



---

Universidad de Valladolid



**PROGRAMA DE DOCTORADO EN QUÍMICA: QUÍMICA DE  
SÍNTESIS, CATÁLISIS Y MATERIALES AVANZADOS**

**TESIS DOCTORAL:**

**Experimental and Computational Studies on  
the Catalytic and Luminescent Properties of Ni,  
Pd and Au Complexes with 2-Chalcone or  
2-Biaryl Phosphines**

Presentada por **Jaime Ponce de León Pintado** para  
optar al grado de  
Doctor/a por la Universidad de Valladolid

Dirigida por:  
Prof. Dr. Pablo Espinet Rubio





Universidad de Valladolid



Documento / Document 8T

## INFORME DEL DIRECTOR O DIRECTORA DE TESIS PARA VALIDAR LA SOLICITUD DE DEPÓSITO / THESIS SUPERVISOR'S REPORT TO VALIDATE THE DEPOSIT REQUEST

Esta autorización debe estar firmada por todos los directores o directoras de la tesis / This authorisation must be signed by all the thesis supervisors.

Dr./Dra: Prof. Dr. Pablo Espinet Rubio

con D.N.I./Pasaporte / with National Identity Card/Passport Number: 17176361F

email: [espinet@qi.uva.es](mailto:espinet@qi.uva.es)

como Director/a de la Tesis Doctoral titulada / as Director/Supervisor of the Doctoral Thesis entitled

Experimental and computational studies on the catalytic and luminescent properties of Ni, Pd and Au complexes with 2-chalcone or 2-biaryl phosphines

realizada por D./D<sup>a</sup> / written by Mr./Ms Jaime Ponce de León Pintado

Programa de Doctorado / Doctoral Programme

Doctorado en Química: Química de Síntesis, Catálisis y Materiales Avanzados

autoriza la solicitud del depósito de la misma, considerando que / *authorises the application to deposit this thesis, considering that*

esta tesis cumple sobradamente las condiciones de publicaciones en revistas de alto índice de impacto para ser presentada como compendio de publicaciones, contiene una investigación novedosa y original en el campo de la química que demuestra la madurez científica del doctorando, su dominio de las metodologías de investigación y, en un grado extraordinario, su capacidad para aplicar y combinar técnicas instrumentales avanzadas y programas de cálculo computacional.

Valladolid, a fecha de firma electrónica / Valladolid, as of the date of the electronic signature (firma de todos los directores o directoras / signature of all the directors)

ESPINET RUBIO  
PABLO -  
17176361F  
Fecha: 2022.12.06 23:37:51  
+01'00'

Nota: Incorporar este documento con las dos firmas electrónicas visibles, en la pantalla documentación (documento 3) de la aplicación para el depósito de la tesis de la UVa /Note: Include this document with visible electronic signatures in the documentation screen (document 3) of the thesis deposit web application

PRESIDENCIA DE LA COMISIÓN DE TESIS DOCTORALES  
PRESIDENT OF THE DOCTORAL THESIS COMMITTEE





La Tesis Doctoral titulada “*Experimental and Computational Studies on the Catalytic and Luminescent Properties of Ni, Pd and Au Complexes with 2-Chalcone or 2-Biaryl Phosphines*” ha sido realizada gracias al apoyo económico del Ministerio de Economía, Industria y Competitividad y de la Agencia Estatal de Investigación (contrato predoctoral para la Formación de Doctores BES-2017-080726), del Ministerio de Economía, Industria y Competitividad (proyectos CTQ2016-80913-P, CTQ2017-89217-P), del Ministerio de Ciencia e Innovación y de la Agencia Estatal de Investigación (proyecto PID2020-118547GB-I00) y de la Junta de Castilla y León (proyectos VA051P17, VA062G18, VA224P20).

Se agradece su contribución al desarrollo de los trabajos descritos en esta memoria al resto de coautores de las publicaciones: Prof. Dr. Pablo Espinet, Dra. Rebeca Infante, Dra. Estefanía Gioria, Prof. Dr. Jesús M<sup>a</sup> Martínez de Ilarduya, Guillermo Marcos, Sara Villalba, Dr. Marconi N. Peñas, Dra. Andrea Vélez, Dr. Myles Drance, Prof. Dr. Alexander T. Radosevich, Prof. Dr. Gabriel Aullón, Prof. Dr. Juan Casares, Dra. María Pérez. Además, se agradece la ayuda puntual del Prof. Dr. Agustí Lledós.



## Contents

<b>Resumen</b> .....	<b>1</b>
<b>Introduction</b> .....	<b>7</b>
<b>Chapter I: Evaluation of Ligand Ability to Promote Difficult Couplings in Nickel</b> ....	<b>15</b>
<b>Chapter II: New Methodologies for the Selective Synthesis of Highly Fluorinated Biaryls</b> .....	<b>25</b>
<b>Chapter III: Synthesis and Evaluation as Precatalysts of <i>cis</i>-[PdR<sub>2</sub>(L)<sub>n</sub>] Complexes (R = Partially Fluorinated Aryl)</b> . ....	<b>41</b>
<b>Chapter IV: Analysis of Metal-Ligand Interactions in [AuCl(L)] Complexes with Fluorinated PR<sub>2</sub>(biaryl) Phosphines</b> .....	<b>59</b>
<b>Chapter V: Synthesis of Fluorophosphoranes from Fluorinated Biaryl Phosphines by Intramolecular S<sub>N</sub>Ar</b> .....	<b>69</b>
<b>Chapter VI: Luminescent Behavior of Chalcone-derived Phosphines (PEWO) and their Metal Complexes</b> .....	<b>81</b>
<b>Chapter VII: Synthesis of Group 10 Metallophosphoranes (M = Ni, Pd) and Selective Substitution Reactions</b> .....	<b>89</b>
<b>Conclusions</b> .....	<b>97</b>
<b>Methods</b> .....	<b>99</b>
<b>List of Publications</b> .....	<b>101</b>





## Resumen

El trabajo realizado en esta Tesis abarca diversas temáticas, tales como el estudio de las etapas y los mecanismos de una reacción, el desarrollo de nuevas metodologías sintéticas de productos orgánicos relevantes, o el análisis de las propiedades fisicoquímicas que presentan nuevos compuestos relacionados por la presencia destacada de dos fragmentos moleculares a lo largo de toda la tesis. Estos fragmentos son los arilos fluorados y los ligandos fosfina. Estos grupos y su combinación, fosfinas fluoradas, han jugado un papel imprescindible en el desarrollo de la Tesis.

En el desarrollo de la Tesis, se han empleado intensamente técnicas instrumentales de uso común en la investigación química, entre las que destacan la resonancia magnética nuclear (RMN) y la difracción de rayos X. Adicionalmente, técnicas como la espectroscopía de infrarrojo (IR), la cromatografía de gases acoplada a espectrometría de masas o la luminiscencia UV-Vis han sido empleadas de forma complementaria cuando ha sido necesario. Finalmente, el estudio computacional (DFT) ha resultado un importante apoyo para las propuestas realizadas en alguno de los estudios realizados. Todas las técnicas, incluidos los estudios computacionales, han sido utilizadas personalmente por quien presenta esta memoria.

### **Capítulo I: *Evaluación de la capacidad de los ligandos para facilitar acoplamientos difíciles en Ni***

El interés en procesos sintéticos catalizados por níquel se ha incrementado exponencialmente en la última década. No obstante, la información disponible para elegir el ligando apropiado en un proceso de acoplamiento C–C en Ni es escasa en comparación con Pd, donde esta etapa ha sido estudiada en profundidad.

El compuesto previamente descrito *cis*-[Ni(C<sub>6</sub>F<sub>5</sub>)<sub>2</sub>(THF)<sub>2</sub>] es un precursor ideal para medir y comparar la capacidad de diversos ligandos de promover la etapa de eliminación reductora en Ni, crucial en muchos procesos sintéticos, y evitar reacciones competitivas.

Se ha evaluado una gran variedad de ligandos: bipyridinas, fosfinas monodentadas, fosfinas quelatantes, fosfinas biarílicas y fosfinas PEWO. Estas últimas presentan una olefina deficiente en electrones que puede actuar como quelato al centro metálico.

Los resultados obtenidos son muy variados, desde ligandos que producen complejos altamente estables a ligandos que son capaces de promover la eliminación reductora de manera instantánea.

Las fosfinas biarílicas, muy eficaces en Pd, son lentas y poco eficientes en Ni. Sin embargo, los ligandos PEWO son extraordinariamente activos y son capaces de promover el acoplamiento incluso a -50 °C.

### **Capítulo II: *Nuevos métodos para la síntesis selectiva de biarilos altamente fluorados***

La presencia de átomos de flúor en una molécula modifica sus propiedades fisicoquímicas frente a su análogo no fluorado. Esto ha llevado a un incremento del número de

compuestos fluorados que son utilizados en diversos campos, como la industria farmacéutica y la ciencia de materiales. No obstante, el grado de fluoración en estas moléculas puede considerarse como bajo, ya que es raro encontrar ejemplos que presenten 4 átomos de flúor o más.

Esta escasez puede explicarse por la falta de métodos generales para la preparación de biarilos con alto grado de fluoración. Y es que, si bien hay una gran cantidad de procedimientos de síntesis para obtener biarilos con uno de sus arilos fluorados, solo existían dos ejemplos para obtener biarilos con ambos arilos fluorados. No obstante, estos métodos presentan ciertas limitaciones, como la inestabilidad de algunos reactivos en las condiciones de reacción o un alcance limitado en los posibles productos.

Por este motivo, se procedió al diseño de nuevas metodologías que nos han permitido obtener biarilos fluorados en altos rendimientos, con condiciones suaves de reacción y reduciendo la cantidad de subproductos generados.

En primer lugar, y apoyándonos en los resultados del Capítulo I, se utilizaron los ligandos PEWO para la obtención de biarilos catalizada tanto por Ni como por Pd. En esta reacción, de tipo Negishi, se emplea  $Zn(C_6F_5)_2$  como nucleófilo. Los rendimientos obtenidos son notablemente mejores que los descritos previamente, y los tiempos de reacción se reducen sensiblemente. En algunos casos, donde el electrófilo (ArI) presenta alto grado de fluoración, se detectó una pérdida de rendimiento, en especial con el sistema de Ni. El análisis de alícuotas de reacción por RMN de  $^{19}F$  permitió asociar la pérdida de rendimiento a la formación de subproductos debidos a una transmetalación no deseada.

Con el objetivo de incrementar la selectividad en la etapa de transmetalación, se procedió al desarrollo de un segundo método. En esta ocasión, se optó por un sistema catalítico bimetalico Pd/Cu, ya que la transmetalación de arilos desde el Cu al Pd se encuentra muy favorecida y la formación del nucleófilo en cantidades catalíticas reduce la competencia de otras reacciones paralelas.

### **Capítulo III: Síntesis y evaluación como precatalizadores de complejos $cis-[Pd(Ar^F)_2(L)]$ ( $Ar^F$ = arilo parcialmente fluorado)**

El desarrollo de nuevos métodos sintéticos facilitados por Pd, que implican moléculas complejas o reactivos sensibles, ha tenido asociado un interés creciente en el diseño de nuevos precatalizadores que permitan acceder a la especie catalíticamente activa en condiciones suaves de reacción. No obstante, muchos de estos precatalizadores consumen parte de los reactivos o generan subproductos no inertes, que pueden afectar al buen funcionamiento de las catálisis.

En 2016, nuestro grupo de investigación utilizó el complejo  $cis-[Pd(C_6F_5)_2(THF)_2]$  como un medidor de la capacidad de diversos ligandos para promover acoplamientos difíciles. En este estudio se destacó que, tras la eliminación reductora, se genera el correspondiente  $[Pd^0(L)]$ , que se considera la especie catalíticamente activa. Con estos antecedentes, se decidió valorar la capacidad de distintos compuestos  $cis-[Pd(Ar^F)_2(L)]$  con arilos parcialmente fluorados como precatalizadores.

En primer lugar, se evaluó la estabilidad de los complejos sintetizados. Aquellos compuestos que presentan ciclooctadieno (COD) como ligando son estables en disolución incluso a temperaturas moderadas. En cambio, los compuestos con tetrahidrofurano (THF) se descomponen progresivamente. La velocidad de descomposición es mayor en los compuestos que presentan menor grado de fluoración en su estructura.

El grado de activación de estos complejos en pruebas estequiométricas, tras la adición de ligandos voluminosos, se estudió tanto a temperatura ambiente como a 60 °C. Como esperábamos, los complejos con THF, que es un ligando lábil en Pd<sup>II</sup>, reaccionan más rápido que los de COD. Además, la alta labilidad del THF, incluso a baja temperatura, permitió aislar complejos de tipo *cis*-[Pd(Ar<sup>F</sup>)<sub>2</sub>(L)] con los ligandos XantPhos y SPhos. En condiciones normales resulta muy difícil aislar este tipo de compuestos, debido a su reactividad.

Finalmente, los complejos de COD y THF fueron empleados como precatalizadores en tres reacciones modelo. Los resultados obtenidos indican que el complejo de THF es el indicado a emplear en condiciones de reacción suaves o con nucleófilos débiles. No obstante, los compuestos con COD son competentes con nucleófilos fuertes, como los organozíncicos, o en condiciones de alta temperatura.

#### ***Capítulo IV: Análisis de la interacción ligando-metal en complejos [AuCl(L)] con fosfinas fluoradas de tipo PR<sub>2</sub>(2-biarilo)***

Las fosfinas 2-biarílicas son ampliamente utilizadas como ligandos en procesos catalizados por oro. En las estructuras de los complejos [AuX{PR<sub>2</sub>(2-biarilo)}], ya sean catiónicos o neutros, se observa que el biarilo se encuentra localizado sobre el átomo de oro. La proximidad entre el arilo inferior y el oro sugiere la existencia de interacciones estabilizantes entre ambos.

Con el objetivo de analizar la naturaleza de estas interacciones, se sintetizó una serie de fosfinas biarílicas que presentan uno de sus arilos, superior o inferior, o ambos fluorados. Así, es posible relacionar el grado de interacción con las propiedades electrónicas de la fosfina.

El estudio de las fuerzas implicadas se llevó a cabo combinando datos experimentales, obtenidos mediante difracción de rayos X de los compuestos [AuCl(L)] sintetizados, y computacionales, tales como análisis de la estabilidad termodinámica de posibles isómeros, teoría cuántica de átomos en moléculas (QTAIM), análisis de interacciones no covalentes (NCI) y análisis de orbitales naturales enlazantes (NBO).

Los resultados obtenidos indican que la distancia entre el átomo de oro y el arilo inferior de los ligandos se encuentra por debajo de la correspondiente suma de radios de van der Waals. Esto demuestra la presencia de interacciones de tipo no covalente entre estos dos fragmentos de la molécula, que perturban a la densidad electrónica  $\pi$  del arilo sin establecer solapamiento orbital (covalencia). El análisis NBO permitió cuantificar el valor de esta interacción, que se sitúa en el orden de 2–10 kcal·mol<sup>-1</sup> en función del complejo analizado.

### **Capítulo V: Síntesis de fluorofosforanos a partir de fosfinas biarílicas fluoradas mediante $S_NAr$ intramolecular**

Las fosfinas no son simplemente ligandos para complejos metálicos, también presentan su propia reactividad. En este sentido, cabe destacar la formación de iluros de fósforo, empleados como reactivos en la reacción de Wittig, y la utilización de pares de Lewis impedidos en la activación de moléculas pequeñas. Las propiedades de las fosfinas como base de Lewis permiten además su aplicación como especies nucleófilas. Esta reactividad ha sido aplicada a reacciones de sustitución nucleófila aromática intermolecular.

Además, diversas especies de fósforo heterocíclicas presentan comportamiento luminiscente. Esta propiedad emisiva suele ir asociada a la presencia de un grupo dibenzofosfol en la molécula. Esto ha hecho que numerosos compuestos con átomos de fósforo en su estructura encuentren utilidad en la ciencia de materiales.

En este contexto, consideramos que las fosfinas 2-biarílicas fluoradas sintetizadas previamente, y descritas en el capítulo IV, suponen una buena plataforma para la obtención de especies de fósforo (V). El acceso a estas especies se produjo de manera sencilla y eficiente, mediante calentamiento de la fosfina en disolución. Estas especies fueron identificadas como fluorofosforanos, que presentan un enlace P–F, y se pueden considerar formalmente como el producto de adición oxidante del enlace C–F al átomo de fósforo. La temperatura necesaria para el proceso de isomerización depende de los sustituyentes en el átomo de fósforo, que regulan su nucleofilia, así como de los del biarilo, que modulan la electrofilia del átomo de carbono reactivo.

Los compuestos obtenidos presentan además comportamiento luminiscente, con emisión fluorescente en la región UV-azul, dependiendo del compuesto analizado. Este comportamiento se debe a la presencia del grupo dibenzofosfol.

El mecanismo de reacción fue analizado mediante estudios cinéticos de velocidad de reacción, y complementado por métodos DFT. Las medidas cinéticas indican que la reacción es de orden 1 frente a la fosfina, lo que implica una reacción intramolecular. Además, el empleo de química computacional permite identificar el proceso como una sustitución nucleófila aromática, en la que el fósforo actúa como grupo entrante y el flúor como grupo saliente. La posterior coordinación del átomo de flúor al fosfonio generado forma el fluorofosforano final.

### **Capítulo VI: Comportamiento luminiscente de fosfinas derivadas de chalcona (PEWO) y de sus complejos metálicos**

Los compuestos con sistemas poliaromáticos conjugados suelen presentar propiedades luminiscentes, lo que los hace atractivos para el desarrollo de nuevos materiales. Las propiedades emisivas de estos compuestos pueden modificarse mediante variaciones en sus sustituyentes o con la incorporación de un fragmento metálico a su estructura.

Los ligandos PEWO previamente descritos presentan un fragmento chalcona en su esqueleto. A diferencia de otras chalconas, en las que se observa un efecto electrónico de tipo *push-pull*, ya que presentan sustituyentes dadores y atractores respectivamente en

cada uno de sus extremos, los ligandos fluorados PEWO actúan como *pull-pull* al tener sustituyentes atractores en ambos extremos de la olefina.

Cuando se exponen a luz UV, los ligandos PEWO fluorados presentan emisión fluorescente, en la zona amarilla del espectro visible. En cambio, una vez coordinados dos ligandos a Pd, formando complejos de tipo *trans*-[PdX<sub>2</sub>(PEWO)<sub>2</sub>] (X = Cl, Br), en los que la olefina no está coordinada, el máximo de emisión se desplaza hacia mayores longitudes de onda, y su naturaleza pasa a ser de tipo fosforescente.

El comportamiento luminiscente es altamente dependiente del metal y los sustituyentes que presenta. Así, tanto el complejo análogo de Pt, *trans*-[PtCl<sub>2</sub>(PEWO)<sub>2</sub>], como el derivado de cianuro, *trans*-[Pd(CN)<sub>2</sub>(PEWO)<sub>2</sub>], no presentan propiedades emisivas. El análisis de las transiciones electrónicas en estos complejos metálicos mediante cálculos TD-DFT permite comprender las diferencias en el comportamiento emisivo de estas especies. Así, se observa la hibridación entre los orbitales del fragmento chalcona con los del PdX<sub>2</sub> en el LUMO de los compuestos luminiscentes, a diferencia de los derivados no emisivos, donde esta hibridación no tiene lugar.

### **Capítulo VII: Síntesis de metalofosforanos del grupo 10 (M = Ni, Pd) y reacciones de sustitución selectivas**

Como se ha comentado en el resumen del Capítulo V, las fosfinas presentan carácter básico en términos de la teoría ácido/base de Lewis. Esto se debe a la presencia de un par electrónico disponible en el átomo de fósforo, lo que abre su utilización como reactivos nucleófilos. No obstante, esta reactividad puede modularse modificando la estructura de la fosfina. Así, el diseño de nuevas fosfinas con geometría restringida, fijada por su esqueleto, permite abrir el camino a reactividades de tipo bifílico, donde la fosfina puede actuar tanto como dadora como aceptora de electrones.

Las fosfinas coordinadas a metales de transición suelen ser simplemente un espectador en las reacciones, aportando estabilidad al complejo metálico o modulando la reactividad del metal. No obstante, el uso de fosfinas con geometría restringida como ligandos ha permitido desarrollar sistemas con reactividad cooperativa metal-ligando o incluso reactividad localizada en el ligando, con el metal actuando simplemente como espectador.

En este contexto, se sintetizaron una serie de complejos de metales del grupo 10 de tipo [MX<sub>2</sub>(L)] con el ligando quelato *py*<sub>2</sub>-*NNP*. Este ligando presenta un grupo fosfina con geometría distorsionada *C<sub>s</sub>*. En los complejos sintetizados se observa una migración del grupo X al átomo de fósforo, es decir, la fosfina actúa como ácido de Lewis, una vez coordinada al metal como base de Lewis.

Los complejos de paladio sintetizados se emplearon en reacciones de sustitución del ligando aniónico. El diferente carácter duro/blando así como la mayor oxofilia del fósforo frente al paladio permiten la sustitución selectiva del grupo unido al fósforo o al paladio en función del reactivo y el complejo empleado. La reversibilidad de este proceso fue demostrada para la reacción de intercambio de fenol. En conjunto, la nueva reactividad observada en este tipo de complejos abre la puerta al diseño de nuevos procesos sintéticos mediante la cooperación metal-ligando.



## Introduction

At first sight, the studies carried out in this thesis may look unrelated, as they approach very different topics, spanning from metal to ligand bonding interactions to catalysis, with a stop in materials science and luminescence. However, once a closer look is taken, some similarities between the chapters can be found, and the major presence of two moieties can be distinguished. These two moieties are phosphines and fluorinated aryls. They separately and their combination, fluorinated phosphines, play an important role in the research reported in this Thesis.

Phosphines are, probably, the most widely used ligands in reactions involving transition metals, both in stoichiometric reactions and in catalysis. They were the solution to provide stability to the transition metal organometallic species in the seminal research of the early 1950's. The development of homogeneous catalysis is, in many instances, based on the versatility of the P atom to be modified with different substituents that modulate its features, allow tailoring of the steric and electronic properties of the ligand, its resistance to oxidation, or the introduction of chirality. Hence, phosphines are in the origin of the extraordinary development of the field *transition metal homogeneous catalysis*, which has been growing since then.

Among the most known phosphine ligands with an on-purpose design, we find the dialkyl 2-biarylphosphines, developed by Buchwald group.<sup>1</sup> These ligands have been employed in many transition metal catalyzed reactions, such as C–C Suzuki couplings and C–N Buchwald-Hartwig aminations with palladium, or in cyclization and cycloaddition reactions with gold. These ligands combine bulky aryls that make a good donor phosphine facilitating the oxidative addition step in catalysis and the biaryl moiety that becomes acceptor in low oxidation state metal intermediates and facilitates the reductive elimination step. In this way, with the appropriate phosphine, the success of the cycle only depends on a reasonably efficient transmetalation.

Alternatively, our group has worked on a family of chelating fluorinated aryl phosphines named PEWO with an electron withdrawing olefin. These ligands can be seen as derivatives of a chalcone moiety, which acts as the acceptor of electron density from the metal center. The withdrawing effect of these ligands has direct consequences when PEWOs are employed in catalysis. The reductive elimination barrier is highly decreased, sometimes impressively, although at the cost of making oxidative addition more difficult (but accessible with ArI and ArBr).<sup>2</sup> The structural similarity between Buchwald's biarylphosphines and PEWO ligands can be observed in Figure 1.

---

<sup>1</sup> Arrechea, P. L.; Buchwald, S. L. Biaryl Phosphine Based Pd(II) Amido Complexes: The Effect of Ligand Structure on Reductive Elimination. *J. Am. Chem. Soc.*, **2016**, *138*, 12486–12493.

<sup>2</sup> Gioria, E.; del Pozo, J.; Lledós, A.; Espinet, P. Understanding the Use of Phosphine-(EWO) Ligands in Negishi Cross-Coupling: Experimental and Density Functional Theory Mechanistic Study. *Organometallics*, **2021**, *40*, 2272–2282.

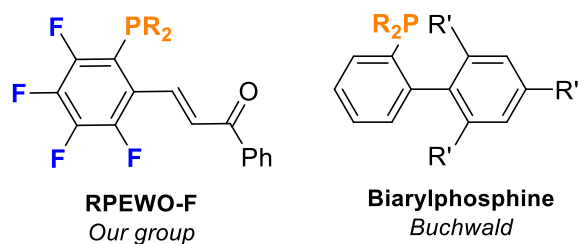


**Figure 1.** General structure of PEWO and biarylphosphine ligands.

Concerning fluorinated aryls, molecules containing them are very valuable due to the singular properties that this moiety offers in comparison with their non-fluorinated counterparts. The metal complexes with highly fluorinated aryls show remarkably high stability because of the strong  $M-C_{Ar}$  bond formed. This, and the rich information obtained from  $^{19}F$  NMR studies was crucial and allowed our group to carry out many basic mechanistic and catalytic studies with Pd, that in the previous decades could only be approached with the wrong Pt model. Fluorinated aryls are a sufficiently slow but correct model in Pd of systems involving conventional aryls that react too fast to be studied. Two research lines derive from here, the mechanistic studies, and the synthesis of molecules with fluorinated aryls.

There is an increasing interest in molecules bearing highly fluorinated aryls, in pharmaceuticals to increase their effectiveness, stability or bioabsorption,<sup>3</sup> and in materials as molecules with highly polarized zones. In group 10 TM-catalyzed reactions, such as Suzuki, Negishi or Stille couplings, the reductive elimination step is crucial for the yield and selectivity of the catalysis, as it is the irreversible step that pulls the whole cycle on. However, the coupling of highly fluorinated aryls is difficult and the molecules containing specially fluorinated biaryl is scarce, mainly due to the lack of methodologies to synthesize this kind of compounds in comparison to biaryl with only one or zero fluorinated aryls. Hence, identifying ligands that reduce the activation barrier for this step is highly advisable, especially when the fragments are difficult to couple, in order to avoid the formation of other by-products. At this point the confluence of the two main characters in the play occurs: in order to facilitate the coupling of fluorinated aryls, Buchwald phosphines and fluorinated PEWO phosphines are very efficient.

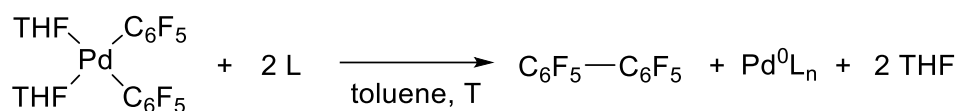
In 2016, our group reported a methodology to obtain accurate values for the activation barrier of the reductive elimination process in Pd.<sup>4</sup> The method allowed to rank the ability of several phosphine ligands to promote the coupling from  $cis-[Pd(C_6F_5)_2(THF)_2]$  (Scheme 1). Interestingly, one of the PEWO ligands developed by our group, with *o*-tolil substituents in the phosphorous, produced the reductive elimination at a rate comparable to that of the very bulky tBuXPhos and P<sup>t</sup>Bu<sub>3</sub> ligands. We wondered whether a similar system would be feasible employing nickel instead of palladium, since its use has vastly increased in the last decade due to its unique properties.<sup>5</sup>

<sup>3</sup> Gillis, E. P.; Eastman, K. J.; Hill, M. D.; Donnelly, D. J.; Meanwell, N. A. Applications of Fluorine in Medicinal Chemistry. *J. Med. Chem.*, **2015**, *58*, 8315–8359.

<sup>4</sup> Gioria, E.; del Pozo, J.; Martínez-Irarduya, J. M.; Espinet, P. Promoting Difficult Carbon-Carbon Couplings: Which Ligand Does Best? *Angew. Chem., Int. Ed.*, **2016**, *55*, 13276–13280.

<sup>5</sup> Ananikov, V. P. Nickel: The “Spirited Horse” of Transition Metal Catalysis. *ACS Catal.*, **2015**, *5*, 1964–1971.



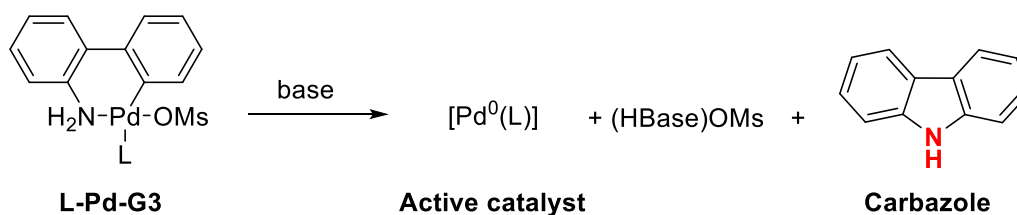


**Scheme 1.** Protocol for the experimental evaluation of reductive elimination process.

As a first-row transition metal, nickel is cheaper and more abundant. Moreover, it shows an enhanced reactivity, as one-electron processes and different oxidation states are more accessible for it. The smaller atomic radius of nickel makes it a harder metal center compared to palladium. Thus, coordination to nickel of small molecules with hard atoms, such as O- and N-donors, is usually favored. The ability of different ligands, such as olefins, bipyridines and phosphines, to promote difficult couplings in nickel and to prevent competitive processes is evaluated in **Chapter I**.

The design of systems to obtain highly fluorinated biaryls in good yields with high selectivity is very appealing. To get to this goal, two different methodologies were applied. Firstly, a catalytic system where the ligand design is decisive to reduce the amount of by-products obtained, such as homocoupling and hydrolysis, favoring the formation of the desired product. This approach, shown in the first part of **Chapter II**, can be considered an extension of the results obtained in **Chapter I**, where the ideal ligand (PEWO) was identified from stoichiometric reactions. Secondly, a bimetallic Pd/Cu system, shown in the second part of **Chapter II**, where the *in situ* generation of the nucleophile reduces the amount of homocoupling products. In this case, the choice of ligands for each metal is crucial to avoid the failure of any of the catalytic cycles that work simultaneously.

During the development of these catalytic systems, an interesting feature caught our attention. In some cases, the efficiency of the reaction was highly dependent on the precatalyst employed and, obviously, different byproducts were formed during their activation. For the PEWO system, 2 equivalents of nucleophile,  $\text{Zn}(\text{C}_6\text{F}_5)_2$ , were consumed for the  $[\text{MCl}_2(\text{CH}_3\text{CN})_2]$  precatalyst activation, generating fairly inert  $\text{C}_{12}\text{F}_{10}$ . For the bimetallic system, the widely employed XPhos-Pd-G3 precatalyst consumed one equivalent of base and generated a carbazole, which could further react under the reaction conditions (Scheme 2). These observations suggested us to develop general precatalysts, that would be activated simply by addition of the preferred ligand, without consuming any other reagent, and whose activation would not form reactive species. To this end, and with the previous 2016 work with Pd in mind, we prepared a series of *cis*- $[\text{Pd}(\text{Ar}^{\text{F}})_2(\text{L})]$  complexes bearing partially fluorinated aryls and labile ligands. These complexes would enter the catalytic cycle as active  $[\text{Pd}^0(\text{L})]$  species simply by reductive elimination of  $(\text{Ar}^{\text{F}})_2$ . Indeed, both stoichiometric reactions, where the generated  $[\text{Pd}^0(\text{L})]$  is trapped as  $[\text{Pd}(\text{Ar})\text{X}(\text{L})]$ , as well as catalytic reactions prove the high efficiency of these complexes as precatalysts, as described in **Chapter III**.



**Scheme 2.** Activation reaction of L-Pd-G3 precatalysts. OMs = Mesylate.

The easy ligand substitution in *cis*-[Pd(Ar<sup>F</sup>)<sub>2</sub>(L)] also allowed us to isolate some intermediates with biarylphosphines. As said before, in complexes with this kind of ligands, the biaryl usually interacts with the metal center. Nevertheless, the nature of this interaction is different for each metal. For palladium, the biaryl moiety is placed in one of the four available coordination positions. A strong interaction between the metal and the ipso carbon of the biaryl is inferred by the X-ray structures reported in the literature, as the geometry of this carbon atom is slightly distorted to a tetrahedral one, typical of sp<sup>3</sup> hybridization. This observation suggests that the interaction has some degree of covalency. However, the nature of this interaction with other metals is not so clear. Gold (I) complexes, neutral or cationic, bearing biarylphosphines are two-coordinated and show a linear geometry.<sup>6</sup> Nevertheless, the biaryl moiety is directed toward the gold atom too (Figure 2). In these cases, the ipso carbon of the biaryl shows a trigonal geometry, typical of sp<sup>2</sup> hybridization, which indicates that the metal-ligand interaction is different to that observed for palladium. The analysis of this interaction is discussed in **Chapter IV**, employing biarylphosphine ligands with similar steric hindrance but different electronic richness. For this study, some unreported 2-biaryl phosphine partially or fully fluorinated that had not been tested before were synthesized.

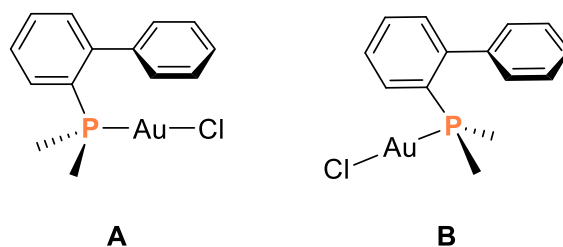


**Figure 2.** Alternative conformations of [AuCl(L)] complexes with biaryl phosphines. Only A is observed experimentally.

Phosphines also have their own reactivity. Well-known examples of synthetic reactions with phosphines as substrates are the preparation of phosphorous ylides, employed in the Wittig reaction,<sup>7</sup> and frustrated Lewis pairs (FLPs), used for the activation of small molecules.<sup>8</sup> In some cases, this reactivity can be made catalytic in the phosphine, such as in deoxygenation reactions, where the phosphorous follows a P(III)/P(V) redox cycle, or

<sup>6</sup> Pérez-Galán, P.; Delpont, N.; Herrero-Gómez, E.; Maseras, F.; Echavarren, A. M. Metal-Arene Interactions in Dialkylbiarylphosphane Complexes of Copper, Silver, Gold. *Chem. - Eur. J.*, **2010**, *16*, 5324–5332.

<sup>7</sup> Byrne, P. A.; Gilheany, D. G. The modern interpretation of the Wittig reaction mechanism. *Chem. Soc. Rev.*, **2013**, *42*, 6670–6696.

<sup>8</sup> Stephan, D. W.; Erker, G. Frustrated Lewis Pair Chemistry: Development and Perspectives. *Angew. Chem., Int. Ed.*, **2015**, *54*, 6400–6441.

in the activation of X–H bonds. In this context, the work at Goicoechea and Radosevich groups, employing geometrically constrained biphilic phosphines clearly stands out.<sup>9,10</sup>

Moreover, some phosphine derivatives exhibit interesting properties for application in materials science, such as luminescence and conductivity. These properties have been thoroughly studied for P(III) dibenzophospholes and their P(V) chalcogen derivatives.<sup>11</sup> The Lewis basicity of P(III) in some phosphines allows their use as nucleophiles too. This reactivity has been utilized for intermolecular nucleophilic aromatic substitutions. In this thesis, an example of  $S_NAr$  is studied in **Chapter V**, where a formal oxidative addition of phosphorous to a C–F bond enables the formation of elusive pentacoordinated P(V) fluorophosphoranes. These complexes also exhibit fluorescent emission, localized in the cyclic dibenzophosphole moiety.

Luminescent properties are usually observed for compounds that can permit electron delocalization through their skeleton, mainly involving  $\pi$ -electronic systems, such as functionalized polycyclic aromatic hydrocarbons (PAHs) and polyenes. The luminescence of these systems can also be modulated upon ligation to a metal, which typically takes part in the process involving its *d* orbitals.<sup>12</sup> Considering the presence of a conjugated chalcone moiety in our PEWO ligands, it is logical to think that they may exhibit luminescent properties. The evaluation of the emissive properties is shown in **Chapter VI** (Figure 3). Interestingly, in the solid state, PEWOs show fluorescent emission, which is turned into phosphorescence when coordinated in some Pd complexes.

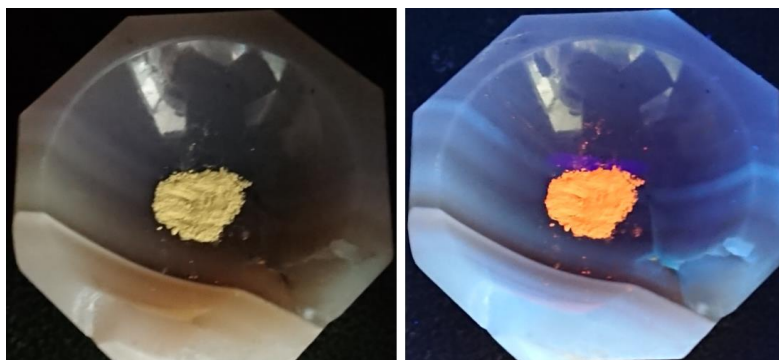


**Figure 3.** Pictures of complex  $\text{trans-[PdCl}_2(\text{PhPEWO-F})_2]$  without (left) and with (right) irradiation.

When coordinated to a metal center, phosphine ligands typically act as spectators, modulating the electronic properties of the metal they are bonded to. However, with the appropriate ligand design, it is possible to observe a cooperative M–L reactivity,<sup>13</sup> or even

<sup>9</sup> Abbenseth, J.; Goicoechea, J. M. Recent developments in the chemistry of non-trigonal pnictogen pincer compounds: from bonding to catalysis. *Chem. Sci.*, **2020**, *11*, 9728–9740.

<sup>10</sup> Lipshultz, J. M.; Li, G.; Radosevich, A. T. Main Group Redox Catalysis of Organopnictogens: Vertical Periodic Trends and Emerging Opportunities in Group 15. *J. Am. Chem. Soc.*, **2021**, *143*, 1699–1721.

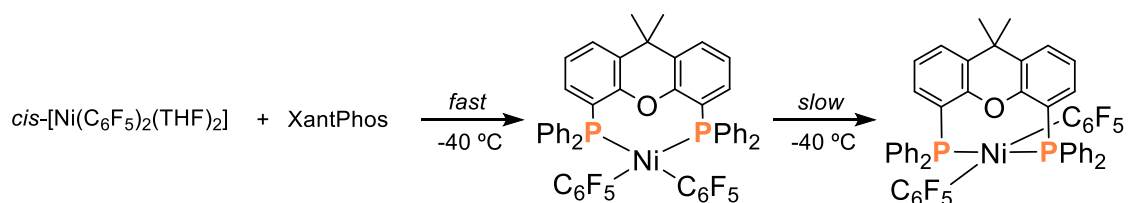
<sup>11</sup> Hibner-Kulicka, P.; Joule, J. A.; Skalik, J.; Bałczewski, P. Recent studies of the synthesis, functionalization, optoelectronic properties and applications of dibenzophospholes. *RSC Adv.*, **2017**, *7*, 9194–9236.

<sup>12</sup> Kalinowski, J.; Fattori, V.; Cocchi, M.; Williams, J. A. G. Light-emitting devices based on organometallic complexes as emitters. *Coord. Chem. Rev.*, **2011**, *255*, 2401–2425.

<sup>13</sup> Drance, M. J.; Tanushi, A.; Radosevich, A. T. Two-Site O–H Addition to an Iridium Complex Featuring a Nonspectator Tricoordinate Phosphorus Ligand. *J. Am. Chem. Soc.*, **2022**, *144*, 20243–20248.

a reversal reactivity, where it is the metal the one that acts as spectator.<sup>14</sup> The unusual behavior of a geometrically distorted phosphine ligand upon coordination to some group 10 metal precursors is discussed in **Chapter VII**. The work shown in this chapter has been performed during a stay at Professor Radosevich's research group (MIT).

The study of reaction mechanisms has played a key role in this thesis. The use of nuclear magnetic resonance (NMR) techniques, apart from the typical characterization purposes, has been important to obtain accurate kinetic data as well as to detect reaction intermediates (Scheme 3). Most of the synthesized compounds present NMR active nuclei <sup>19</sup>F and <sup>31</sup>P. Compared to <sup>1</sup>H, they have a larger spectral width, which provides a lot of information from a single spectrum. In addition, the sensitivity of these nuclei is quite high, making the observation of reaction intermediates at low concentrations feasible. Sometimes, a concentration vs time plot of the experimental data obtained from a kinetic study is not enough to confirm or discard a proposed mechanism or to obtain accurate rate values. In these cases, the application of non-linear adjustments through microkinetic modelling can be very helpful. This kind of data analysis has been carried out employing the COPASI software.<sup>15</sup>



**Scheme 3.** Low temperature NMR allows to detect the *cis* isomer and its isomerization to *trans* complex.

Often, NMR and X-ray diffraction have given complementary information about the species involved in a reaction and their reactivity. Additionally, other techniques such as IR spectroscopy, combined GC-MS or UV-Vis luminescence may be useful in some cases. These techniques are, however, useless if the proper experiment design is not well planned. Working under inert atmosphere or at low temperatures may be required when attempting to isolate a new compound. Looking for previously reported similar products as well as the experience acquired during several hours of experimentation provide the answers to what is needed for each reaction.

In summary, this thesis exploits the advantages that offer on-purpose designed phosphines and their derivatives to conduct different kinds of mechanistic or synthetic research. The use of the appropriate techniques has allowed us to disclose the identity of reaction intermediates, to measure reaction rates or to understand unexpected properties.

To finish this introduction, it is worth commenting that this Thesis was trapped by the long confinement period associated to the pandemic and working in the lab was not permitted for some months. It is obvious that this circumstance was not in the original

<sup>14</sup> Bruch, Q. J.; Tanushi, A.; Müller, P.; Radosevich, A. T. Metal–Ligand Role Reversal: Hydride-Transfer Catalysis by a Functional Phosphorus Ligand with a Spectator Metal. *J. Am. Chem. Soc.*, **2022**, *144*, 21443–21447.

<sup>15</sup> Hoops, S.; Sahle, S.; Gauges, R.; Lee, C.; Pahle, J.; Simus, N.; Singhal, M.; Xu, L.; Mendes, P.; Kummer, U. COPASI—a Complex Pathway Simulator. *Bioinformatics*, **2006**, *22*, 3067–3074.

program of research. In order not to waste these months, a computational research based on QTAIM theory and NCI studies was planned, far from any previous computational experience of the student and the supervisor. This is now **Chapter IV** and its acceptance and publication in *Inorganic Chemistry* was an injection of optimism and self-confidence in that black period.



## Chapter I: Evaluation of Ligand Ability to Promote Difficult Couplings in Nickel

The interest in Ni-catalyzed cross-coupling reactions has vastly increased in the last two decades.<sup>1</sup> Compared to the deeply studied Pd processes, the available information to select appropriate ligands for Ni-catalyzed C–C couplings is still scarce. In general, extrapolation of ligand behavior from Pd to Ni is likely to fail due to different factors. One reason, analyzed by Doyle,<sup>2</sup> is that due to the smaller radius of Ni, for the same ancillary ligand, the cone angle  $\theta$ , proposed long ago by Tolman,<sup>3,4</sup> is smaller on Pd than that on Ni. This reduces the volume available to accommodate the reacting groups coordinated to Ni and may prevent the approach of some of the reagents to the metal center. In fact, ligands designed with large  $\theta$  but low %V<sub>bur</sub>, this is, with remote steric hindrance, make operative some Ni catalyzed couplings that fail with classical bulky ligands such as P<sup>t</sup>Bu<sub>3</sub> or JohnPhos (Figure 1).

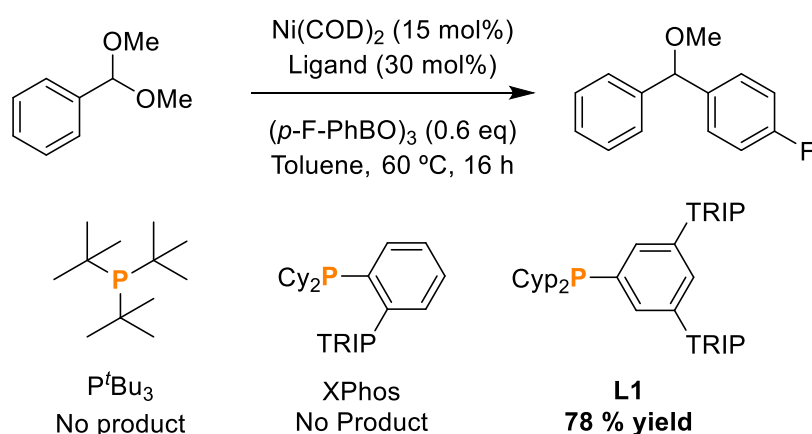


**Figure 1.** Ligand design enables Ni-catalyzed Suzuki coupling of acetals. Cy = cyclohexyl, Cyp = cyclopentyl, TRIP = 2,4,6-tri-isopropylphenyl

A second reason is the different ability of the ligand bonded to the metal center to promote the reductive elimination step. In contrast to the oxidative addition and transmetalation steps, where the choice of reagents (electrophile and nucleophile) may allow these stages of the catalysis to take place, reductive elimination depends only on the ligand, as it is an intramolecular step from a kinetic point of view. Hence, for some processes, the ligand

<sup>1</sup> (a) A. Correa, in Topics in Current Chemistry. Ni- and Fe-Based Cross-Coupling Reactions. Springer International Publishing: Switzerland, 2016; (b) Tasker, S. Z.; Standley, E. A.; Jamison, T. F. Recent advances in homogeneous nickel catalysis. *Nature*, **2014**, *509*, 299–309; (c) Han, F.-S. Transition-metal-catalyzed Suzuki–Miyaura cross-coupling reactions: a remarkable advance from palladium to nickel catalysts. *Chem. Soc. Rev.*, **2013**, *42*, 5270–5298.

<sup>2</sup> Wu, K.; Doyle, A. G. Parameterization of phosphine ligands demonstrates enhancement of nickel catalysis via remote steric effects. *Nat. Chem.*, **2017**, *9*, 779–784.

<sup>3</sup> (a) Tolman, C. A. Phosphorus ligand exchange equilibria on zerovalent nickel. Dominant role for steric effects. *J. Am. Chem. Soc.*, **1970**, *92*, 2956–2965; (b) Tolman, C. A.; Seidel, W. C.; Gosser, L. W. Formation of three-coordinate nickel(0) complexes by phosphorus ligand dissociation from NiL<sub>4</sub>. *J. Am. Chem. Soc.*, **1974**, *96*, 53–60; (c) Tolman, C. A. Steric effects of phosphorus ligands in organometallic chemistry and homogeneous catalysis. *Chem. Rev.*, **1977**, *77*, 313–348.

<sup>4</sup> Since the early estimations in physical models (using Ni as the metal center), other methods have been incorporated, including the modern application of computational methods to different coordination geometries and metal centers: Jover, J.; Cirera, J. Computational assessment on the Tolman cone angles for P-ligands. *Dalton Trans.*, **2019**, *48*, 15036–15048.

employed will be crucial to obtain the desired product and reduce the amount of possible formed byproducts. Previously, our group had proposed the use of complex *cis*-[Pd(C<sub>6</sub>F<sub>5</sub>)<sub>2</sub>(THF)<sub>2</sub>] as a Pd<sup>II</sup>-meter to experimentally rank the different ligands according to their ability to facilitate the difficult C<sub>6</sub>F<sub>5</sub>–C<sub>6</sub>F<sub>5</sub> coupling. The procedure consists of measuring the activation energy for C<sub>6</sub>F<sub>5</sub>–C<sub>6</sub>F<sub>5</sub> formation ( $\Delta G^\ddagger(\text{C}_6\text{F}_5\text{--C}_6\text{F}_5)_{\text{Pd}}$ ) upon addition of the ligand being tested to *cis*-[Pd(C<sub>6</sub>F<sub>5</sub>)<sub>2</sub>(THF)<sub>2</sub>].<sup>5</sup> For identical structures of group 10 metals, a modeled computational study showed that the activation energy for C–C reductive elimination from 4-coordinated *cis*-[M(CH<sub>3</sub>)<sub>2</sub>(PH<sub>3</sub>)<sub>2</sub>] species follows the trend Ni < Pd < Pt.<sup>6</sup> However, this trend may not apply when employing bulky ligands in Ni, as the metal center would be very crowded and the ligand may not accommodate as comfortably as with Pd or Pt. For this reason, we decided to extend the idea of the Pd<sup>II</sup>-meter to nickel, to be able to experimentally compare the ligand behavior in both metals. Note that in Ni detrimental hydrolysis may be more competitive due to the higher oxophilic character of Ni compared to Pd.

The design of an appropriate Ni<sup>II</sup>-meter is not a trivial task, as several ligands with different steric and electronic properties would be evaluated. Therefore, we sought for a starting material that would allow easy coordination of every ligand tested. In order to have a direct comparison with the results obtained with the Pd<sup>II</sup>-meter, we prepared three different Ni complexes bearing C<sub>6</sub>F<sub>5</sub> moieties and easily displaceable stabilizing ligands (Figure 2). The modular nature of these precursors should allow for direct evaluation of the ligand effects, in order to obtain both qualitative and quantitative information.

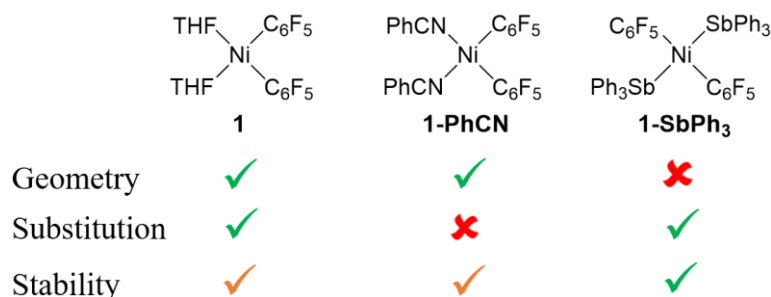


**Figure 2.** [Ni(C<sub>6</sub>F<sub>5</sub>)<sub>2</sub>L<sub>2</sub>] complexes and evaluation of their properties

Initially, *trans*-[Ni(C<sub>6</sub>F<sub>5</sub>)<sub>2</sub>(SbPh<sub>3</sub>)<sub>2</sub>] (**1-SbPh<sub>3</sub>**), an air and moisture stable solid that can be readily obtained in one step,<sup>7</sup> was tested. SbPh<sub>3</sub> ligands are easy to displace, as they are loosely bound to nickel. However, the big volume of the Sb atom makes the *trans* geometry the most stable one thermodynamically, due to the high repulsion between the ligands if they were in *cis* geometry. Hence, a presumably dissociative *trans* to *cis* isomerization is required prior to reductive elimination. The rate of this isomerization process, involving the perfluorinated aryls, could be slower than the reductive elimination step for some of the ligands tested, giving rise to a wrong measure of the coupling efficiency. Therefore, **1-SbPh<sub>3</sub>** was discarded for the study.

<sup>5</sup> Gioria, E.; del Pozo, J.; Martínez-Illarduya, J. M.; Espinet, P. Promoting Difficult Carbon-Carbon Couplings: Which Ligand Does Best? *Angew. Chem., Int. Ed.*, **2016**, *55*, 13276–13280.

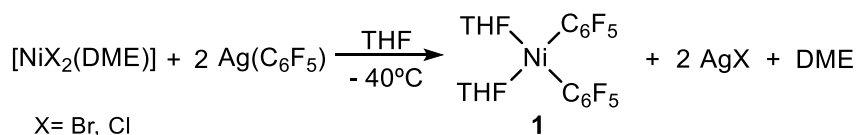
<sup>6</sup> Ananikov, V. P. Nickel: The “Spirited Horse” of Transition Metal Catalysis. *ACS Catal.*, **2015**, *5*, 1964–1971.

<sup>7</sup> Casares, J. A.; Espinet, P.; Martín-Alvarez, J. M.; Martínez-Illarduya, J. M.; Salas, G. Stable Nickel Catalysts for Fast Norbornene Polymerization: Tuning Reactivity. *Eur. J. Inorg. Chem.*, **2005**, 3825–3831.



Complex **1-PhCN** was then evaluated.<sup>8</sup> This complex is not as stable as **1-SbPh<sub>3</sub>** and must be handled under inert conditions. The *cis* geometry of the complex is confirmed by IR spectroscopy. However, the PhCN ligands are not so easily displaced from Ni, making ligand substitution the rds in some cases. For this reason, **1-PhCN** is not suitable for quantitative analysis of the reductive elimination.

At this point, we focused on *cis*-[Ni(C<sub>6</sub>F<sub>5</sub>)<sub>2</sub>(THF)<sub>2</sub>] (**1**) which is the analog complex to the Pd<sup>II</sup>-meter. This complex shows a *cis* geometry and THF ligands are easily substituted. Although **1** is slightly sensitive to oxygen and moisture, it can be stored for long periods under inert atmosphere at low temperature without signs of decomposition. Therefore, **1** was chosen as Ni<sup>II</sup>-meter, as it fulfills the proper requirements in terms of stability, ligand substitution and ease of handling. Two different synthetic routes toward **1** can be found in the literature:<sup>9</sup> firstly, a direct transmetalation from MgBr(C<sub>6</sub>F<sub>5</sub>) to NiBr<sub>2</sub>; secondly, removal of bridging halides from the dimeric species [NBu<sub>4</sub>]<sub>2</sub>[Ni(C<sub>6</sub>F<sub>5</sub>)<sub>2</sub>(μ-Cl)]<sub>2</sub> using a silver salt of a poorly coordinating anion (AgClO<sub>4</sub>). The first procedure allowed to obtain **1** in one step, but with low yields and impurified with magnesium salts. Although with the second protocol the product can be obtained with high purity from the dimer, the whole procedure is a four-step route with low atom efficiency, as it requires a high excess of LiC<sub>6</sub>F<sub>5</sub> (8:1 vs Ni). Therefore, we envisioned a new synthetic route to prepare **1** (Scheme 1). It was directly obtained in good yields from commercially available [NiX<sub>2</sub>(dme)] (X = Cl, Br) and AgC<sub>6</sub>F<sub>5</sub> in THF at -40 °C. Evaporation, extraction with Et<sub>2</sub>O, and filtration to remove the insoluble silver salts, followed by evaporation to dryness affords **1** as an orange solid with >97% purity.



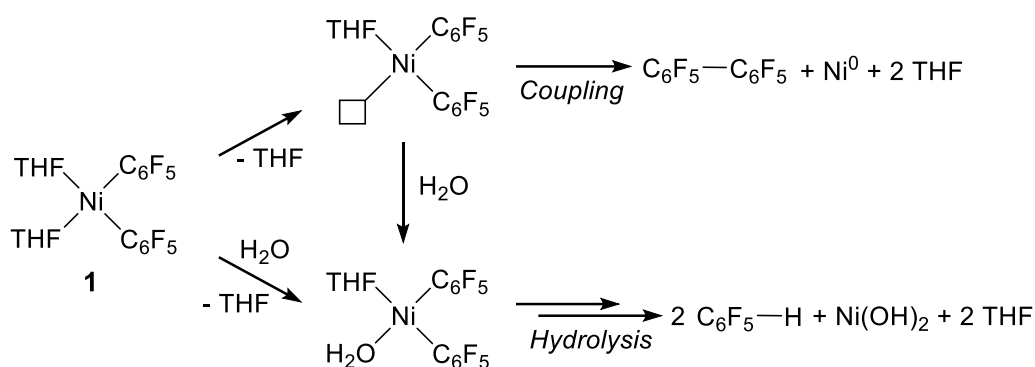
**Scheme 1.** One-step synthesis of *cis*-[Ni(C<sub>6</sub>F<sub>5</sub>)<sub>2</sub>(THF)<sub>2</sub>] (**1**).

While complex **1** is stable in THF solution for a few days, in noncoordinating solvents, it decomposes noticeably quick to a mixture of the coupling product (C<sub>6</sub>F<sub>5</sub>-C<sub>6</sub>F<sub>5</sub>) and the hydrolysis byproduct (C<sub>6</sub>F<sub>5</sub>-H). This is presumably due to easy THF dissociation to form the three-coordinate [Ni(C<sub>6</sub>F<sub>5</sub>)<sub>2</sub>(THF)] that undergoes reductive elimination more quickly than the four-coordinate **1** and competitive substitution to [Ni(C<sub>6</sub>F<sub>5</sub>)<sub>2</sub>(THF)(OH<sub>2</sub>)] followed by hydrolysis (Scheme 2).<sup>10</sup>

<sup>8</sup> Lopez, G.; Garcia, G.; Sanchez, G.; Garcia, J.; Ruiz, J.; Hermoso, J. A.; Vegas, A.; Martinez-Ripoll, M. Hydroxo and azolate derivatives of pentafluorophenyl-nickel(II) complexes. Crystal structure of [NBu<sub>4</sub>]<sub>2</sub>[{Ni-(C<sub>6</sub>F<sub>5</sub>)<sub>2</sub>(μ-OH)}<sub>2</sub>] and [NBu<sub>4</sub>]<sub>2</sub>[{Ni(C<sub>6</sub>F<sub>5</sub>)<sub>2</sub>}(μ-OH)(μ-pyrazolato)]. *Inorg. Chem.*, **1992**, *31*, 1518–1523.

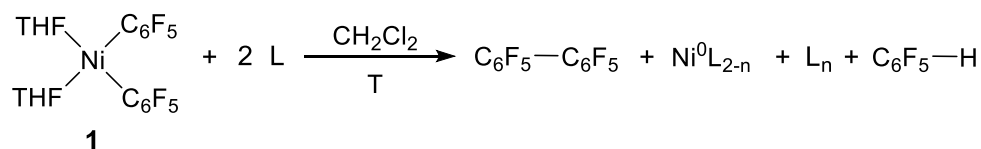
<sup>9</sup> Forniés, J.; Martín, A.; Martín, L. F.; Menjón, B.; Kalamarides, H. A.; Rhodes, L. F.; Day, C. S.; Day, V. W. Synthesis and Characterization of a New Family of Square-Planar Nickel(II) Carbonyl Derivatives. *Chem. - Eur. J.*, **2002**, *8*, 4925–4934.

<sup>10</sup> For hydrolysis by adventitious water see: Casares, J. A.; Espinet, P.; Martínez-Ilarduya, J. M.; Mucientes, J. J.; Salas, G. Study of the replacement of weak ligands on square-planar organometallic nickel(II) complexes. Organo-nickel aqua-complexes. *Inorg. Chem.*, **2007**, *46*, 1027–1032.



**Scheme 2.** Coupling versus Hydrolysis from the Ni<sup>II</sup>-Meter

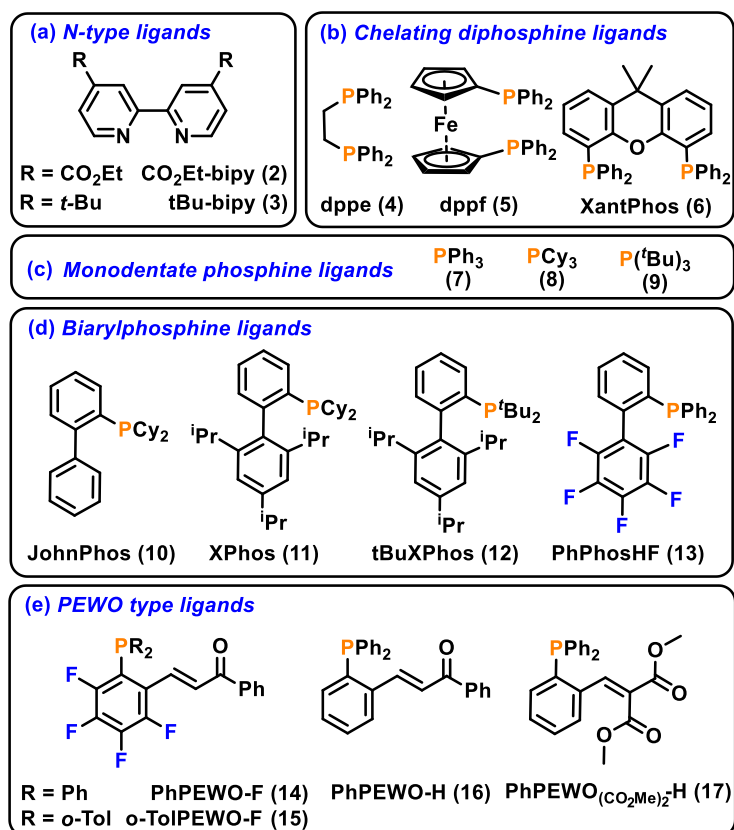
The protocol for the coupling/hydrolysis measurements shown in Scheme 3 (where each L stands for one potentially bidentate ligand or for two monodentate ligands) is as follows: The reactions are carried out in CH<sub>2</sub>Cl<sub>2</sub>, due to the low solubility of **1** in other solvents at low temperature. The reaction progress is monitored by <sup>19</sup>F NMR, checking for product formation. The addition of L is made at low temperature, and the NMR tube is brought to the coupling temperature once the ligand coordination has reached equilibrium. Excess ligand (L/Ni molar ratio: 2:1 for chelating ligands, 4:1 for monodentate ligands) is used to stabilize the reduction product as [Ni<sup>0</sup>L<sub>n</sub>] (n = 2–4 depending on L), in order to prevent initially formed Ni<sup>0</sup> from sequestering a portion of the L needed for full consumption of Ni<sup>II</sup> complex.



**Scheme 3.** Protocol for the coupling vs hydrolysis measurements.

Ni-meter **1** itself undergoes coupling and hydrolysis (Scheme 2) and can be taken as a reference to compare with the ligand added measurements. It immediately reveals much higher hydrolysis:coupling ratio (53:47 mol %) at 25 °C than observed for the equivalent Pd-meter (87:13 mol %).<sup>5</sup> In general, higher participation of hydrolysis is found in Ni compared to Pd for all the tested ligands, consistent with both the more favorable coordination of water to Ni, due to its higher oxophilicity character, and its higher acidity on the harder Ni<sup>II</sup> center than on the softer Pd<sup>II</sup>. A control experiment in the presence of added D<sub>2</sub>O confirmed that the hydrolysis product was enriched in C<sub>6</sub>F<sub>5</sub>-D.

The ligands tested are grouped into five types (Scheme 4): (a) bipyridines; (b) chelating diphosphines; (c) monodentate phosphines; (d) dialkyl biarylphosphines (Buchwald type); and (e) PEWO type ligands (phosphine-EWO ligands). Upon addition of these ligands to **1**, results spanning from formation of totally inert complexes to instantaneous C<sub>6</sub>F<sub>5</sub>-C<sub>6</sub>F<sub>5</sub> coupling, as well as diverse C<sub>6</sub>F<sub>5</sub>-C<sub>6</sub>F<sub>5</sub>:C<sub>6</sub>HF<sub>5</sub> ratios, were observed at 25 °C.



**Scheme 4.** Ligand Types Tested with the Ni<sup>II</sup>-Meter

The bipy ligands (**2** and **3**) immediately form the X-ray characterized *cis*-[Ni(C<sub>6</sub>F<sub>5</sub>)<sub>2</sub>L] chelated complexes (**18** and **19**) (Figure 3, above). Symmetrical diphosphine ligands **4** and **5** also lead to stable *cis*-[Ni(C<sub>6</sub>F<sub>5</sub>)<sub>2</sub>L] chelated complexes **20** and **21**, respectively, which were isolated and X-ray characterized (Figure 3, below). X-ray structures show a square planar geometry at Ni, with the C<sub>6</sub>F<sub>5</sub> moieties in *cis* position imposed by the ligand. As reported by Yamamoto for the *cis*-[Ni(C<sub>6</sub>F<sub>5</sub>)<sub>2</sub>(2,2'-bipy)] complex,<sup>11</sup> coupling on **18–21** does not occur at 25 °C. Moreover, all these complexes are stable not only at 25 °C in CH<sub>2</sub>Cl<sub>2</sub> but also at 80 °C in 1,4-dioxane. These results highlight the difficulty to promote the C<sub>6</sub>F<sub>5</sub>–C<sub>6</sub>F<sub>5</sub> coupling in Ni.

<sup>11</sup> (a) Yamamoto, T.; Yamamoto, A.; Ikeda, S. Organo (dipyridyl) nickel complexes. I. Stability and activation of the alkyl-nickel bonds of dialkyl (dipyridyl) nickel by coordination with various substituted olefins. *J. Am. Chem. Soc.*, **1971**, *93*, 3350–3359; (b) Yamamoto, T.; Yamamoto, A.; Ikeda, S. Organo (dipyridyl) nickel complexes. II. Stabilities of olefin-nickel bonds in olefin-coordinated dipyridylnickel and dialkyl (dipyridyl) nickel complexes. *J. Am. Chem. Soc.*, **1971**, *93*, 3360–3364; (c) Yamamoto, T.; Abila, M. Reductive elimination of Et–Et from NiEt<sub>2</sub>(bpy) promoted by electron-accepting aromatic compounds. *J. Organomet. Chem.*, **1997**, *535*, 209–211.

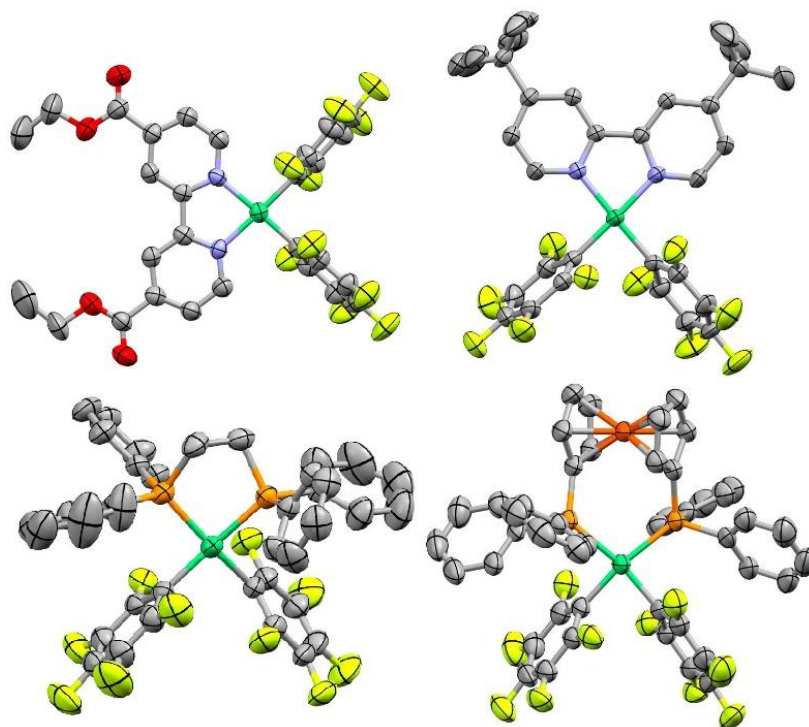


**Figure 3.** Top Left: Ni(C<sub>6</sub>F<sub>5</sub>)<sub>2</sub>(CO<sub>2</sub>Et-bipy) (**18**); Top Right: Ni(C<sub>6</sub>F<sub>5</sub>)<sub>2</sub>(*t*Bu-bipy) (**19**). Bottom Left: Ni(C<sub>6</sub>F<sub>5</sub>)<sub>2</sub>(dppe) · 1/2 CH<sub>2</sub>Cl<sub>2</sub> (**20**); Bottom Right: Ni(C<sub>6</sub>F<sub>5</sub>)<sub>2</sub>(dppf) · *n*-pentane (**21**). All solvent molecules and H atoms omitted for clarity.

The reaction of **1** with Xantphos in CH<sub>2</sub>Cl<sub>2</sub> at 25 °C produced *trans*-chelate complex **22**. Its X-ray diffraction structure confirmed the expectations from the NMR studies, and it is shown in Figure 4. Monitoring of the reaction of **1** with Xantphos at -40 °C showed that *cis*-[Ni(C<sub>6</sub>F<sub>5</sub>)<sub>2</sub>(Xantphos)] (**23**) was initially formed and then isomerized to the thermodynamically favored *trans*-[Ni(C<sub>6</sub>F<sub>5</sub>)<sub>2</sub>(Xantphos)] (**22**) (Scheme 5). This supports that isomerization of the initially formed *cis* complex is considerably faster than coupling even at 25 °C.

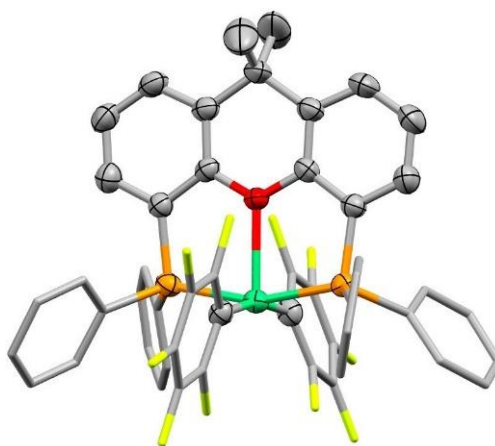
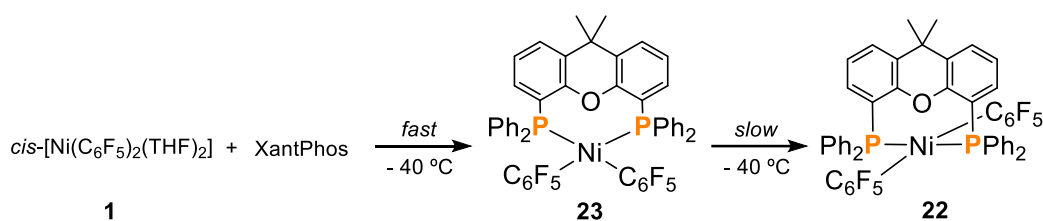


**Figure 4.** X-ray diffraction structure of *trans*-[Ni(C<sub>6</sub>F<sub>5</sub>)<sub>2</sub>(XantPhos)] · toluene (**22**). Solvent molecule and H atoms omitted for clarity.



**Scheme 5.** Reaction sequence observed at  $-40\text{ }^\circ\text{C}$  in the formation of *trans*-[Ni(C<sub>6</sub>F<sub>5</sub>)<sub>2</sub>(XantPhos)] (**22**)

In contrast to the stability of the precedent complexes, coupling (C<sub>6</sub>F<sub>5</sub>–C<sub>6</sub>F<sub>5</sub>) and hydrolysis (C<sub>6</sub>F<sub>5</sub>–H) was observed at  $25\text{ }^\circ\text{C}$  for all the other ligands in Scheme 2 (mainly groups d and e). Some specific reactions with addition of *p*-benzoquinone (bzq) were also carried out. For complex **1**, the reactions in Scheme 1 are sensitive to addition of bzq (Table 1, entry 2 vs. 1). Presumably, the coupling occurs on Ni<sup>II</sup> species with at least one coordinated bzq in equilibrium with free bzq, since broad signals are observed in the Ni-bounded C<sub>6</sub>F<sub>5</sub> region of the <sup>19</sup>F NMR in these reactions. Bzq accelerates the coupling reaction and noticeably improves the coupling/hydrolysis ratio. Consistently, increasing the bzq concentration (entry 3 in Table 1) has a large positive effect on the degree of substitution and on the coupling/hydrolysis ratio.

**Table 1.** Conversion (%) of **1**, and coupling/hydrolysis ratio.

Entry/ L	time	Conversion/ %	(C <sub>6</sub> F <sub>5</sub> ) <sub>2</sub> :C <sub>6</sub> F <sub>5</sub> –H/ %
<b>1</b> / THF	2 h	85	49:51
	4 h	100	47:53
<b>2</b> / bzq (2 eq)	4 h	100	66:34
<b>3</b> / bzq (20 eq)	1.5 h	100	89:11

Monodentate phosphines with different molecular sizes totally replace THF. The small PPh<sub>3</sub> (**7**) and PCy<sub>3</sub> (**8**) form stable *trans*-[Ni(C<sub>6</sub>F<sub>5</sub>)<sub>2</sub>(PR<sub>3</sub>)<sub>2</sub>] complexes **24** and **25**. The *trans* arrangement of the two C<sub>6</sub>F<sub>5</sub> groups prevents reductive elimination. In contrast, the <sup>31</sup>P NMR spectra show that only one molecule of P<sup>*t*</sup>Bu<sub>3</sub> (**9**) can coordinate to the Ni<sup>II</sup> center, producing the reactive *cis*-[Ni(C<sub>6</sub>F<sub>5</sub>)<sub>2</sub>(P<sup>*t*</sup>Bu<sub>3</sub>)] (**26**). Complex **26** undergoes fast evolution at  $25\text{ }^\circ\text{C}$ , mainly to C<sub>6</sub>F<sub>5</sub>H, in less than 2 h (Table 2, entry 1). Since two nonequivalent C<sub>6</sub>F<sub>5</sub> groups are observed in the <sup>19</sup>F NMR spectrum, it cannot be discarded that complex **26** could be [Ni(C<sub>6</sub>F<sub>5</sub>)<sub>2</sub>(P<sup>*t*</sup>Bu<sub>3</sub>)(THF)]. The efficient formation of the hydrolysis product shows that complex **26** allows for easy water coordination and subsequent hydrolysis.

Biarylphosphines **10–13** are very inefficient (entries 2–6, Table 2): It took 6–9.5 h at  $25\text{ }^\circ\text{C}$  to reach 47–77 % conversion in CH<sub>2</sub>Cl<sub>2</sub>, showing slower coupling than hydrolysis with only 20–24% of coupling product (entry 3). The reaction in toluene instead of dichloromethane (entry 4) was not any faster, but it produced a better (still bad) coupling/hydrolysis ratio of 42:58 in 6 h and 59:41 in 9.5 h, possibly due to the lower water content in the toluene. The possible cooperative effect of addition of *p*-benzoquinone (L:bzq = 1:1) was checked with ligand **11**, hoping for a higher rate of the coupling reaction and better protection against hydrolysis, but no improvement was observed (entry 5). Probably, the bulkiness of the ligand prevents bzq approaching to the

Ni center. The less bulky PhPhosHF (**13**) produced a slightly better coupling/hydrolysis ratio, although longer reaction times were necessary.

**Table 2.** Conversion (%) of **1**, and coupling/hydrolysis ratio with bulky ligands.

Entry/ L	time	Conversion/ %	(C <sub>6</sub> F <sub>5</sub> ) <sub>2</sub> :C <sub>6</sub> F <sub>5</sub> -H/ %
1/ 9 <sup>a</sup>	2 h	100	11:89
2/ 10	6 h	78	20:80
3/ 11	6 h	47	29:71
	9.5 h	77	24:76
4/ 11 <sup>a</sup>	6 h	45	42:58
	9.5 h	68	59:41
5/ 11 + bzq	18 h	76	20:80
6/ 12	6 h	83	23:77
7/ 13	28 h	100	40:60

<sup>a</sup> In toluene.

Finally, PEWO ligands **14–17** of group (e) in Scheme 2 were evaluated (Table 3). Their P–olefin chelate coordination in solution is unambiguously confirmed by observation of four nonequivalent *Ortho* signals in their <sup>19</sup>F NMR spectra. PEWO ligands **14–17** show an exceptional performance inducing C<sub>6</sub>F<sub>5</sub>–C<sub>6</sub>F<sub>5</sub> coupling due to the effect of coordination of the EWO olefin moiety.<sup>12</sup> Total conversion of complex **1** at 25 °C occurs just in seconds, rather than hours. Furthermore, the conversion at this temperature affords very predominantly coupling product (82–96 %). To the best of our knowledge, these coupling rates are the fastest ever observed in Ni<sup>II</sup> → Ni<sup>0</sup> reductive elimination processes of this kind and are comparable to related processes taking place at Ni<sup>III</sup> species.<sup>13</sup> In fact, they are too fast to be measured by NMR at 25 °C by applying the initial rates method.

**Table 3.** Conversion (%) of **1** (eq. 2), and coupling/hydrolysis ratio with PEWO ligands.

Entry/ L	time	Conversion/ %	(C <sub>6</sub> F <sub>5</sub> ) <sub>2</sub> :C <sub>6</sub> F <sub>5</sub> -H/ %
1/ 14	< 5 min	100	95:5
2/ 15	< 5 min	100	82:18
3/ 16	< 5 min	100	89:11
4/ 17	< 5 min	100	96:4

The greatly different behavior of PR<sub>2</sub>(biaryl) and PEWO ligands in the Ni-meter, in contrast to their similar behavior in the Pd-meter, must have a structural origin. There is no structural X-ray information available for Ni complexes with PR<sub>2</sub>(biaryl) ligands, and we have not been able to obtain single crystals either. The NMR spectra for these complexes in CH<sub>2</sub>Cl<sub>2</sub>, in Ni/L = 1:2 solutions, always show one equivalent of free L and one coordinated L. In fact, their chemical behavior is very similar to that of P<sup>t</sup>Bu<sub>3</sub>, as the

<sup>12</sup> Pérez-Rodríguez, M.; Braga, A. A. C.; García-Melchor, M.; Pérez-Temprano, M. H.; Casares, J. A.; Ujaque, G.; de Lera, A. R.; Álvarez, R.; Maseras, F.; Espinet, P. C–C Reductive Elimination in Palladium Complexes, and the Role of Coupling Additives. A DFT Study Supported by Experiment. *J. Am. Chem. Soc.*, **2009**, *131*, 3650–3657.

<sup>13</sup> Bour, J. R.; Camasso, N. M.; Meucci, E. A.; Kampf, J. W.; Canty, A. J.; Sanford, M. S. Carbon–Carbon Bond-Forming Reductive Elimination from Isolated Nickel(III) Complexes. *J. Am. Chem. Soc.*, **2016**, *138*, 16105–16111.

hydrolysis product is mainly obtained when they are employed. This suggests that the PR<sub>2</sub>(biaryl) phosphines are behaving as bulky monodentate ligands in the Ni complexes *cis*-[Ni(C<sub>6</sub>F<sub>5</sub>)<sub>2</sub>{PR<sub>2</sub>(biaryl)}] or *cis*-[Ni(C<sub>6</sub>F<sub>5</sub>)<sub>2</sub>{PR<sub>2</sub>(biaryl)}(THF)], allowing for easy coordination of water and subsequent hydrolysis.

In the absence of more detailed experimental information, we performed DFT calculations to evaluate the stabilization of the putative Pd and Ni complexes formed by reaction of one molecule of the ligand JohnPhos (**10**) to complex *cis*-[M(C<sub>6</sub>F<sub>5</sub>)<sub>2</sub>(THF)<sub>2</sub>] (M = Pd and Ni), taking the starting complex in each case as zero energy. The results in Table 4 shows that, in dichloromethane, the displacement of one or the two THF ligands in Pd produces more stable complexes, supporting a chelating coordination of the ligand along the coupling evolution. On the other hand, the calculations show that displacement of one THF is clearly favorable for Ni, but displacement of the second THF molecule results in a species that is even higher in energy than the starting complex. This observation supports a monodentate coordination of JohnPhos, like P<sup>t</sup>Bu<sub>3</sub>, along the process.

**Table 4.** DFT Calculations for the thermodynamic effect of displacing 1 or 2 THF molecules upon addition of ligand **10**.<sup>a</sup>

Compound	$\Delta\Delta G^0$	Compound	$\Delta\Delta G^0$
[Pd(C <sub>6</sub> F <sub>5</sub> ) <sub>2</sub> (THF) <sub>2</sub> ]	0.0	[Ni(C <sub>6</sub> F <sub>5</sub> ) <sub>2</sub> (THF) <sub>2</sub> ]	0.0
[Pd(C <sub>6</sub> F <sub>5</sub> ) <sub>2</sub> (THF)(L)]	-11.8	[Ni(C <sub>6</sub> F <sub>5</sub> ) <sub>2</sub> (THF)(L)]	-6.7
[Pd(C <sub>6</sub> F <sub>5</sub> ) <sub>2</sub> (L)]	-6.6	[Ni(C <sub>6</sub> F <sub>5</sub> ) <sub>2</sub> (L)]	4.5

<sup>a</sup> In CH<sub>2</sub>Cl<sub>2</sub> solution. L = JohnPhos.  $\Delta\Delta G^0$  in kcal x mol<sup>-1</sup>.

With these computational results and considering the overall evidence collected, it is reasonable to propose for each of the ligand/metal pairs the structures in solution depicted in Figure 5. For Pd, the structure in CH<sub>2</sub>Cl<sub>2</sub> solution of the complex with JohnPhos must be **A**. For Ni, the distal aryl would be unable to chelate Ni in competence with the smaller and harder THF (or eventually water), and structure **B** is preferred. Finally, the chelate coordination of PEWO affords structure **C** for the Ni complexes in solution, as it had been previously observed in Pd.<sup>5</sup>

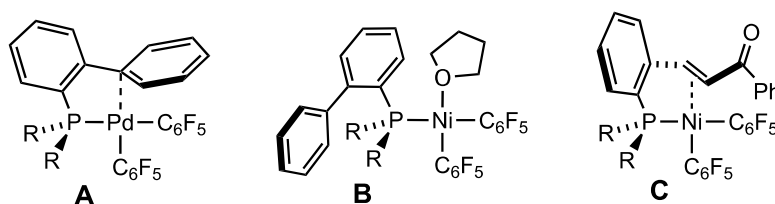


**Figure 5.** Proposed structures for PR<sub>2</sub>(biaryl) and PEWO M(C<sub>6</sub>F<sub>5</sub>)<sub>2</sub> complexes in solution.

It is noteworthy that the coupling power of the PEWO ligands is much higher in Ni than in Pd. Quantitative analysis of the activation barrier for the reductive elimination was carried out. The measured  $\Delta G^\ddagger(\text{C}_6\text{F}_5\text{-C}_6\text{F}_5)_{\text{Ni}}$  barriers at the corresponding experimental temperature required in each case are collected in Table 5, column 4. Additionally, we determined  $\Delta H^\ddagger(\text{C}_6\text{F}_5\text{-C}_6\text{F}_5)_{\text{Ni}}$  and  $\Delta S^\ddagger(\text{C}_6\text{F}_5\text{-C}_6\text{F}_5)_{\text{Ni}}$  for ligand **16** in an experimental variable-temperature study. Assuming that the entropic contribution  $\Delta S^\ddagger(\text{C}_6\text{F}_5\text{-C}_6\text{F}_5)_{\text{Ni}}$  is

unlikely to vary too much from one PEWO ligand to another, a unified comparative scale at 0 °C was also calculated (Table 5, column 5).

**Table 5.** Experimental  $\Delta G^\ddagger(\text{C}_6\text{F}_5\text{-C}_6\text{F}_5)_{\text{Ni}}$  (kcal mol<sup>-1</sup>) for reductive elimination of *cis*-[Ni(C<sub>6</sub>F<sub>5</sub>)<sub>2</sub>(THF)<sub>2</sub>] (**1**) upon addition of PEWO ligands.

Entry/ L	T/ °C	(C <sub>6</sub> F <sub>5</sub> ) <sub>2</sub> :C <sub>6</sub> F <sub>5</sub> -H/ %	$\Delta G^\ddagger$ at T °C	$\Delta G^\ddagger$ at 0 °C
1/ THF	10	61:39	21.9	—
2/ 14	-53	100:0	16.7	17.7
3/ 15	-52	100:0	17.0	18.1
4/ 16	-22	100:0	19.5	19.9
5/ 17	-36	100:0	18.1	18.8

Comparing the data in Table 5 with those at 25 °C, it is clear that lower temperatures increase the conversion times but they also favor higher C<sub>6</sub>F<sub>5</sub>-C<sub>6</sub>F<sub>5</sub>:C<sub>6</sub>F<sub>5</sub>-H ratios. For the PEWO ligands, their reactions are complete in about 8 h and do not show any sign of hydrolysis. The temperature-unified column in Table 5 clearly shows that, the more electron deficient the olefin group is, the faster the couplings are: (i) PEWO-F ligands (**14** and **15**) are faster than PEWO-H ligands (**16** and **17**). (ii) PEWO-F ligand **14** is faster than its PEWO-H homologue **16**. (iii) PEWO-H ligand **17** (with two CO<sub>2</sub>Me substituents) is faster than PEWO-H ligand **16** (with only one C(=O)Ph group). However, contrary to the results obtained for Pd, for Ni PhPEWO-F (**14**) promotes faster reductive eliminations than *o*-TolPEWO-F (**15**), suggesting that bulky R groups on phosphorus can be beneficial in Pd but detrimental in Ni.

In summary, the described protocol allows not only to analyze ligand behavior in Ni-catalyzed reactions, but also how residual water can interfere in these processes. Moreover, the reasons behind the poor performance in Ni of ligands widely employed in Pd are explained. Figure 6 summarizes graphically, for representative ligands, the most significant experimental results of this study.

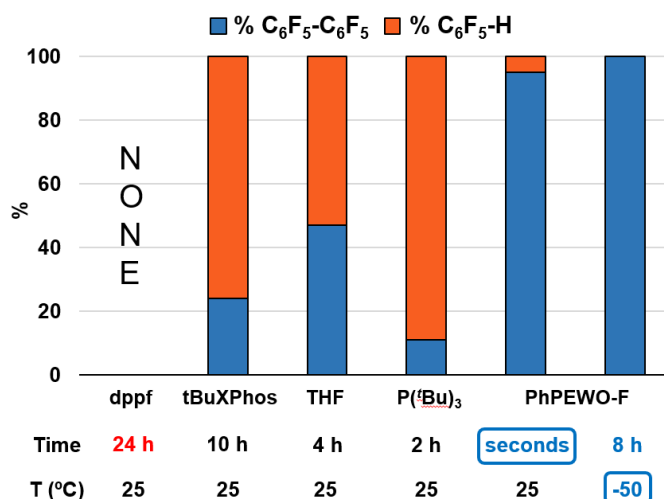


**Figure 6.** L and T dependence of coupling vs hydrolysis.



## Chapter II: New Methodologies for the Selective Synthesis of Highly Fluorinated Biaryls.

In general, cross-coupling reactions may suffer from variable contamination by homocoupling products, due to the operation of undesired transmetalation processes.<sup>1</sup> These are facilitated when Ar<sup>F</sup> groups are involved, due to the slowness of the reductive elimination step. Encouraged by the excellent results obtained for the stoichiometric C<sub>6</sub>F<sub>5</sub>–C<sub>6</sub>F<sub>5</sub> reductive elimination promoted by PEWO ligands shown in Chapter I, we wondered whether this kind of ligands could be employed in a catalytic system preventing the formation of big amounts of side products. Considering the ability of the PEWO ligands to promote the C<sub>6</sub>F<sub>5</sub>–C<sub>6</sub>F<sub>5</sub> coupling, it seemed reasonable to test them in a catalysis where the product would be a highly fluorinated biaryl, be it symmetric or not.

The presence of fluorine atoms tunes the electronic and physicochemical properties of a molecule, compared to its non-fluorinated congener. This has led to an increased use of fluorine containing compounds in several fields, such as pharmaceutical and materials science (Figure 1). However, the degree of fluorination in these molecules can be considered low, since it is rare to observe more than four fluorine atoms in the whole molecule. This fact can be explained by the scarcity of methods to obtain highly fluorinated biaryls.

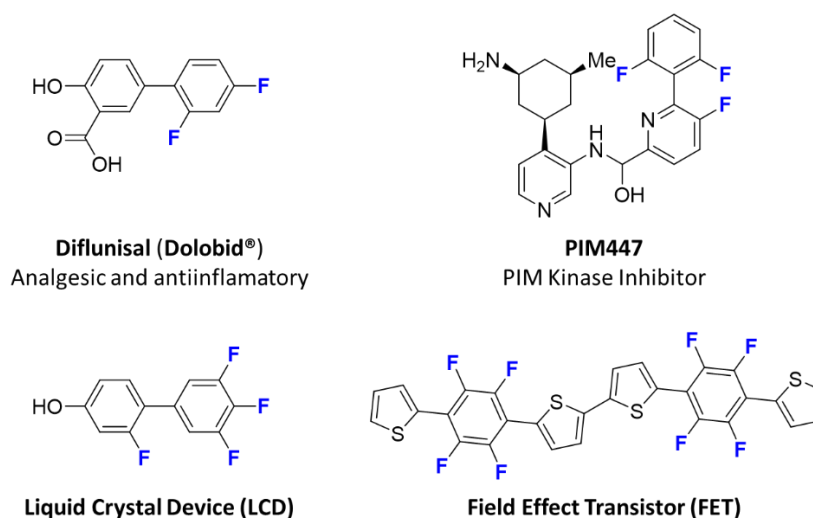


**Figure 1.** Selected molecules with fluorinated biaryl moieties.

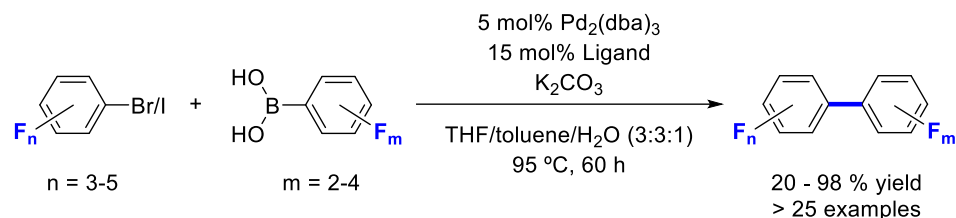
Although there are several catalytic methodologies to access biaryls with one fluorinated aryl,<sup>2</sup> only two examples were found in the literature where both aryls showed a high

<sup>1</sup> del Pozo, J.; Salas, G.; Álvarez, R.; Casares, J. A.; Espinet, P. The Negishi Catalysis: Full Study of the Complications in the Transmetalation Step and Consequences for the Coupling Products. *Organometallics*, **2016**, *35*, 3604–3611.

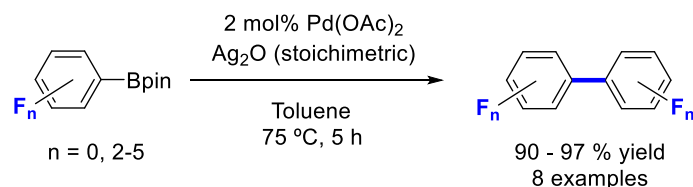
<sup>2</sup> (a) Chen, L.; Francis, H.; Carrow, B. P. An “On-Cycle” Precatalyst Enables Room-Temperature Polyfluoroarylation Using Sensitive Boronic Acids. *ACS Catal.*, **2018**, *8*, 2989–2994; (b) Golding, W. A.; Phipps, R. J. Electrostatically-directed Pd-catalysis in combination with C–H activation: site-selective coupling of remote chlorides with fluoroarenes and fluoroheteroarenes. *Chem. Sci.*, **2020**, *11*, 3022–3027; (c) Wang, J.; Meng, G.; Xie, K.; Li, L.; Sun, H.; Huang, Z. Mild and Efficient Ni-Catalyzed Biaryl Synthesis with Polyfluoroaryl Magnesium Species: Verification of the Arrest State, Uncovering the Hidden Competitive Second Transmetalation and Ligand-Accelerated Highly Selective Monoarylation. *ACS Catal.*, **2017**, *7*, 7421–7430.

fluorination degree (Scheme 1). Firstly, a Suzuki coupling that requires high temperatures and long reaction times (95 °C, 60 h).<sup>3</sup> Moreover, this system provided low yields when both aryls have two fluorine atoms in ortho position, mainly due to a competitive protodeboronation process of the boronic acid,<sup>4</sup> as well as a higher inefficiency in the transmetalation step due to the lower nucleophilicity of these reagents. Indeed, this fact is taken to the extreme with pentafluorophenylboronic acid, (C<sub>6</sub>F<sub>5</sub>)B(OH)<sub>2</sub>, for which no reaction product is obtained at all. Interestingly, in the reaction scope the authors reported the use of a different dialkyl biarylphosphine ligand for each product. On the other hand, the ligandless Pd-catalyzed oxidative homocoupling of fluorinated arylboronates,<sup>5</sup> which takes place under milder conditions compared to the previous method (75 °C, 5h), but the use of a stoichiometric amount of Ag<sub>2</sub>O as oxidant is required and its scope is limited to the synthesis of symmetrical biaryls. The reaction is extremely solvent dependent. While it works great in toluene with yields up to 98%, no product is obtained in acetonitrile, due to the formation of stable *cis*-[Pd(Ar<sup>F</sup>)<sub>2</sub>(NCMe)<sub>2</sub>] complexes. At this point, we hypothesized that the use organozinc reagents as nucleophiles might alleviate the problems associated to boron derivatives in terms of both stability and reactivity.

Huber *et al.*, 2017, Suzuki Coupling



Marder *et al.*, 2020, Oxidative Homocoupling



**Scheme 1.** Literature syntheses of polyfluorinated biaryls.

Based on a successful preliminary test of catalytic synthesis to produce C<sub>6</sub>F<sub>5</sub>-C<sub>6</sub>F<sub>5</sub> from C<sub>6</sub>F<sub>5</sub>-I and Zn(C<sub>6</sub>F<sub>5</sub>)<sub>2</sub> working at 80 °C, with a combination of *trans*-[PdCl<sub>2</sub>(NCMe)<sub>2</sub>] and one equivalent of PhPEWO-F as precatalyst,<sup>6</sup> we decide to explore the feasibility of nickel- and palladium-catalyzed Ar-C<sub>6</sub>F<sub>5</sub> Negishi couplings, employing commercially available Zn(C<sub>6</sub>F<sub>5</sub>)<sub>2</sub> as a nucleophile. This reagent, containing the most fluorinated aryl,

<sup>3</sup> Bulfield, D.; Huber, S. M. Synthesis of Polyfluorinated Biphenyls; Pushing the Boundaries of Suzuki-Miyaura Cross Coupling with Electron-Poor Substrates. *J. Org. Chem.*, **2017**, *82*, 13188–13203.

<sup>4</sup> Cox, P. A.; Reid, M.; Leach, A. G.; Campbell, A. D.; King, E. J.; Lloyd-Jones, G. C. Base-Catalyzed Aryl-B(OH)<sub>2</sub> Protodeboronation Revisited: From Concerted Proton Transfer to Liberation of a Transient Aryl Anion. *J. Am. Chem. Soc.*, **2017**, *139*, 13156–13165.

<sup>5</sup> Budiman, Y. P.; Jayaraman, A.; Friedrich, A.; Kerner, F.; Radius, U.; Marder, T. B. Palladium-Catalyzed Homocoupling of Highly Fluorinated Arylboronates: Studies of the Influence of Strongly vs. Weakly Coordinating Solvents on the Reductive Elimination Process. *J. Am. Chem. Soc.*, **2020**, *142*, 6036–6050.

<sup>6</sup> Gioria, E.; del Pozo, J.; Lledós, A.; Espinet, P. Understanding the Use of Phosphine-(EWO) Ligands in Negishi Cross-Coupling: Experimental and Density Functional Theory Mechanistic Study. *Organometallics*, **2021**, *40*, 2272–2282.

should be a good model for other catalysis employing organozinc derivatives with less polyfluorinated aryls.

The reaction conditions were chosen after some solvent and temperature trials on the highly challenging C<sub>6</sub>F<sub>5</sub>-C<sub>6</sub>F<sub>5</sub> coupling (Eq. 1). The reaction did not work at room temperature and performed poorly at 60 °C. Therefore, it was required a higher temperature for the catalysis to be effective, 80 °C, probably due to the low nucleophilicity of the Zn(C<sub>6</sub>F<sub>5</sub>)<sub>2</sub> reagent. At this temperature, 1,4-dioxane was an efficient solvent, whereas less polar or more coordinating solvents, such as toluene or acetonitrile respectively, were not. Coordination strength of the solvent plays a crucial role. It has been reported that linear ZnR<sub>2</sub> species can accommodate up to 2 molecules of solvent, changing the geometry around the Zn atom to a tetrahedral environment.<sup>7</sup> This geometrical modification enhances the nucleophilicity of the organozinc reagent. In this situation, for an effective transmetalation of the R group, decoordination of one of the solvent molecules is required, in order to form a bimetallic intermediate. This might be the main reason for which the strongly coordinating acetonitrile is not a good solvent in this system. Transmetalation was more efficient for the transfer of the first C<sub>6</sub>F<sub>5</sub> group, which determined the use of a slightly excess of the nucleophile, 1.5 mol of Zn(C<sub>6</sub>F<sub>5</sub>)<sub>2</sub> per mol of C<sub>6</sub>F<sub>5</sub>I. The ligand screening experiments (Table 1) showed that, at a 5% of Ni precatalyst loading, the use of PhPEWO-F (entry 3, >99% yield) makes a drastic difference with other common ligands, such as PPh<sub>3</sub> or XPhos (entries 1 and 2, 0% yield). These results fully agree with the previous observations for the stoichiometric reductive elimination of C<sub>6</sub>F<sub>5</sub>-C<sub>6</sub>F<sub>5</sub> from *cis*-[Ni(C<sub>6</sub>F<sub>5</sub>)<sub>2</sub>(THF)<sub>2</sub>], where PhPEWO-F was extremely effective while PPh<sub>3</sub> and XPhos were not. It was also found that the direct use of the isolable [PdCl<sub>2</sub>(PhPEWO-F)] complex as precatalyst improved the results initially obtained by its *in situ* formation from [PdCl<sub>2</sub>(NCMe)<sub>2</sub>],<sup>6</sup> providing quantitative C<sub>6</sub>F<sub>5</sub>-C<sub>6</sub>F<sub>5</sub> coupling with only 3% of this precatalyst and in shorter reaction times compared to Ni.

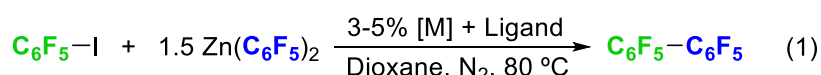


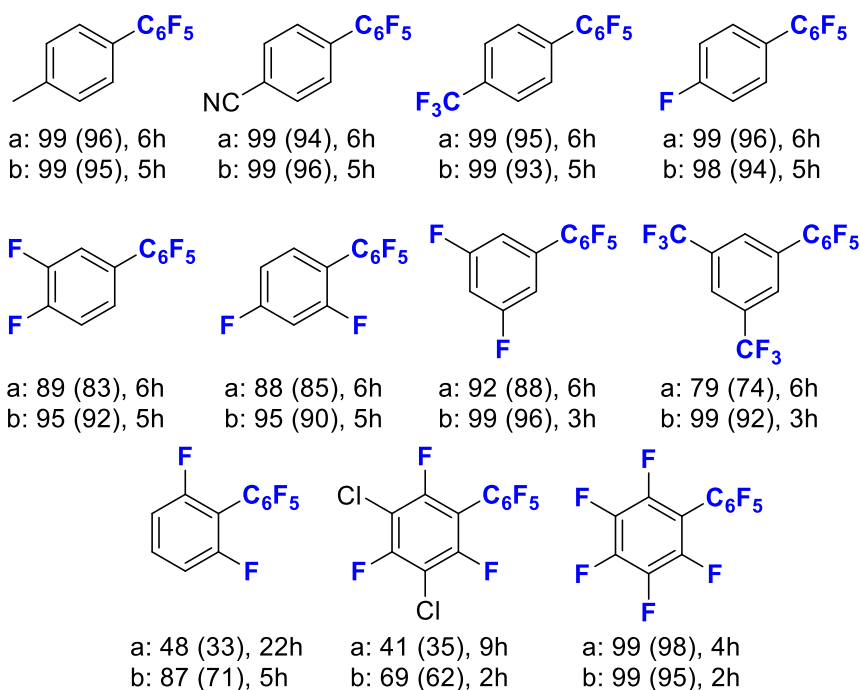
**Table 1.** Preliminary tests of catalytic C<sub>6</sub>F<sub>5</sub>-C<sub>6</sub>F<sub>5</sub> coupling efficiency of PhPEWO-F compared to other phosphines in Ni, and improved results in Pd. [Ni] = [NiCl<sub>2</sub>(NCMe)<sub>2</sub>]; ArI = C<sub>6</sub>F<sub>5</sub>I. [ArI] = 0.05 M.

Entry/Catalyst	[M] %	t/ h	Yield/ %
1/ [Ni] + 2 PPh <sub>3</sub>	5	24	0
2/ [Ni] + 1 XPhos	5	24	0
3/ [Ni] + 1 PhPEWO-F	5	4	>99
4/ [PdCl <sub>2</sub> (PhPEWO-F)]	3	2	>99

These optimized reaction conditions (Table , entries 3 and 4) were then applied to the preparation of the Ar-C<sub>6</sub>F<sub>5</sub> biaryls shown in Scheme 2. The ArI reagent was varied in order to cover a reasonable scope, from para-substituted aryls presumably leading to

<sup>7</sup> del Pozo, J.; Pérez-Iglesias, M.; Álvarez, R.; Lledós, A.; Casares, J. A.; Espinet, P. Speciation of ZnMe<sub>2</sub>, ZnMeCl, and ZnCl<sub>2</sub> in Tetrahydrofuran (THF), and Its Influence on Mechanism Calculations of Catalytic Processes. *ACS Catal.*, **2017**, *7*, 3575–3583.

easier coupling (*p*-Me, *p*-CN, *p*-F, *p*-CF<sub>3</sub>) to others with different and increased F or CF<sub>3</sub> substitution patterns. Monitoring of the catalytic reactions by <sup>19</sup>F NMR provided excellent identification of the conversion efficiency for the starting materials, the F containing products, and the yields in each of them. In all cases, the out-of-cycle initial formation of [M<sup>0</sup>(L)] (L = PhPEWO-F) from the [MCl<sub>2</sub>(L)] precatalyst (3% for Pd, 5% for Ni) produces a small amount of C<sub>6</sub>F<sub>5</sub>-C<sub>6</sub>F<sub>5</sub>, 3 mol% and 5 mol% respectively. Also, a small amount of C<sub>6</sub>HF<sub>5</sub> is formed by reaction of Zn(C<sub>6</sub>F<sub>5</sub>)<sub>2</sub> with the last traces of water in the "dry" solvent. These processes do not alter the reaction outcome due to the excess of Zn(C<sub>6</sub>F<sub>5</sub>)<sub>2</sub> employed in the reaction.



**Scheme 2.** Scope of Ar-C<sub>6</sub>F<sub>5</sub> synthesis comparing Ni (a) and Pd (b) catalysts and different Ar groups. C<sub>6</sub>Cl<sub>3</sub>F<sub>3</sub> was employed as internal standard. Isolated yields in parenthesis.

It is interesting to note that no catalytic intermediates were observed during the reactions, and the consumption of ArI and formation of Ar-C<sub>6</sub>F<sub>5</sub> and other products were simultaneous. This means that all the steps in the catalytic cycle subsequent to the oxidative addition (OA), namely transmetalations (TM), undesired transmetalations (UTM), and reductive eliminations (RE), are faster than OA. Yet, they have their own different rates for each case of aryl group and are consequently determinant of the products composition when more than one product is observed. On the other hand, the very similar catalytic behavior observed for Ni and Pd supports a M<sup>0</sup>/M<sup>II</sup> cycle for both metal centers (Figure 2).

Some significant observations can be made on the results in Scheme 2. For the biphenyls in the first row of Scheme 2, the cross-coupling yields are essentially quantitative. Neither Ar-Ar nor C<sub>6</sub>F<sub>5</sub>-C<sub>6</sub>F<sub>5</sub> (except the 3 or 5% formed in precatalyst activation) are observed. The cross-coupling reaction induced by PhPEWO-F is so much faster than the undesired transmetalations, that these have no chance to compete, and the cross-couplings are fully selective.

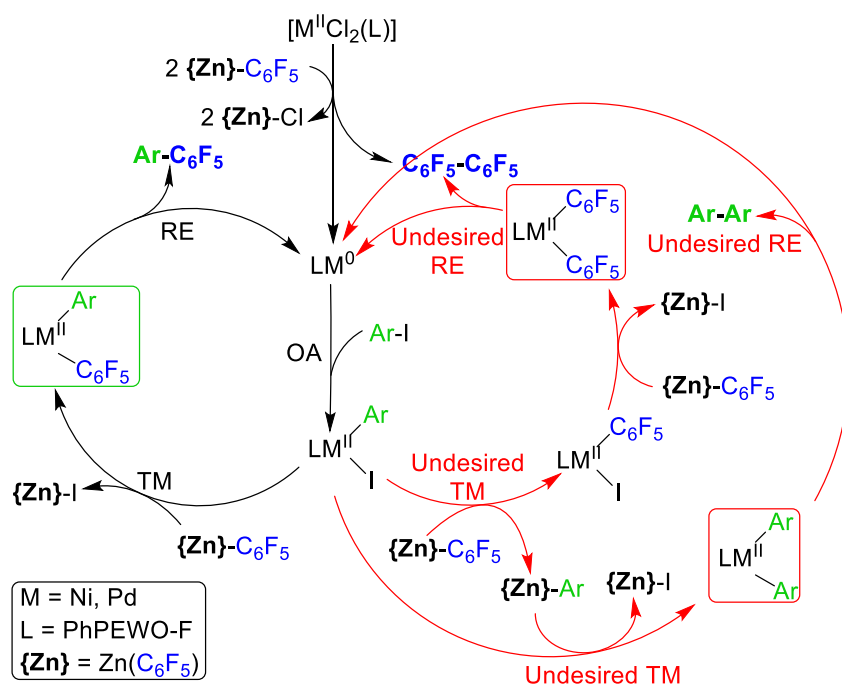


**Figure 2.** Desired (left, in black) and undesired (right, in red) cycles competing in the Ar-C<sub>6</sub>F<sub>5</sub> cross-coupling Negishi process. In addition, ArH and C<sub>6</sub>HF<sub>5</sub> are generated from Ar-{Zn} species after hydrolysis.

However, for the other substrates of Scheme 2, the polarization of the electron density of the aryls, away from C<sub>ipso</sub>, makes the coupling rates from [M(C<sub>6</sub>F<sub>5</sub>)(Ar)(L)] progressively slower. This slowness allows for rate competence of the undesired processes in red in Figure 2, *via* retro-transmetalation to [M(C<sub>6</sub>F<sub>5</sub>)I(L)], and of other exchanges non specified in Figure 2 (e.g. C<sub>6</sub>F<sub>5</sub>/Ar) that lead eventually to the same undesired coupling products.<sup>1</sup> Consequently, other products of the reaction are formed (Table 2). Moreover, this detrimental effect is higher with the more acidic Ni catalyst; the Pd catalyst works significantly better than Ni in all cases, showing higher selectivity to the cross-coupling and shorter reaction times, although the results with Ni are still very satisfactory, with only one case with yield lower than 85 %.

**Table 2.** Products observed for reactions (Eq. 1) at the times indicated in Scheme 1, given in mol%.

Entry/ Ar	Cat.	ArI	ArC <sub>6</sub> F <sub>5</sub>	Ar <sub>2</sub>	ArH <sup>a</sup>	(C <sub>6</sub> F <sub>5</sub> ) <sub>2</sub>
1/ 3,4-C <sub>6</sub> H <sub>3</sub> F <sub>2</sub>	[Ni]+L	9	89	0	2	6
2/ 2,4-C <sub>6</sub> H <sub>3</sub> F <sub>2</sub>	[Ni]+L	1	88	8	3	9
3/ 3,5-C <sub>6</sub> H <sub>3</sub> F <sub>2</sub>	[Ni]+L	0	92	6	2	8
4/ 3,5-C <sub>6</sub> H <sub>3</sub> (CF <sub>3</sub> ) <sub>2</sub>	[Ni]+L	0	79	16	5	12
5/ 3,4-C <sub>6</sub> H <sub>3</sub> F <sub>2</sub>	[Pd]	5	95	0	0	4
6/ 2,4-C <sub>6</sub> H <sub>3</sub> F <sub>2</sub>	[Pd]	4	95	0	1	3
7/ 3,5-C <sub>6</sub> H <sub>3</sub> F <sub>2</sub>	[Pd]	0	>99	0	0	3
8/ 3,5-C <sub>6</sub> H <sub>3</sub> (CF <sub>3</sub> ) <sub>2</sub>	[Pd]	0	>99	0	0	3

<sup>a</sup> ArH comes from the Ar groups trapped as Ar-{Zn} at the end of the reaction and is obtained and measured after hydrolysis.

For the two cross-coupling products of the third row, involving compounds with two F atoms in the 2,6 positions, the cross-coupling selectivity lowers more significantly, although it is still very high for Pd (87% and 69% respectively) compared to Ni (48% and 41%) (Table 3). As expected, the presence of F atoms in 2,6 positions produces the highest polarization of the  $C_{\text{ipso}}$  electron density and the slowest coupling rates and, consequently, the highest incidence of undesired transmetalations and couplings. The significant formation of  $C_6F_5-C_6F_5$  and Ar-Ar in the mixtures confirms this effect. Due to the reversibility of all the transmetalations, the aryl groups have the opportunity to re-enter the catalytic cycle from Ar-{Zn}, but not from irreversible undesired Ar-Ar homocoupling products. This can eventually affect seriously its concentration and its activity as nucleophile, to the point that full conversion of ArI may not be achieved, as in the two reactions with Ar = 2,6- $C_6H_3F_2$  in Table 3.

**Table 3.** Products observed for reactions (Eq. 1) at the times indicated in Scheme 1, given in mol%.

Entry/ Ar	Cat.	ArI	ArC <sub>6</sub> F <sub>5</sub>	Ar <sub>2</sub> <sup>a</sup>	ArH <sup>b</sup>	(C <sub>6</sub> F <sub>5</sub> ) <sub>2</sub> <sup>a</sup>
1/ 2,6- $C_6H_3F_2$	[Ni]+L	7	48	13	19	24
2/ 2,4,6- $C_6Cl_2F_3$	[Ni]+L	0	41	10	39	28
3/ 2,6- $C_6H_3F_2$	[Pd]	8	87	0.5	4	5
4/ 2,4,6- $C_6Cl_2F_3$	[Pd]	0	69	8	16	20
5/ $C_6F_5$	[Ni]+L	0	–	–	– <sup>c</sup>	>99 <sup>d</sup>
6/ $C_6F_5$	[Pd]	0	–	–	– <sup>c</sup>	>99 <sup>e</sup>

<sup>a</sup> For Ar and  $C_6F_5$  groups balance to 100 these molar number have to be multiplied by 2. <sup>b</sup> ArH comes from the Ar groups trapped as Ar-{Zn} at the end of the reaction and is obtained and measured after hydrolysis. <sup>c</sup> Cannot be measured because all the hydrolysis product of Ar-{Zn} is  $C_6HF_5$  in this case. <sup>d</sup> A total of 105 mol% could be produced. <sup>e</sup> A total of 103 mol% could be produced.

In catalysis focused on Ar-Ar homocouplings, the desired and undesired transmetalations in the cycle of Figure 2 (which presumably are operative although they are undetectable), as well as the precatalyst activation, lead all to the same product, Ar-Ar. The irreversible formation of  $C_6F_5-C_6F_5$  is, for the cross-couplings catalysis studied here, a sterile source of consumption of  $Zn(C_6F_5)_2$  but, in catalytic reactions oriented to homocoupling (last two entries of Table 3),  $C_6F_5-C_6F_5$  is the wanted product. In this situation, the Ni system recovers full conversion of the starting materials, although still at longer reaction times than Pd (4 h for Ni, 2 h for Pd). Thus, Negishi homocoupling with PhPEWO-F as coupling promoter ligand is able to produce quantitative conversion to  $C_6F_5-C_6F_5$  in short reaction times. From the reactions studied, only 2,6- $C_6H_3F_2$ -2,6- $C_6H_3F_2$  and  $C_6Cl_2F_3-C_6Cl_2F_3$  couplings look comparable in difficulty to  $C_6F_5-C_6F_5$ , and any other Ar-Ar homocouplings should be even faster. Consequently, the catalytic synthesis of Ar<sup>F</sup>-Ar<sup>F</sup> through Negishi homocouplings, exemplified by  $C_6F_5-C_6F_5$  in this study, is a reasonable alternative to the previously reported use of boronic acids or boronates in combination with stoichiometric  $Ag_2O$  as oxidant of the  $Pd^0$  catalyst.<sup>5</sup>

Finally, with the percentages of catalyst tested, we have observed, mainly for Ni, some cases of uncomplete conversion of ArI (9% at most). These are, of course, due to catalyst decomposition. The easily observed formation of a red product in the reaction media supports the formation of a highly unreactive  $Ni^0$  species, which has been eventually

identified as  $[\text{Ni}^0(\text{PhPEWO-F})_2]$ . This complex was independently synthesized and fully characterized, including its X-ray diffraction structure (Figure 3).<sup>8</sup> The two ligands are coordinated to the Ni atom in a chelating fashion, both by the P atom and the olefin moiety. Thus, the Ni atom is fully enveloped in a tetrahedral environment and inaccessible to the reagents. Indeed, when this complex was employed as precatalyst, no conversion of the starting materials was observed at all, supporting its identification as a highly stable off-cycle species.

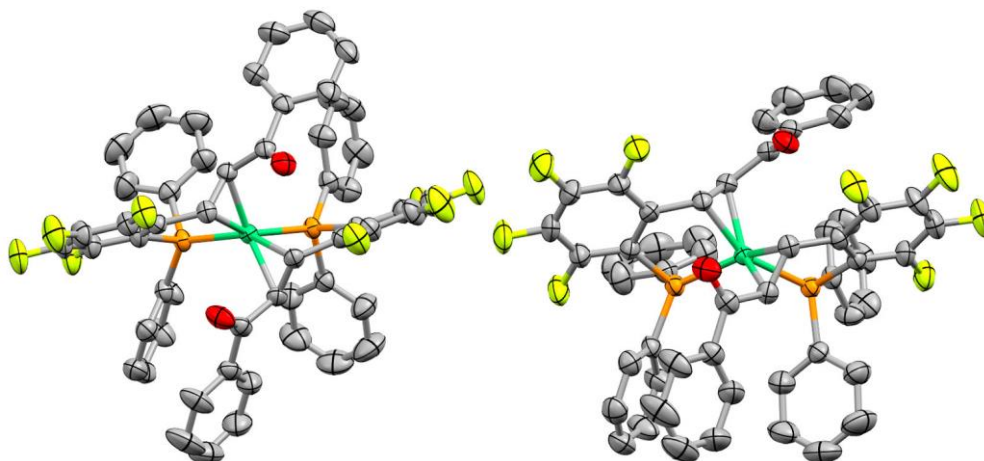
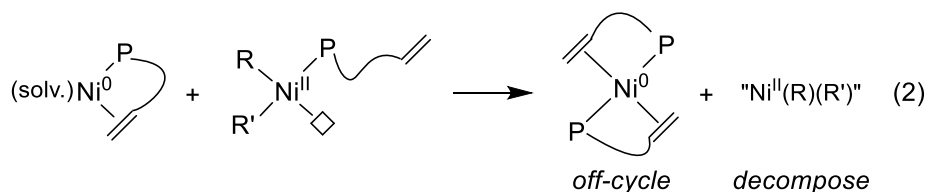


**Figure 3.** Two views of the distorted tetrahedral X-ray molecular structure of  $[\text{Ni}(\text{PhPEWO-F})_2]$ .

A plausible mechanistic interpretation of the catalytic differences observed for Ni and Pd is that the worse performance of Ni at 80 °C, in contrast with it being more efficient than Pd at very low temperatures, is due to the higher lability of  $\text{Ni}^{\text{II}}$ -olefin bonds, which can induce a higher percentage of olefin decoordination at 80 °C than for Pd. This lability can be explained with the higher acidic character of  $\text{Ni}^{\text{II}}$  compared to  $\text{Pd}^{\text{II}}$ . Moreover, the use of a quite acidic fluorinated PEWO ligand and poorly donor fluorinated aryls does not help to lower this acidic character. Since coupling promotion requires chelating coordination of PhPEWO-F (remember the inefficiency of  $\text{PPh}_3$  in Table , entry 1) the  $\text{Ni}^{\text{II}}$ -olefin lability explains the much lower performance of PhPEWO-F as coupling promoter in Ni at high temperature, and also higher catalyst decomposition from P-monodentate intermediates (Eq. 2).

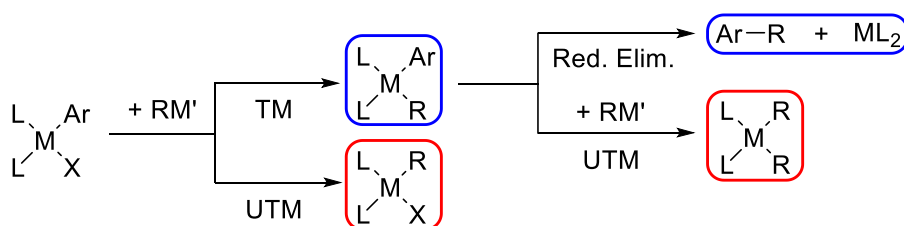


The results obtained for the Negishi cross-coupling of fluorinated aryls with PhPEWO-F as ligand show total selectivity toward the product when the two aryls to couple are dissimilar enough, with full conversion of the aryl iodide in most cases. However, when the aryl iodide is electronically similar to  $\text{C}_6\text{F}_5$ , such as 2,6-difluoroiodobenzene, the

<sup>8</sup> A similar product  $[\text{Pd}^0(\text{PhPEWO-F})_2]$  has already been reported for Pd. See reference 6.

selectivity lowers, obtaining higher amounts of homocoupling and hydrolysis byproducts. In addition, this loss of selectivity is more marked when Ni was employed than with Pd.

These byproducts are formed by different undesired Ar/C<sub>6</sub>F<sub>5</sub> transmetalations (UTM) that can take place during the catalysis (Scheme 3). Firstly, an Ar/ C<sub>6</sub>F<sub>5</sub> exchange between the oxidative addition complex [M(Ar)X(L)] and the nucleophile Zn(C<sub>6</sub>F<sub>5</sub>)<sub>2</sub>, generating [M(C<sub>6</sub>F<sub>5</sub>)X(L)] and Zn(Ar)(C<sub>6</sub>F<sub>5</sub>), instead of the desired C<sub>6</sub>F<sub>5</sub>/X transmetalation. Secondly, an Ar/C<sub>6</sub>F<sub>5</sub> exchange prior to reductive elimination at the [M(Ar)(C<sub>6</sub>F<sub>5</sub>)(L)] complex, producing [M(C<sub>6</sub>F<sub>5</sub>)<sub>2</sub>(L)]. ArH byproduct is formed from Zn(Ar)(C<sub>6</sub>F<sub>5</sub>) hydrolysis, while homocoupling Ar–Ar byproduct is generated after subsequent transmetalations of Zn(Ar)(C<sub>6</sub>F<sub>5</sub>) with the catalyst.



**Scheme 3.** Unwanted transmetalations leading to byproducts (circled in red) (R = C<sub>6</sub>F<sub>5</sub>).

In order to reduce these parasite reactions, different strategies can be carried out. The selectivity in the transmetalation step can be enhanced with the choice of an appropriate nucleophile for which the Ar/X exchange is preferred over the Ar/Ar' UTM. To reduce the UTM at the [M(Ar)(Ar')(L)] complex, reductive elimination should be kinetically favored over the UTM. This goal can be achieved by two approaches. Ligand promotion of the reductive elimination step, as shown previously with PEWO ligands, and reducing the amount of nucleophile employed by its *in situ* generation. The latter option would enhance the rate ratio toward reductive elimination, as it is a unimolecular step, while transmetalations are, at least, bimolecular.

Our research group has previously worked with bimetallic systems involving two transition metals. This methodology has been applied to the cross-coupling of aryls with bulky substituents, be it in a Pd/Au system with arylstannanes,<sup>9</sup> or in a Pd/Cu system with aryl silanes.<sup>10</sup> The ability of organocopper species to transmetalate the organic moiety to palladium has been exploited in several catalysis.<sup>11</sup> Moreover, some copper complexes can perform C–H activation of acidic protons and allow *in situ* generation of the corresponding copper nucleophile in low concentration.<sup>12</sup> Hence, we considered that a Pd/Cu bimetallic system, employing aryl halides and fluorinated arenes with an acidic proton as substrates, might reduce the formation of byproducts in the synthesis of highly

<sup>9</sup> del Pozo, J.; Carrasco, D.; Pérez-Temprano, M. H.; García-Melchor, M.; Álvarez, R.; Casares, J. A.; Espinet, P. Stille Coupling Involving Bulky Groups Feasible with Gold Cocatalyst. *Angew. Chem., Int. Ed.*, **2013**, *52*, 2189–2193.

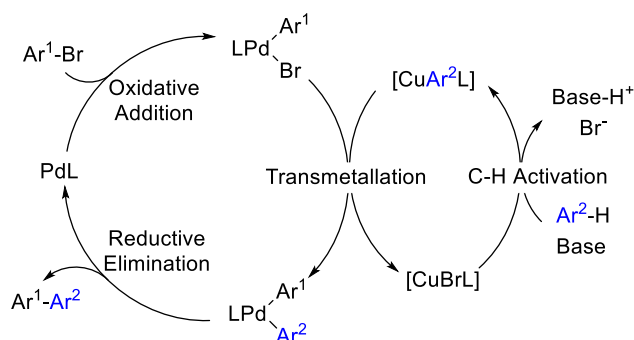
<sup>10</sup> del Pozo, J.; Casares, J. A.; Espinet, P. In Situ Generation of ArCu from CuF<sub>2</sub> Makes Coupling of Bulky Aryl Silanes Feasible and Highly Efficient. *Chem. - Eur. J.*, **2016**, *22*, 4274–4284.

<sup>11</sup> (a) Wu, Y.; Huo, X.; Zhang, W. Synergistic Pd/Cu Catalysis in Organic Synthesis. *Chem. - Eur. J.* **2020**, *26*, 4895–4916; (b) Kim, U. B.; Jung, D. J.; Jeon, H. J.; Rathwell, K.; Lee, S.-g. Synergistic Dual Transition Metal Catalysis. *Chem. Rev.*, **2020**, *120*, 13382–13433.

<sup>12</sup> Fortman, G. C.; Slawin, A. M. Z.; Nolan, S. P. A Versatile Cuprous Synthon: [Cu(IPr)(OH)] (IPr = 1,3-Bis(Diisopropylphenyl)Imidazol-2-Ylidene). *Organometallics*, **2010**, *29*, 3966–3972.

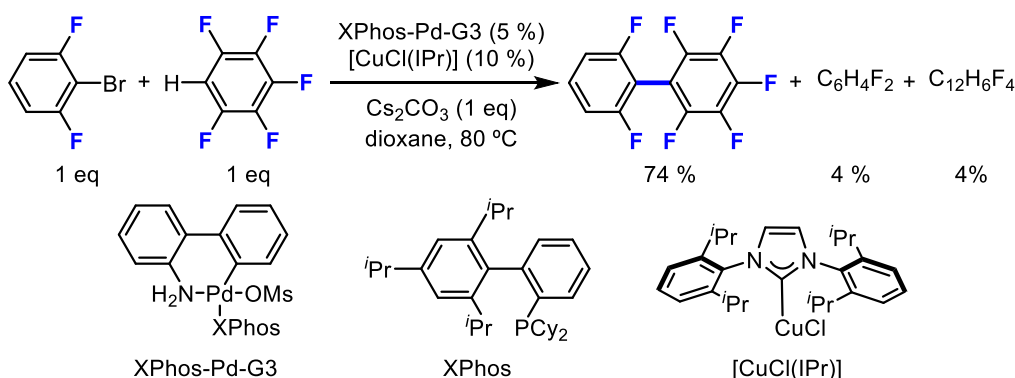


fluorinated biaryls (Scheme 4). A similar process has been previously evaluated by Cazin *et al.* by using Pd and Cu precatalysts with NHC ligands on both metals.<sup>13</sup>



**Scheme 4.** Mechanism for the Pd/Cu bimetallic cross-coupling between aryl bromides and arenes containing an acidic proton.

Initially, we essayed a system similar to the one used by Cazin group,<sup>13</sup> using [Pd(allyl)Cl(IPr)] and [CuCl(IPr)] as co-catalysts for the cross-coupling of 1-Br-2,6-C<sub>6</sub>H<sub>3</sub>F<sub>2</sub> (**1a**) as fluorinated aryl electrophile and C<sub>6</sub>HF<sub>5</sub> (**2n**) as precursor of the Cu nucleophile. Cs<sub>2</sub>CO<sub>3</sub> was employed as base. However, no cross-coupling biaryl product was formed and only C<sub>6</sub>F<sub>5</sub>-allyl from Pd precatalyst activation was detected. This frustrating result suggests that the C–H activation by the copper catalyst and the Cu-to-Pd transmetalation steps are working, but the carbene ligand on Pd is not efficient to promote the reductive elimination of two highly fluorinated aryls and generate the palladium cycle. Therefore, we carried out a systematic study of the reaction looking for ligands and Pd precatalysts that could favor a productive cycle in palladium, and copper precatalysts and bases compatible with them. The precatalysts XPhos-Pd-G3 (5 %) and [CuCl(IPr)] (10 %) combined with Cs<sub>2</sub>CO<sub>3</sub> as base, at 80 °C, gave the best yield (74 %) of the cross-coupling product **3an** (Scheme 5). Along with the desired cross-coupling product **3an**, very small amounts of the hydrolysis product 1,3-difluorobenzene (**4a**, 4%) and the homocoupling biaryls of both aryls (**3aa**, 4% and **3nn**, 3%) were identified by <sup>19</sup>F NMR.



**Scheme 5.** Preliminary experiments for precatalysts choice. [ArBr] = 0.08 M.

Other reaction conditions were tested (Table 4). When the amount of copper precatalyst was reduced to a half, the yield dropped significantly (entry 2). This result is consistent

<sup>13</sup> Lesieur, M.; Lazreg, F.; Cazin, C. S. A Cooperative Pd–Cu System for Direct C–H Bond Arylation. *Chem. Commun.*, **2014**, 50, 8927–8929.

with the nature of the bimetallic catalysis, where the transmetalation step involves both catalyst. Thus, if this step is too slow, it may lead to decomposition of the catalysts. The use of less bulky ligands in copper lead to a very low yield, presumably due to ligand exchange between Pd and Cu catalysts (entry 3).<sup>14</sup> Once a carbene ligand is accommodated in the Pd, the catalysis does not work, as discussed before. On the other hand, the use of the bulkier tBuXPhos, which is an excellent promoter of C<sub>6</sub>F<sub>5</sub>–C<sub>6</sub>F<sub>5</sub> coupling in Pd,<sup>15</sup> also reduced the yield of the reaction (entry 4). In this case, the problem is a conflict of bulky ligands at both metals, where the transmetalation step becomes more difficult as the bulkiness of the ligand at Pd increases. The use of acetonitrile as reaction solvent was again detrimental and no coupling product was observed (entry 5). Other bases did not improve the yield (entries 6 and 7). When <sup>t</sup>BuONa was employed, activation of the fluorine atom of C<sub>6</sub>F<sub>5</sub> in para position was observed. The catalysis proceeded similarly when an aryl chloride was employed instead of an aryl bromide (entry 8). Finally, increasing the concentration in the system improved the yield, up to an 84 %, keeping the selectivity of the process intact (entry 9).

**Table 4.** Screening of optimized reaction conditions.

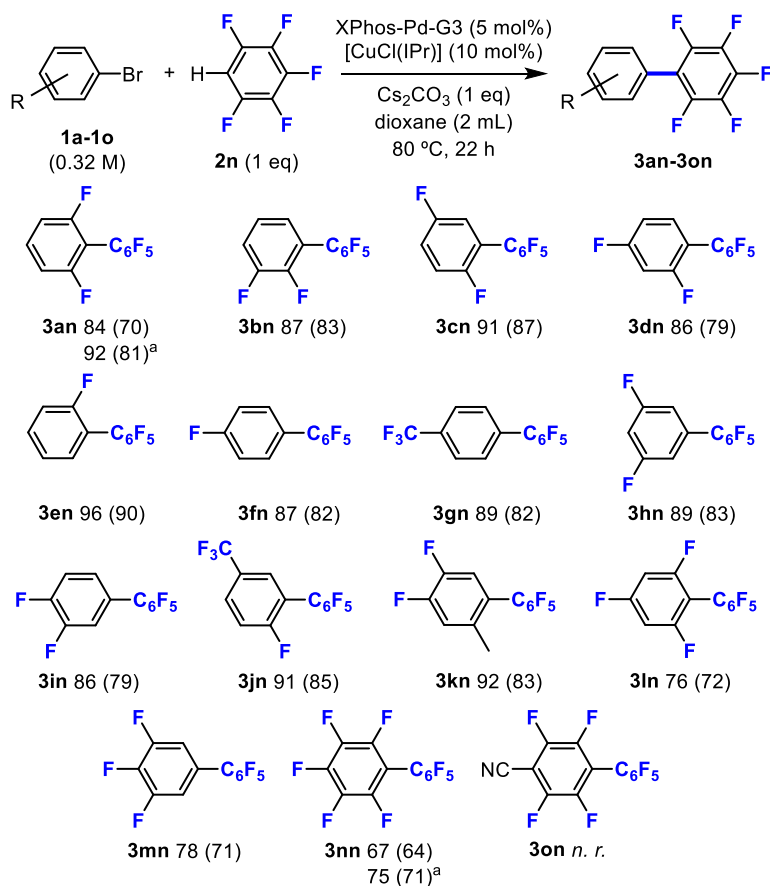
Entry	Variation of conditions	3an yield/ % <sup>a</sup>
1	None	74
2	5 mol% [Cu] instead of 10 mol% [Cu]	6
3	[CuCl(IDm)] instead of [CuCl(IPr)]	2
4	tBuXPhos-Pd-G3 instead of XPhos-Pd-G3	27
5	Acetonitrile as solvent	<i>n. r.</i>
6	CsOH as base	55
7	<sup>t</sup> BuONa as base	17
8	ArCl instead of ArBr	70
9	[ArBr] = 0.32 M instead of 0.08 M	84

<sup>a</sup> Yields determined by <sup>19</sup>F NMR employing  $\alpha,\alpha,\alpha$ -trifluorotoluene as internal standard.

The scope of the reaction was evaluated first for different bromoaryls (**1a-1o**) with C<sub>6</sub>H<sub>5</sub>F<sub>5</sub> (**2n**) as nucleophile source (Scheme 6). The protocol is very efficient for mono-, di- and trifluorinated aryl bromides, affording yields in the range 75–90 % (**3an-3mn**), and almost 70 % yield for the C<sub>6</sub>F<sub>5</sub>–C<sub>6</sub>F<sub>5</sub> coupling (**3nn**). The higher yields obtained for the less fluorinated aryl bromides are presumably due to a faster reductive elimination compared to that for C<sub>6</sub>F<sub>5</sub>–C<sub>6</sub>F<sub>5</sub>. Small amounts of homocoupling and hydrolysis products were detected in all cases (< 4%). Alkyl or fluoroalkyl substituents at the bromoaryl ring, such as Me (**3kn**) and CF<sub>3</sub> (**3gn** and **3jn**), are compatible with this synthetic protocol. In contrast, the presence of a nitrile moiety blocks the reaction and no coupling product is observed (**3on**). This quenching is probably due to coordination of the nitrile to some metal intermediates and is in good agreement with the previous experiment that discarded acetonitrile as reaction solvent. In some selected cases we also employed 1.5 eq of **2n**, which resulted in an improved yield of the catalysis (**3an** and **3nn**).

<sup>14</sup> Furst, M. R. L.; J. Cazin, C. S. Copper N-heterocyclic carbene (NHC) complexes as carbene transfer reagents. *Chem. Commun.*, **2010**, 46, 6924–6925.

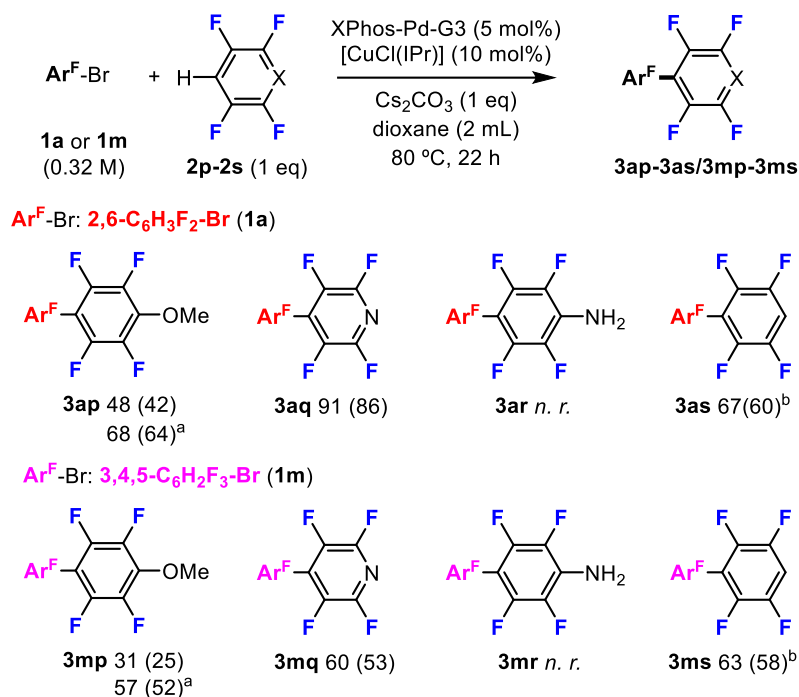
<sup>15</sup> Gloria, E.; del Pozo, J.; Martínez-Ilarduya, J. M.; Espinet, P. Promoting Difficult Carbon-Carbon Couplings: Which Ligand Does Best? *Angew. Chem., Int. Ed.*, **2016**, 55, 13276–13280.



**Scheme 6.** Fluoroaryl bromide scope. Yield determined by <sup>19</sup>F NMR. Isolated yield in parenthesis. <sup>a</sup> 1.5 eq of C<sub>6</sub>H<sub>5</sub>F (**2n**).

Then, we examined the compatibility of different fluoroarenes (Scheme 7). The formation of the CuAr<sup>F</sup> intermediates in the presence of base should be efficient for the tetrafluorinated reagents **2p-2s**, since they all have an Ar<sup>F</sup>-H bond with enhanced acidity. Their catalytic reactions with two electrophiles, 2,6-C<sub>6</sub>H<sub>3</sub>BrF<sub>2</sub> (**1a**) and 3,4,5-C<sub>6</sub>H<sub>2</sub>BrF<sub>3</sub> (**1m**) were studied in order to observe possible effects on the catalysis. The examples studied show that the biphenyl yield is very sensitive to the coordinative strength of the substituents in the **2p-2s** reagent, supporting that in some cases they hamper the Pd cycle probably at the transmetalation step, and their donor strength, that modulates the Ar<sup>F</sup>-H bond acidity: NH<sub>2</sub> quenches their two reactions due to the strong N-coordination ability (as discussed above for the nitrile group);<sup>16</sup> in contrast, 2,3,5,6-tetrafluoropyridine gives very high yields of **3aq** or **3mq** because of the well-known fact that the donor ability of the N electron pair of this tetrafluoropyridine is practically inexistent; in the middle, OMe leads to lower yields of **3ap** and **3mp**, due to a weaker OMe coordination ability compared to NH<sub>2</sub> but higher compared to **2q**. Again, the use of a slight excess of **2p** increased the yield of the products.

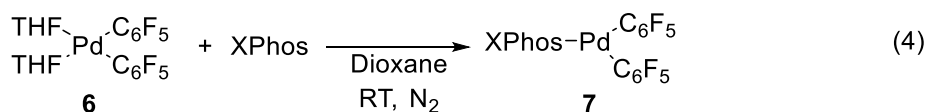
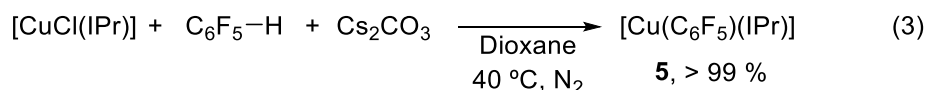
<sup>16</sup> The possible Buchwald-Hartwig amination product was not detected either and only the starting material was recovered.



**Scheme 7.** Fluoroarenes scope. Yield determined by <sup>19</sup>F NMR. Isolated yield in parenthesis. <sup>a</sup> 1.5 eq of **2p** were used. <sup>b</sup> 3.0 eq of **2s** were used.

For 1,2,4,5-tetrafluorobenzene (**2s**), with two acidic C–H bonds, there was competition of mono- and diarylated products. A big excess of the arene **2s** (3 eq) was necessary to diminish the formation of the diarylated product, and monoarylated product (**3as** or **3ms**) was obtained in 67 % and 63 % molar yield respectively. Yet, full conversion of the aryl bromide was observed and the diarylated product was still formed in 33 % yield. This observation highlights that, in the absence of coordinating groups, the cross-coupling process is very efficient.

In order to understand the relevance of the different catalytic steps of the system, some stoichiometric experiments were carried out. The C–H activation of C<sub>6</sub>HF<sub>5</sub> by [CuCl(IPr)] in the presence of Cs<sub>2</sub>CO<sub>3</sub> yields [Cu(C<sub>6</sub>F<sub>5</sub>)(IPr)] (**5**) in almost quantitative yield in two hours at 40 °C (eq. 3). The 1:1 addition of XPhos to *cis*-[Pd(C<sub>6</sub>F<sub>5</sub>)<sub>2</sub>(THF)<sub>2</sub>] (**6**) at room temperature in 1,4-dioxane affords [Pd(C<sub>6</sub>F<sub>5</sub>)<sub>2</sub>(XPhos)] (**7**) (eq. 4) as a moderately stable compound in solution, in contrast to its *t*BuXPhos analogue that easily decomposes at room temperature to C<sub>6</sub>F<sub>5</sub>–C<sub>6</sub>F<sub>5</sub> and [Pd<sup>0</sup>(L)].<sup>15</sup> Its <sup>31</sup>P NMR shows one signal at 27.8 ppm and the <sup>19</sup>F NMR shows six signals, three for each C<sub>6</sub>F<sub>5</sub> ring, due to the inequivalence of both aryls. This suggest a κ<sup>2</sup>-P,C chelating coordination of the XPhos ligand.



Complex **7** was isolated at room temperature as a colorless solid and its X-ray diffraction structure was elucidated (Figure 4). In agreement with the NMR spectra, the structure

shows a P,C-chelating coordination of XPhos, involving predominantly C1 of the distal ring (the Kochi hapticity of this interaction is  $h = 1.37$ ).<sup>17</sup> The most remarkable structural aspect of **7** is the small C2-Pd-C3 angle ( $82.3^\circ$ ) forced by the crowding with the biaryl phosphine. This forced angle shortens the distance between C2 and C3 to 2.69 Å, reducing the activation energy for Aryl-Aryl reductive elimination.

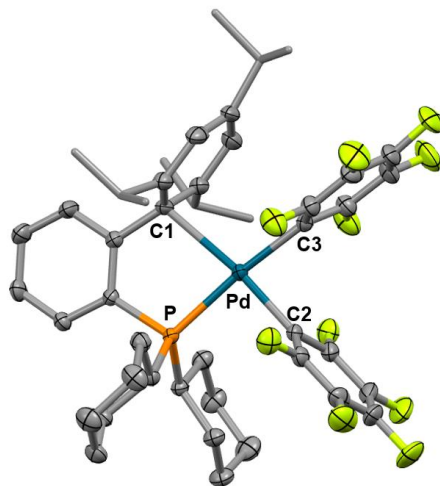
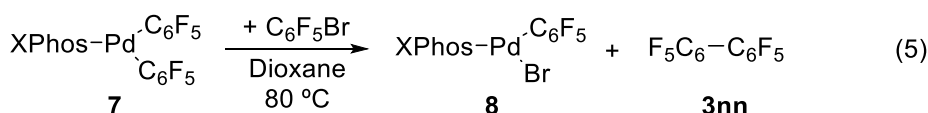


**Figure 4.** X-ray structure of *cis*-[Pd(C<sub>6</sub>F<sub>5</sub>)<sub>2</sub>(XPhos)] (**7**). H atoms omitted for clarity. Selected bond distances (Å) and angles (°): Pd–P = 2.328, Pd–C1 = 2.478, Pd–C2 = 2.013, Pd–C3 = 2.080. P–Pd–C1 = 81.58, P–Pd–C2 = 91.72, C2–Pd–C3 = 82.32, C1–Pd–C3 = 104.32. Pd–C distances to the two distal ring atoms *ortho* to C1 = 2.784, 3.002.

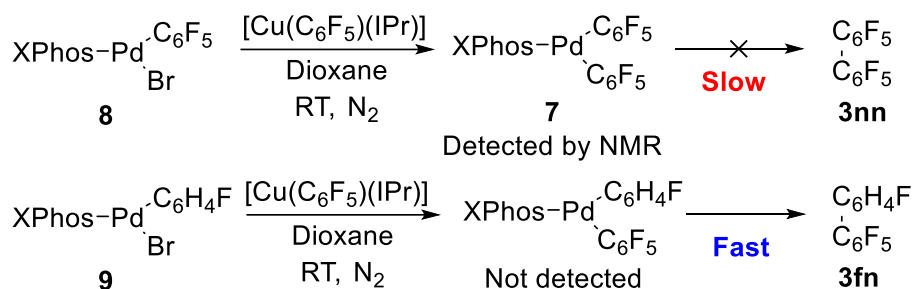
When a solution of **7** in dioxane was heated at 80 °C in the presence of C<sub>6</sub>F<sub>5</sub>–Br, reductive elimination of C<sub>6</sub>F<sub>5</sub>–C<sub>6</sub>F<sub>5</sub> followed by instantaneous oxidative addition to the *in situ* generated [Pd<sup>0</sup>(XPhos)] complex (the Pd<sup>0</sup> complex was never observed) was complete in 180 min, generating [PdBr(C<sub>6</sub>F<sub>5</sub>)(XPhos)] (**8**) (eq. 5). At room temperature, **8** shows an equilibrium in solution between monomer and halogen bridged dimers [Pd(μ-Br)(C<sub>6</sub>F<sub>5</sub>)(XPhos)]<sub>2</sub>, giving rise to broadening of its <sup>19</sup>F and <sup>31</sup>P NMR signals.



Interestingly, a close inspection of the <sup>19</sup>F NMR monitoring of the catalytic experiments, using C<sub>6</sub>F<sub>5</sub>–Br (**1n**) and C<sub>6</sub>HF<sub>5</sub> (**2n**) as reagents, led to the identification of the NMR signals of [Cu(C<sub>6</sub>F<sub>5</sub>)(IPr)] (**5**) and [Pd(C<sub>6</sub>F<sub>5</sub>)<sub>2</sub>(XPhos)] (**7**) in the reaction mixture. This suggests that, when **1n** and **2n** are employed as reagents, the reductive elimination at Pd is the slowest transformation in the catalytic cycle. Finally, the transmetalation/reductive elimination sequence was also evaluated for C<sub>6</sub>F<sub>5</sub>–C<sub>6</sub>F<sub>5</sub> (**3nn**) and *p*-C<sub>6</sub>H<sub>4</sub>F–C<sub>6</sub>F<sub>5</sub> (**3fn**) couplings, by following the reactivity of [Cu(C<sub>6</sub>F<sub>5</sub>)(IPr)] (**5**) with the oxidative addition complexes [PdBr(C<sub>6</sub>F<sub>5</sub>)(Xphos)](**8**) or [PdBr(*p*-C<sub>6</sub>H<sub>4</sub>F)(Xphos)] (**9**) in dioxane at room

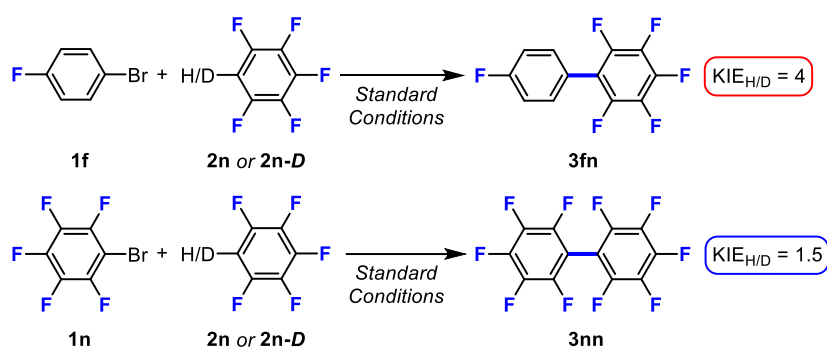
<sup>17</sup> (a) Vasilyev, A. V.; Lindeman, S. V.; Kochi, J. K. Noncovalent Binding of the Halogens to Aromatic Donors. Discrete Structures of Labile Br<sub>2</sub> Complexes with Benzene and Toluene. *Chem. Commun.*, **2001**, 909–910; (b) Ogawa, K.; Kitagawa, T.; Ishida, S.; Komatsu, K. Synthesis and Structure of a New Tetrakis(pentafluorophenyl)borate Salt of the Silver(I) Cation with Novel Trigonal Planar Tris(benzene) Coordination. *Organometallics*, **2005**, *24*, 4842–4844.

temperature (Scheme 8). The reaction of **8** with **5** at room temperature did not produce the biaryl product (**3nn**), but full conversion to Pd biaryl complex **7** in four hours. Obviously, the reductive elimination is much slower than the transmetalation for these highly fluorinated reagents. In contrast, when **5** and **9** were mixed at room temperature the reaction took place in two hours, and only the coupling product (**3fn**) was detected along the reaction, showing that in this case, with one little fluorinated aryl, the reductive elimination is much faster than the transmetalation.



**Scheme 8.** Transmetalation studies.

This analysis of the transmetalation/reductive elimination in stoichiometric conditions and at room temperature may not have direct translation to the catalytic conditions at 80 °C due to the different concentrations of the catalytic species and reagents. We know from the stoichiometric results that the transmetalations are fast for both reactions at room temperature, so they must be very fast at 80 °C. Moreover, for Pd, the transformation of [Pd<sup>0</sup>(XPhos)] to [Pd(Aryl)Br(XPhos)] can be considered complete and instantaneous.<sup>18</sup> For Cu, however, the [Cu(C<sub>6</sub>F<sub>5</sub>)(IPr)] concentration depends on a deprotonation equilibrium of aryl-H, which is influencing the Cu availability at the transmetalation and, consequently, the rate of this step. Information about the influence of the arene deprotonation step in the transmetalation/reductive elimination process could be obtained from KIE experiments with C<sub>6</sub>F<sub>5</sub>-H/D. To this end, we conducted KIE experiments with **1f** or **1n** under catalytic conditions (Scheme 9).<sup>19</sup>



**Scheme 9.** KIE experiments. Standard conditions as in Scheme 6.

<sup>18</sup> Wagschal, S.; Perego, L. A.; Simon, A.; Franco-Espejo, A.; Tocqueville, C.; Albaneze-Walker, J.; Jutand, A.; Grimaud, L. Formation of XPhos-Ligated Palladium(0) Complexes and Reactivity in Oxidative Additions. *Chem. - Eur. J.*, **2019**, *25*, 6980–6987.

<sup>19</sup> KIE values were determined as the ratio of product formation between the deuterated and protic reagents in separated vessels: Simmons, E. M.; Hartwig, J. F. On the Interpretation of Deuterium Kinetic Isotope Effects in C-H Bond Functionalizations by Transition Metal Complexes. *Angew. Chem., Int. Ed.*, **2012**, *51*, 3066–3072.

With *p*-C<sub>6</sub>H<sub>4</sub>BrF (**1f**) a KIE value of  $\approx 4$  was obtained, indicating that the C–H activation is largely determinant on the overall reaction rate. In contrast, with C<sub>6</sub>BrF<sub>5</sub> (**1n**) the KIE value is  $\approx 1.5$ , which, along with the NMR detection of the intermediate Pd biaryl complex **7**, supports that reductive elimination is the slowest step in this occasion. This is an extreme example of difficult cross-coupling but, in less clear cases with fast oxidative addition, the KIE experiments can determine which step, reductive elimination or C–H activation, is more rate determining.

In conclusion, two complementary protocols for the synthesis of symmetric and asymmetric biaryls fluorinated at one or the two aryls have been developed. Highly fluorinated species, such as C<sub>6</sub>F<sub>5</sub>–C<sub>6</sub>F<sub>5</sub> or C<sub>6</sub>Cl<sub>2</sub>F<sub>3</sub>–C<sub>6</sub>F<sub>5</sub>, are easily obtained by Ni- or Pd-catalysed Negishi processes using the chelating ligand PhPEWO-F in M:L = 1:1 ratio. This ligand facilitates fast and selective coupling even for highly fluorinated aryls, and allows for general application, fairly mild conditions, short reaction times and unusually high cross-coupling selectivity of alike fluorinated aryls, particularly with the Pd catalyst.

In addition, the bimetallic Pd/Cu system allows to employ commercially available Ar<sup>F</sup>–H active reagents, avoiding a previous step of nucleophile preparation. The choice of ligands for Pd and Cu is crucial for the good outcome of the reaction, since all the steps in the mechanism can be limiting for the overall reaction rate. The access to different precursors and the remarkable selectivity of this catalytic bimetallic system, preventing unwanted transmetalations to avoid homocoupling side-reactions, is a very valuable addition and complementary to the PEWO method, giving access to the use of additional commercial reagents (Ar–Cl and Ar–Br instead of Ar–I electrophiles, Ar<sup>F</sup>–H active instead of Ar<sup>F</sup>–M active nucleophile precursors) and to higher cross-coupling selectivity in difficult cases of aryls with efficient undesired transmetalations.





### Chapter III: Synthesis and Evaluation as Precatalysts of cis-[PdR<sub>2</sub>(L)<sub>n</sub>] Complexes (R = Partially Fluorinated Aryl).

The development of new Pd-catalyzed processes has had a great impact in synthetic methodologies, specially in the last two decades.<sup>1</sup> In parallel, the design of new Pd precatalysts has been crucial for the good outcome of some of these reactions, which may not succeed employing classic precatalysts such as PdCl<sub>2</sub>, Pd(OAc)<sub>2</sub> and Pd<sub>2</sub>(dba)<sub>3</sub>.<sup>2</sup> Among the Pd<sup>II</sup> sources, two of them stand out. PEPPSI precatalysts have been proven as an excellent platform for carbene ligands (Figure 1, left);<sup>3</sup> while L-Pd-G3 precatalysts (Figure 1, middle),<sup>4</sup> where L is a phosphine ligand, have become widely employed due to their high stability and ease of synthesis, even at multigram scale. Recently, an air stable Pd<sup>0</sup> complex, <sup>DMP</sup>DAB-Pd-MAH (Figure 1, right), was found to be an extremely active precatalyst, due to the ease of DAB ligand substitution.<sup>5</sup>

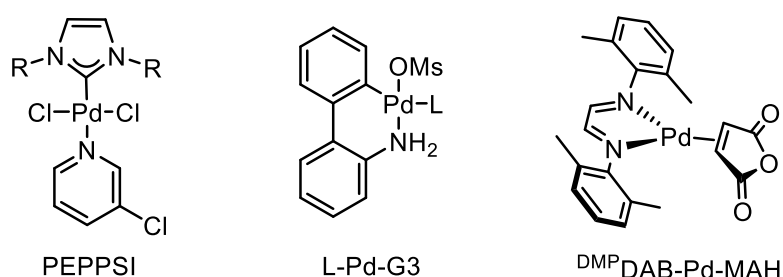


**Figure 1.** Selected rationally designed Pd precatalyst.

Although these three types of precatalysts are very effective, their design shows some disadvantages that may go unnoticed. Pd<sup>II</sup> precatalysts require reduction to Pd<sup>0</sup> active species, and this process is carried out at the cost of one of the reagents in the catalysis, mainly the nucleophile or the base. Moreover, the activation product may not be innocent at all and interfere with the active catalyst species. This is the case of L-Pd-G3, where a reactive carbazole is produced during precatalyst activation. On the other hand, the Pd<sup>0</sup> precatalyst <sup>DMP</sup>DAB-Pd-MAH release N,N'-diaryldiazabutadiene and maleic anhydride.

<sup>1</sup> (a) Johansson Seechurn, C. C. C.; Kitching, M. O.; Colacot, T. J.; Snieckus, V. Palladium-Catalyzed Cross-Coupling: A Historical Contextual Perspective to the 2010 Nobel Prize. *Angew. Chem. Int. Ed.*, **2012**, *51*, 5062–5085; (b) Wu, X. F.; Anbarasan, P.; Neumann, H.; Beller, M. From Noble Metal to Nobel Prize: Palladium-Catalyzed Coupling Reactions as Key Methods in Organic Synthesis. *Angew. Chem. Int. Ed.*, **2010**, *49*, 9047–9050; (c) Ruiz-Castillo, P.; Buchwald, S. L. Applications of Palladium-Catalyzed C–N Cross-Coupling Reactions. *Chem. Rev.*, **2016**, *116*, 12564–12649.

<sup>2</sup> (a) Li, H.; Johansson Seechurn, C. C. C.; Colacot, T. J. Development of Preformed Pd Catalysts for Cross-Coupling Reactions, Beyond the 2010 Nobel Prize. *ACS Catal.*, **2012**, *2*, 1147–1164; (b) Hazari, N.; Melvin, P. R.; Beromi, M. M. Well-defined nickel and palladium precatalysts for cross-coupling. *Nat. Rev. Chem.*, **2017**, *1*, 0025.

<sup>3</sup> Froese, R. D. J.; Lombardi, C.; Pompeo, M.; Rucker, R. P.; Organ, M. G. Designing Pd–N-Heterocyclic Carbene Complexes for High Reactivity and Selectivity for Cross-Coupling Applications. *Acc. Chem. Res.*, **2017**, *50*, 2244–2253.

<sup>4</sup> Bruno, N. C.; Tudge, M. T.; Buchwald, S. L. Design and Preparation of New Palladium Precatalysts for C–C and C–N Cross-Coupling Reactions. *Chem. Sci.*, **2013**, *4*, 916–920.

<sup>5</sup> Huang, J.; Isaac, M.; Watt, R.; Becica, J.; Dennis, E.; Saidaminov, M. I.; Sabbers, W. A.; Leitch, D. C. <sup>DMP</sup>DAB-Pd-MAH: A Versatile Pd(0) Source for Precatalyst Formation, Reaction Screening, and Preparative-Scale Synthesis. *ACS Catal.*, **2021**, *11*, 5636–5646.

The latter is a highly electron deficient olefin and, consequently, can have a great impact in the catalysis.<sup>6</sup>

These observations prompted us to synthesize Pd complexes that could act as precatalysts, avoiding the problems previously observed. Ideally, the Pd precatalyst should be an on-cycle species with the appropriate ligand coordinated. Hence, an oxidative addition complex of the type [PdRX(L)] would be an excellent choice, as long as the R group employed is the same one as the electrophile that would be oxidatively added to Pd during the catalysis. However, if the R group is different, activation of the precatalyst would consume one equivalent of the nucleophile. In addition, the evaluation of a reaction scope would require synthesizing in advance every [PdRX(L)] complex for each electrophile to be tested, which would make the whole process tedious and highly time consuming.

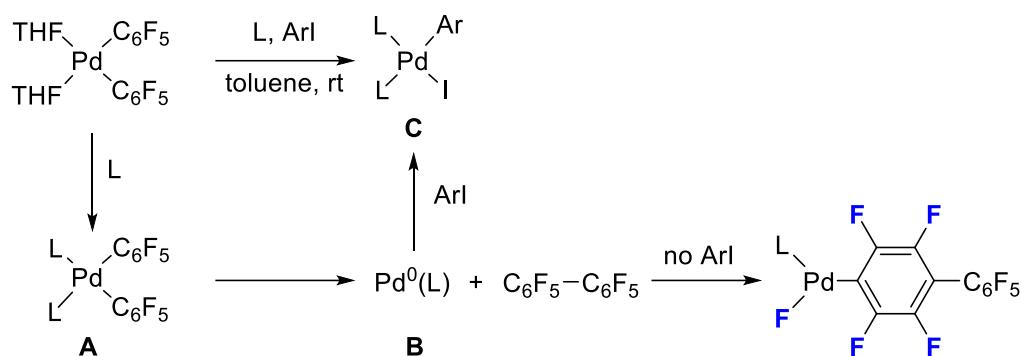
For these reasons, a much better alternative would be the use of [PdRR'(L)] complexes, that would enter the cycle as [Pd<sup>0</sup>(L)] species after reductive elimination. This ideal complex should meet some requisites to be considered an effective general precatalyst. Firstly, it should be an easy to prepare and handle complex. Secondly, reductive elimination of the R and R' groups should take place under mild conditions, so that the precatalyst can be employed in several systems and the active species is formed in short times. Finally, the stabilizing ligand L should be easily displaced by the added ligand, in order to avoid any side reaction under the catalytic conditions. For a proper evaluation of the formation rate of the [Pd<sup>0</sup>(L)] species, which are sometimes quite unstable, stoichiometric experiments trapping them as stable oxidative addition complexes [PdRX(L)] can be carried out.

Previously, our group employed the complex *cis*-[Pd(C<sub>6</sub>F<sub>5</sub>)<sub>2</sub>(THF)<sub>2</sub>] to rank the ability of different phosphine ligands to promote difficult couplings by measuring the rate of the C<sub>6</sub>F<sub>5</sub>–C<sub>6</sub>F<sub>5</sub> reductive elimination (Scheme 1).<sup>7</sup> Firstly, fast THF ligand substitution was observed for the wide range of phosphine ligands evaluated (monocoordinating, chelating, hemilabile, etc.). Then, depending on the phosphine employed, either a stable [Pd(C<sub>6</sub>F<sub>5</sub>)<sub>2</sub>(L)<sub>n</sub>] complex would be formed, or reductive elimination of C<sub>12</sub>F<sub>10</sub> would take place. Interestingly, when tBuXPhos was evaluated, C–F bond activation of coupling product decafluorobiphenyl was observed. Consequently, to obtain an accurate measure, it was necessary to add an ArI to trap the highly active [Pd<sup>0</sup>(tBuXPhos)] species formed after reductive elimination as the oxidative addition complex [Pd(*p*-C<sub>6</sub>H<sub>4</sub>F)IL]. Hence, this study not only allowed to measure the ability of different ligands to promote reductive elimination, but also highlighted that *cis*-[Pd(C<sub>6</sub>F<sub>5</sub>)<sub>2</sub>(THF)<sub>2</sub>] could be employed as an efficient precursor of [Pd(Ar)X(L)] complexes with Buchwald-type biarylphosphines.

---

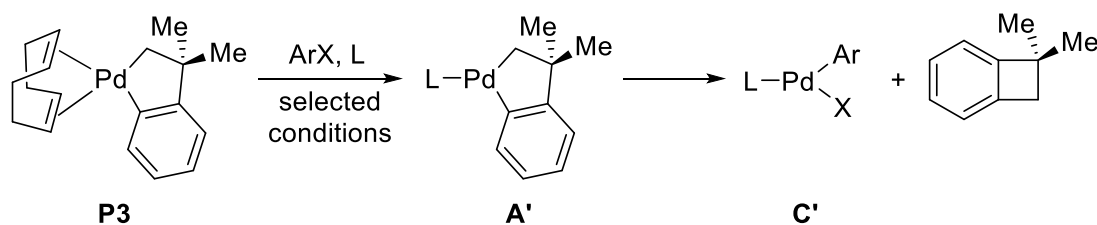
<sup>6</sup> Electron withdrawing olefins can facilitate couplings, a frequently ignored positive effect, but also difficult oxidative additions, due to the strong  $\pi$  back-donation from Pd<sup>0</sup>. Pérez-Rodríguez, M.; Braga, A. C.; García-Melchor, M.; Pérez-Temprano, M. H.; Casares, J. A.; Ujaque, G.; de Lera, A. R.; Álvarez, R.; Maseras, F.; Espinet, P. C–C Reductive Elimination in Palladium Complexes, and the Role of Coupling Additives. A DFT Study Supported by Experiment. *J. Am. Chem. Soc.*, **2009**, *131*, 3650–3657.

<sup>7</sup> Gioria, E.; del Pozo, J.; Martínez-Ilarduya, J. M.; Espinet, P. Promoting Difficult Carbon-Carbon Couplings: Which Ligand Does Best? *Angew. Chem., Int. Ed.*, **2016**, *55*, 13276–13280.



**Scheme 1.** Reactivity and reaction pathways of *cis*-[Pd(C<sub>6</sub>F<sub>5</sub>)<sub>2</sub>(THF)<sub>2</sub>] upon addition of ligands and ArI (ArI = *p*-IC<sub>6</sub>H<sub>4</sub>F).

Recently, Buchwald group has reported a methodology to obtain Pd oxidative addition complexes bearing biarylphosphine ligands, with a similar strategy to ours.<sup>8</sup> They evaluated three different *cis*-[PdR<sub>2</sub>(COD)] complexes as possible candidates: [Pd(CH<sub>2</sub>TMS)<sub>2</sub>(COD)] (**P1**), [Pd(C<sub>6</sub>H<sub>2</sub>F<sub>3</sub>)<sub>2</sub>(COD)<sub>2</sub>] (**P2**) and a neophyl palladacycle [Pd(CH<sub>2</sub>CMe<sub>2</sub>-*o*-C<sub>6</sub>H<sub>4</sub>)(COD)] (**P3**). Both **P1** and **P2** gave moderately good results in the formation of oxidative addition complexes. However, they were discarded in the study; **P1** due to its low thermal stability and **P2** because it did not work properly with the bulkiest ligands. On the other hand, **P3** was considered an appropriate precursor and its reaction with several ligands in the presence of different aryl (pseudo)halides was tested, some of them being pharmaceutical targets. The reaction, shown in Scheme 2, afforded the oxidative addition products in a 54 to 99 % yield range, depending on the reagents and conditions employed.



**Scheme 2.** Reported synthesis of Pd oxidative addition complexes from **P3**.

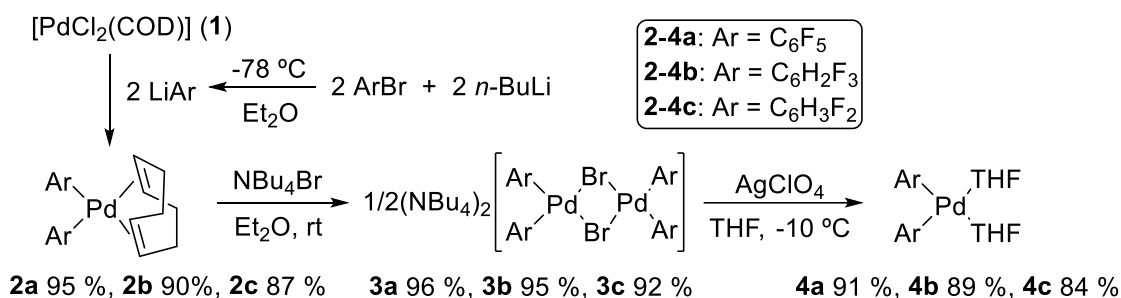
#### *Synthesis and stability of cis*-[Pd(Ar<sup>F</sup>)<sub>2</sub>(COD)] and *cis*-[Pd(Ar<sup>F</sup>)<sub>2</sub>(THF)<sub>2</sub>] complexes

With these two precedents, we considered the evaluation as potential [Pd<sup>0</sup>(L)] precursors of different *cis*-[Pd(Ar<sup>F</sup>)<sub>2</sub>(L)<sub>n</sub>] complexes, bearing partially fluorinated aryls and labile ancillary ligands, namely THF and COD (one of them being **P2** from Buchwald report). *cis*-[Pd(Ar<sup>F</sup>)<sub>2</sub>(THF)<sub>2</sub>] complexes (**4a-c**) are obtained after a 3-step synthesis (Scheme 3).<sup>9</sup> The preparation of these complexes starts with the double arylation of [PdCl<sub>2</sub>(COD)] (**1**) with LiAr<sup>F</sup> salts to give *cis*-[Pd(Ar<sup>F</sup>)<sub>2</sub>(COD)] (Ar<sup>F</sup> = C<sub>6</sub>F<sub>5</sub> (**2a**), 2,4,6-C<sub>6</sub>H<sub>2</sub>F<sub>3</sub>, (**2b**); 2,6-C<sub>6</sub>H<sub>3</sub>F<sub>2</sub>, (**2c**)). Then, COD displacement by addition of a slight excess of (NBu<sub>4</sub>)Br

<sup>8</sup> King, R. P.; Krska, S. W.; Buchwald, S. L. A Neophyl Palladacycle as an Air- and Thermally Stable Precursor to Oxidative Addition Complexes. *Org. Lett.*, **2021**, *23*, 7927–7932.

<sup>9</sup> Espinet, P.; Martínez-Illarduya, J. M.; Pérez-Briso, C.; Casado, A. L.; Alonso, M. A. 3,5-Dichlorotrifluorophenyl complexes, aryl derivatives with simple <sup>19</sup>F NMR structural probes. The synthesis of general precursors for Pd- and Pt complexes. *J. Organomet. Chem.*, **1998**, *551*, 9–20.

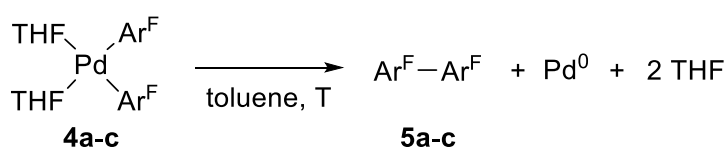
gives the dimeric species (NBu<sub>4</sub>)<sub>2</sub>[Pd<sub>2</sub>(μ-Br)<sub>2</sub>(Ar<sup>F</sup>)<sub>4</sub>] (**3a-c**). Finally, removal of the bromide bridges as insoluble AgBr upon addition of AgClO<sub>4</sub> in THF at low temperature results in the formation of the corresponding *cis*-[Pd(Ar<sup>F</sup>)<sub>2</sub>(THF)<sub>2</sub>] products (**4a-c**).



**Scheme 3.** Synthetic route to **2a-c**, **3a-c** and **4a-c** complexes.

The COD complexes **2a-c** are isolated as colorless solids and are reasonably stable in the solid state at room temperature, where no decomposition is observed even after some months. Nevertheless, when less fluorinated aryls were employed, it was not possible to isolate the complexes due to their instability, even in this step. The pale-yellow dimeric species **3a-c** are indefinitely stable, and can be considered a potential source of any *cis*-[Pd(Ar<sup>F</sup>)<sub>2</sub>(L)<sub>n</sub>] species with weak ligands. Lastly, the colorless **4a-c** require low temperatures for long-term storage to prevent thermal decomposition. At -30 °C, samples checked by <sup>19</sup>F NMR showed no sign of decomposition after 9 weeks. Furthermore, **4a** does not decompose at room temperature, while **4b** is stable for a few days, indicating that they can be safely handled under air at room temperature for short periods of time.

The presence of fluorine atoms in the two ortho positions of the aryl is determinant on the stability of the complexes. For instance, an attempted synthesis of [Pd(Ar<sup>F</sup>)<sub>2</sub>(COD)] complexes with 2,4-C<sub>6</sub>H<sub>3</sub>F<sub>2</sub> or 3,4,5-C<sub>6</sub>H<sub>2</sub>F<sub>3</sub> quickly produced black Pd and the corresponding biaryls instead of the desired complexes. On the other hand, the isolated COD complexes **2a-c** are quite stable in solution even upon heating, as no sign of decomposition was observed after 3 h at 60 °C in toluene. The stability of **4a-c** toward reductive elimination in terms of Gibbs free energy, ΔG<sup>‡</sup>(Ar<sup>F</sup>-Ar<sup>F</sup>)<sub>Pd</sub>, was determined following the protocol previously established in reference 7 (Scheme 4). The values, measured at a convenient temperature in each case, were then transformed to ΔG<sup>‡</sup> at 0 °C for direct comparison under identical T conditions (Table 1, column 5). The effect of fluorine can be clearly observed. While reductive elimination at the perfluorinated **4a** is measured at 25 °C, the less fluorinated **4b** and **4c** require 0 °C to obtain accurate data. ΔG<sup>‡</sup><sub>273K</sub> is reduced from 22.8 to 21.3 (ΔΔG<sup>‡</sup> = 1.5 kcal·mol<sup>-1</sup>) when the meta F atoms are replaced by H atoms (**4a** vs **4b**), and the barrier is further reduced by 0.6 kcal·mol<sup>-1</sup> upon para F atom substitution (**4b** vs **4c**). These differences show that the influence in complex stability of F atoms in meta position is higher than those in para, although the latter cannot be ignored.



**Scheme 4.** Experimental determination of ΔG<sup>‡</sup>(Ar<sup>F</sup>-Ar<sup>F</sup>)<sub>Pd</sub> in toluene.

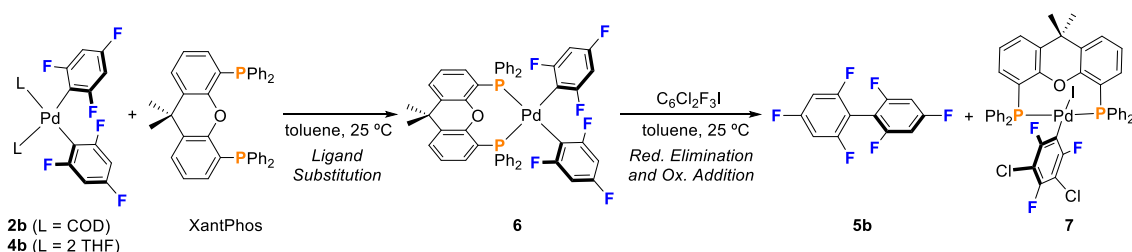
**Table 1.** Experimental  $\Delta G^\ddagger(\text{Ar}^{\text{F}}-\text{Ar}^{\text{F}})_{\text{Pd}}$  (kcal·mol<sup>-1</sup>) for reductive elimination of complexes **4a-c** in toluene. \*From ref. 7.

Entry/ Complex	Aryl	$\Delta G^\ddagger_{\text{T}}$	T/ K	$\Delta G^\ddagger_{273\text{K}}$
1/ 4a	C <sub>6</sub> F <sub>5</sub>	23.1*	298	22.8
2/ 4b	2,4,6-C <sub>6</sub> H <sub>2</sub> F <sub>3</sub>	21.3	273	21.3
3/ 4c	2,6-C <sub>6</sub> H <sub>3</sub> F <sub>2</sub>	20.7	273	20.7

These studies show that COD complexes **2a-c** are way more stable than **4a-c**, which might be important in terms of a potential commercialization. However, this enhanced stability may be detrimental in terms of catalyst activation, since COD ligand is not as easily displaced as THF ligands. Therefore, depending on the conditions employed, access to the active [Pd<sup>0</sup>(L)] species may be easier when THF complexes are employed. For the next the studies, we decided to use Ar<sup>F</sup> = 2,4,6-C<sub>6</sub>H<sub>2</sub>F<sub>3</sub> because of the good stability of both the COD (**2b**) and the THF (**4b**) complexes, their faster reactivity compared to C<sub>6</sub>F<sub>5</sub> analogues, and their very simple <sup>19</sup>F NMR spectral patterns (two signals with no <sup>19</sup>F–<sup>19</sup>F coupling).

#### Steric effects on ligand substitution rates

In a catalytic reaction, addition of the desired ligand is expected to displace COD or THF from the precatalyst, and then produce reductive elimination to generate the active [Pd<sup>0</sup>(L)] species. While the choice of ligand is sometimes imposed by the electrophile employed, to have a productive oxidative addition step, it is sometimes ignored that ligand substitution may suffer from steric hindrance. This difficulty is highly probable when bulky ligands are employed, such as P<sup>t</sup>Bu<sub>3</sub>, PAd<sub>3</sub>, dialkyl biarylphosphines or PEWO ligands. The different rate of COD or THF ligand substitution, and its effect on the formation of [Pd<sup>0</sup>(L)] is clearly observed in Table 2, which show the conversion and evolution of the reaction of XantPhos, a bulky chelating diphosphine ligand, with **2b** and **4b**, in the presence of C<sub>6</sub>Cl<sub>2</sub>F<sub>3</sub>I as oxidant of the [Pd<sup>0</sup>(L)] species formed (Scheme 5). The formation of [Pd<sup>0</sup>(L)] is easily tracked following the formation of biphenyl **5b** in the <sup>19</sup>F NMR spectrum.

**Scheme 5.** Reaction pathway upon addition of XantPhos to **2b** and **4b**.

**Table 2.** Data for ligand substitution and reductive elimination from complexes **2b** and **4b** with XantPhos.

Entry/ [Pd]	t/ min	Conversion/ %	<b>6</b> / %	<b>5b</b> / %
1/ 2b	15	4	4	0
2/ 2b	60	33	25	8
3/ 2b	120	94	40	54
4/ 4b	5	>99	81	19
5/ 4b	30	>99	66	34
6/ 4b	90	>99	31	69

The results show that, for **4b**, THF ligand substitution (LS) by XantPhos is the fastest step. Total conversion to **6** is observed even in the first spectra (entry 4). Reductive elimination (RE) is, in comparison, a much slower process. Consequently, when **4b** is employed, RE can be considered the rate determining step for the formation of the oxidative addition complex *trans*-[Pd(C<sub>6</sub>Cl<sub>2</sub>F<sub>3</sub>)I(XantPhos)] (**7**). In contrast, when **2b** is employed, the COD ligand is not displaced so quickly, and some starting material is observed even after 2 hours (entry 3). The slow rate of COD LS produces lower concentrations of **6** in similar reaction times compared to THF, which directly affects the rate of formation of **7**.

Typically, LS mechanism in Pd is associative, with the entering ligand approaching the Pd empty orbital perpendicular to the square plane. The  $\Delta G^\ddagger$  barrier for this process is increased when the Pd ligands are spanned around the coordination sphere, blocking the approaching route, and when the substituting ligand has an increased bulkiness. Having observed the detrimental effect of COD compared to THF for the formation of *trans*-[Pd(C<sub>6</sub>Cl<sub>2</sub>F<sub>3</sub>)I(XantPhos)] (**7**), LS may play a capital role in reaction with bulkier phosphines, with more hindered P atoms and potential steric conflicts. For the next cases studied, it is difficult to compare directly the steric hindrance of [Pd(neophyl)(COD)] complex (**P3**) used by Buchwald with our [Pd(Ar<sup>F</sup>)<sub>2</sub>(L)] (L = COD, 2 THF) complexes, and also there are no free Gibbs energy data available for the Pd reduction from **P3** to compare to our data. Therefore, we decided to compare the reported data for the sequence LS/RE+OA in Table 1 of reference 8 with the data obtained for complexes **2b** and **4b** in the same conditions (Table 3: room temperature, 60 min.; Table 4: 60 °C, 60 min.).

The data collected at room temperature (Table 3), where **A** is the LS intermediate, and **C** the oxidative addition product, easily identify the different strengths and weaknesses of the tested ligands. The percentage of LS is the sum yield of **A** + **C**, as **C** is formed from **A**. The reactions with COD complexes (**P3** and **2b**) highlight the difficulty to displace COD by the very bulky tBuXPhos and tBuBrettPhos ligands, while the less bulky RuPhos and XPhos, with a less crowded P atom, produce a faster displacement (entries 1-8). Moreover, COD substitution looks easier in **P3** (entries 1 and 2) than in **2b** (entries 5 and 6). The access to the empty orbital in Pd, above the coordination plane, is less hindered in **P3**, with a planar neophyl moiety, than in **2b**, with two aryls almost perpendicular to the coordination plane. Trans influence is also higher for the electron-rich palladacycle than for the fluoroaryl groups, easing the LS process.

The data obtained for tBuXPhos ligand (entries 3 and 7) show that this is the ligand with fastest RE relative to LS, since no LS product **A** is observed, and only the OA product **C** is detected. For RuPhos and XPhos, comparing the yield of **C** formed from **P3** (entries 1 and 2) and **2b** (entries 5 and 6) gives an idea of the relative ease to perform reductive elimination from the corresponding LS complexes. The activation energy for reduction of **A** to [Pd<sup>0</sup>(L)] is lower (the reduction step is faster) for *cis*-[Pd(C<sub>6</sub>H<sub>2</sub>F<sub>3</sub>)<sub>2</sub>(L)] (**A**) than for the homologous palladacyclic [Pd(neophyl)(L)] (**A'**), at least for these two ligands where comparison is possible.

**Table 3.** LS, RE and OA by *p*-BrC<sub>6</sub>H<sub>4</sub>(CF<sub>3</sub>) of precursors **P3**, **2b** and **4b**; 25 °C, 60 min.  
\* Data taken from Table 1 in ref. 8.

Entry/ [Pd]	entering L	% A	% C
1/ [Pd(neophyl)(COD)] ( <b>P3</b> ) *	RuPhos	99	0
2/ [Pd(neophyl)(COD)] ( <b>P3</b> ) *	XPhos	70	0
3/ [Pd(neophyl)(COD)] ( <b>P3</b> ) *	tBuXPhos	0	10
4/ [Pd(neophyl)(COD)] ( <b>P3</b> ) *	tBuBrettPhos	0	0
5/ [Pd(C <sub>6</sub> H <sub>2</sub> F <sub>3</sub> ) <sub>2</sub> (COD)] ( <b>2b</b> )	RuPhos	70	4
6/ [Pd(C <sub>6</sub> H <sub>2</sub> F <sub>3</sub> ) <sub>2</sub> (COD)] ( <b>2b</b> )	XPhos	26	6
7/ [Pd(C <sub>6</sub> H <sub>2</sub> F <sub>3</sub> ) <sub>2</sub> (COD)] ( <b>2b</b> )	tBuXPhos	0	8
8/ [Pd(C <sub>6</sub> H <sub>2</sub> F <sub>3</sub> ) <sub>2</sub> (COD)] ( <b>2b</b> )	tBuBrettPhos	0	0
9/ [Pd(C <sub>6</sub> H <sub>2</sub> F <sub>3</sub> ) <sub>2</sub> (THF) <sub>2</sub> ] ( <b>4b</b> )	RuPhos	91	9
10/ [Pd(C <sub>6</sub> H <sub>2</sub> F <sub>3</sub> ) <sub>2</sub> (THF) <sub>2</sub> ] ( <b>4b</b> )	XPhos	67	33
11/ [Pd(C <sub>6</sub> H <sub>2</sub> F <sub>3</sub> ) <sub>2</sub> (THF) <sub>2</sub> ] ( <b>4b</b> )	tBuXPhos	8	92
12/ [Pd(C <sub>6</sub> H <sub>2</sub> F <sub>3</sub> ) <sub>2</sub> (THF) <sub>2</sub> ] ( <b>4b</b> )	tBuBrettPhos	4	4
13/ [Pd(C <sub>6</sub> H <sub>2</sub> F <sub>3</sub> ) <sub>2</sub> (THF) <sub>2</sub> ] ( <b>4b</b> )	SPhos	90	10

For the THF complex **4b** (entries 9-13), full THF LS substitution is observed for most of the ligands, except tBuBrettPhos, after 1 hour. Considering the previous results in Table 2 for XantPhos, LS probably occurs in seconds for all of them. Consequently, the relative coupling rate constants is related to the **C** yields: tBuXPhos > XPhos > SPhos ≈ RuPhos. These results highlight the better performance of tBuXPhos and XPhos for the *in situ* generation of [Pd(*p*-C<sub>6</sub>H<sub>4</sub>-CF<sub>3</sub>)Br(L)] in short times under mild conditions, once the whole process is not delayed by a slow LS step. It is also clear that the very crowded tBuBrettPhos is almost inactive under these conditions, regardless of the precursor employed.

When the temperature is raised to 60 °C, all the conversions are increased, with many of them up to > 99 % after 1 hour (Table 4). With **4b**, **C** yields are in the range 94-99 % (entries 22-26), except for tBuBrettPhos, which reaches a 44 % conversion with a 35 % yield of **C**. For the cases with COD as initial ligand (**P3** and **2b**), conversions and yields are also clearly improved (entries 14-21). The slow RE observed for RuPhos at 25 °C is negligible for complex **A** from **2b** and **4b** (entries 18 and 22) at 60 °C, but it is still a retarding step from [Pd(neophyl)(RuPhos)] (entry 14). For XPhos, the increase in temperature is enough to obtain full conversion to **C**, both for **P3** (entry 15, 99%) and for **2b** (entry 19, 91%). The lower **C** yield with **2b** is, as commented before, due to a slower

COD LS step (No **A** is observed). The same observation applies to tBuXPhos (entries 16 and 20) and tBuBrettPhos (entries 17, and 21) which suffer an even higher difficulty to be efficient in the LS step. For this reason, in the reactions with **2b**, where LS is more impeded, ligand RuPhos, with the most accessible P atom, affords the highest conversion to **C** (entry 18).

**Table 4.** LS, RE and OA by *p*-BrC<sub>6</sub>H<sub>4</sub>(CF<sub>3</sub>) of precursors **P3**, **2b** and **4b**; 60 °C, 60 min.  
\* Data taken from Table 1 in ref. 8.

Entry/ [Pd]	entering L	% A	% C
14/ [Pd(neophyl)(COD)] ( <b>P3</b> ) *	RuPhos	41	59
15/ [Pd(neophyl)(COD)] ( <b>P3</b> ) *	XPhos	0	99
16/ [Pd(neophyl)(COD)] ( <b>P3</b> ) *	tBuXPhos	0	82
17/ [Pd(neophyl)(COD)] ( <b>P3</b> ) *	tBuBrettPhos	0	24
18/ [Pd(C <sub>6</sub> H <sub>2</sub> F <sub>3</sub> ) <sub>2</sub> (COD)] ( <b>2b</b> )	RuPhos	2	98
19/ [Pd(C <sub>6</sub> H <sub>2</sub> F <sub>3</sub> ) <sub>2</sub> (COD)] ( <b>2b</b> )	XPhos	0	91
20/ [Pd(C <sub>6</sub> H <sub>2</sub> F <sub>3</sub> ) <sub>2</sub> (COD)] ( <b>2b</b> )	tBuXPhos	0	46
21/ [Pd(C <sub>6</sub> H <sub>2</sub> F <sub>3</sub> ) <sub>2</sub> (COD)] ( <b>2b</b> )	tBuBrettPhos	0	6
22/ [Pd(C <sub>6</sub> H <sub>2</sub> F <sub>3</sub> ) <sub>2</sub> (THF) <sub>2</sub> ] ( <b>4b</b> )	RuPhos	6	94
23/ [Pd(C <sub>6</sub> H <sub>2</sub> F <sub>3</sub> ) <sub>2</sub> (THF) <sub>2</sub> ] ( <b>4b</b> )	XPhos	0	99
24/ [Pd(C <sub>6</sub> H <sub>2</sub> F <sub>3</sub> ) <sub>2</sub> (THF) <sub>2</sub> ] ( <b>4b</b> )	tBuXPhos	2	98
25/ [Pd(C <sub>6</sub> H <sub>2</sub> F <sub>3</sub> ) <sub>2</sub> (THF) <sub>2</sub> ] ( <b>4b</b> )	tBuBrettPhos	9	35
26/ [Pd(C <sub>6</sub> H <sub>2</sub> F <sub>3</sub> ) <sub>2</sub> (THF) <sub>2</sub> ] ( <b>4b</b> )	SPhos	3	97

The results collected in Table 3 Table 4 indicate that, given enough time or higher temperature, complexes **P3**, **2b** and **4b** can efficiently generate oxidative addition complexes [Pd(Ar)X(L)] in high yields. Thus, the procedure is potentially useful with several ArX electrophiles that can oxidize the generated [Pd<sup>0</sup>(L)] species formed. For a potential application as precatalysts, a fast and complete in situ formation of [Pd(Ar)X(L)] is required. If the catalysis has to be carried out close to room temperature due to thermal fragility of reagents or products, entry 11 of Table 3 looks the appropriate [Pd+L] combination. If the reagents and products tolerate high temperatures, several options from Table 4 can be considered, such as entry 15 for **P3**, entries 18 and 19 for **2b** and almost all the combinations for **4b**. All of them will form the OA complex in a short time. It is noteworthy that the whole series **4a-c** is available and the clean observation of the starting complex and the coupling biaryls allows to indirectly monitor by <sup>19</sup>F NMR when the formation of the [Pd(Ar)X(L)] is complete. In contrast, **P3** derivatives do not offer equivalent flags for easy observation, and information would need to be acquired from complex <sup>1</sup>H spectra.

#### *Analysis of X-ray structures and their influence in catalysis*

Structural details are easily forgotten when checking long lists of potential catalysts. However, the structures of the complexes are closely related to the thermodynamic stability of intermediates and the Gibbs energy barriers along the whole catalytic process. This should be kept in mind when analyzing the positive or negative catalytic results. For



this reason, X-ray structures of some of the intermediates in the previous reactions were obtained.

XantPhos is a ligand with a singular structural behavior, as it can be coordinated both as *cis*- and *trans*-chelate.<sup>10</sup> In these complexes, the most feasible isomerization mechanism is the classic dissociation of one P–M bond and *topomerization* of the coordinated P atom (change of position to the created vacant) followed by P recoordination. In the context of catalysis, the *trans*-[Pd(R)(R')(XantPhos)] complex, if formed after transmetalation, will then isomerize to the *cis* arrangement needed for R-R' reductive elimination. The hemilability and flexibility of XantPhos is the reason behind its great catalytic success compared to other chelating diphosphines. However, this structural flexibility also warns that increasing the steric factor of the fragments to be coupled may result in a higher structural instability of the intermediates or higher topomerization barriers, blocking the catalysis in some cases. The X-ray structure of *trans*-[Pd(C<sub>6</sub>Cl<sub>2</sub>F<sub>3</sub>)(I)(XantPhos)] (**7**) was determined and confirms the *trans* arrangement of the ligand expected by the equivalence of the P atoms in the <sup>31</sup>P NMR (Figure 2).

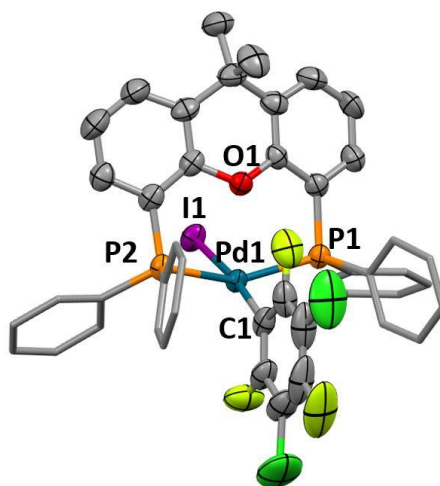


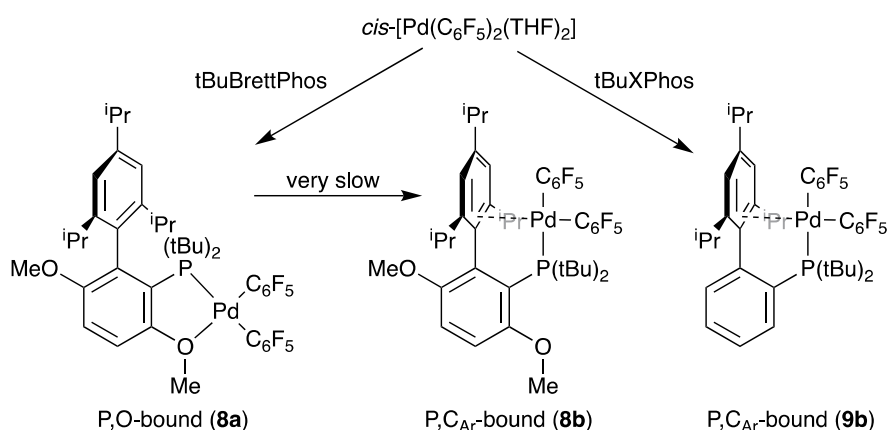
**Figure 2.** X-ray diffraction structure of *trans*-[Pd(2,4,6-C<sub>6</sub>Cl<sub>2</sub>F<sub>3</sub>)(I)(XantPhos)]·2 CH<sub>2</sub>Cl<sub>2</sub> (**7**). H atoms and solvent molecules ( ) omitted for clarity. Significant bond distances (Å): Pd1-P1 = 2.319, Pd1-C1 = 2.030, Pd1-I1 = 2.676, Pd1-P2 = 2.298, Pd1-O1 = 2.636.

The wide family of commercially available 2-biarylphosphines developed by Buchwald are a huge contribution to the Pd-catalyzed synthetic processes. They prevent the decomposition of reaction intermediates and facilitate the OA and RE steps, which are often the obstacles to succeed in the catalysis, depending on the reagents employed. Phosphine coordination mode to Pd is the result of a balance between different factors: attractive Pd-biaryl forces, steric hindrance with other groups in the coordination sphere, presence of heteroatoms, such as in methoxy or dimethylamino groups, and the hydrocarbyl or halo groups in the Pd. The effect on catalysis of these factors has already been studied by Buchwald group.<sup>11</sup>

<sup>10</sup> Adams, G. M.; Weller, A. S. POP-type ligands: Variable coordination and hemilabile behaviour. *Coord. Chem. Rev.*, **2018**, *355*, 150–172.

<sup>11</sup> Arrechea, P. L.; Buchwald, S. L. Biaryl Phosphine Based Pd(II) Amido Complexes: The Effect of Ligand Structure on Reductive Elimination. *J. Am. Chem. Soc.*, **2016**, *138*, 12486–12493.

Looking for phosphine protection, Buchwald group developed some ligands bearing alkoxy substituents. The presence of a –OMe group ortho to the P atom can lead to a P,O-coordination of the phosphine, forming a 5-membered palladacycle. This structure is very reluctant to RE compared to the P,C<sub>Ar</sub>-isomer. The two isomers can coexist in solution, although interconversion is usually slow. This behavior is well known since the trifluoromethylation studies with [Pd(*p*-C<sub>6</sub>H<sub>4</sub>-CO<sub>2</sub>Me)(CF<sub>3</sub>)(CyBrettPhos)],<sup>12</sup> and it is also observed for the complex [Pd(C<sub>6</sub>F<sub>5</sub>)<sub>2</sub>(tBuBrettPhos)],<sup>7</sup> which is P,O-coordinated when formed (**8a**) and only very slowly isomerizes to P,C<sub>Ar</sub> (**8b**), in contrast to [Pd(C<sub>6</sub>F<sub>5</sub>)<sub>2</sub>(tBuXPhos)] which is, necessarily, P,C<sub>Ar</sub>-coordinated (**9b**) (Scheme 6). Hence, the bad results obtained with tBuBrettPhos in Table 3 and Table 4 are not simply a matter of slowness of the reductive elimination, but of slow isomerization to the P,C<sub>Ar</sub> active isomer.



**Scheme 6.** Coordination behavior of tBuBrettPhos and tBuXPhos.

In a similar fashion, the case of SPhos, with two OMe groups in the *distal* aryl needs to be considered. With the ease of substitution of THF in *cis*-[Pd(C<sub>6</sub>H<sub>2</sub>F<sub>3</sub>)<sub>2</sub>(THF)<sub>2</sub>] (**4b**), complex [Pd(C<sub>6</sub>H<sub>2</sub>F<sub>3</sub>)<sub>2</sub>(SPhos)] (**10**) was obtained by reaction of **4b** with SPhos in THF at 0 °C. It shows two inequivalent C<sub>6</sub>H<sub>2</sub>F<sub>3</sub> aryls in the <sup>19</sup>F NMR spectra and two equivalent OMe in the <sup>1</sup>H spectra, discarding P,O-coordination. Indeed, P,O-chelation would lead to a 7-member palladacycle, very high in energy compared to the 5-member palladacycle formed with tBuBrettPhos. The X-ray structure of **10** was determined and confirms the chelating P,C<sub>Ar</sub>-coordination of SPhos to Pd (Figure 3).

<sup>12</sup> Cho, E. J.; Senecal, T. D.; Kinzel, T.; Zhang, Y.; Watson, D. A.; Buchwald, S. L. The Palladium-Catalyzed Trifluoromethylation of Aryl Chlorides. *Science*, **2010**, 328, 1679–1681.

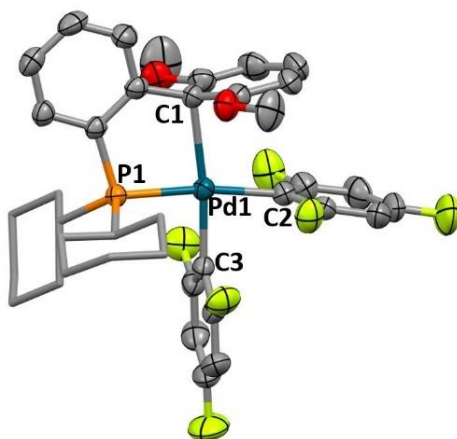


**Figure 3.** X-ray diffraction structure of *cis*-[Pd(C<sub>6</sub>H<sub>2</sub>F<sub>3</sub>)<sub>2</sub>(SPhos)] (**10**). H atoms omitted for clarity. Significant bond distances (Å): Pd1-P1 = 2.307, Pd1-C1 = 2.413, Pd1-C2 = 2.056, Pd1-C3 = 2.007, C2-C3 = 2.679.

A third case with remarkable interest is that of the oxidative addition compounds to the reduction product of **10**, [Pd<sup>0</sup>(SPhos)]. The structure of the complexes upon reaction with *p*-C<sub>6</sub>H<sub>4</sub>FI, C<sub>6</sub>H<sub>2</sub>F<sub>3</sub>I and C<sub>6</sub>H<sub>2</sub>BrF<sub>3</sub> were solved by X-ray diffraction. The product obtained after reaction with *p*-C<sub>6</sub>H<sub>4</sub>FI is the dimer *anti*-[Pd(*p*-C<sub>6</sub>H<sub>4</sub>F)(μ-I)(SPhos)]<sub>2</sub> (**11**), where SPhos acts as monodentate P-coordinated and the coordination square planes of the two Pd atoms make an angle of 116.3° (Figure 4).

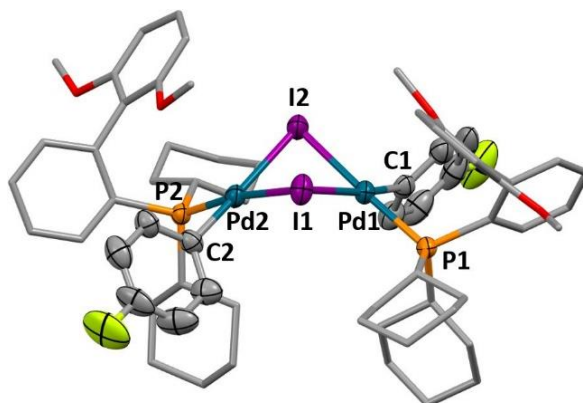
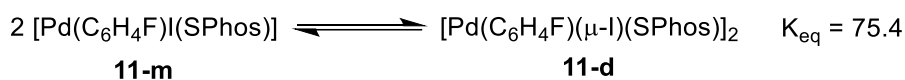


**Figure 4.** X-ray diffraction structure of *anti*-[Pd(*p*-C<sub>6</sub>H<sub>4</sub>F)(μ-I)(SPhos)]<sub>2</sub> · 2 CH<sub>2</sub>Cl<sub>2</sub> (**11**). H atoms and solvent molecules omitted for clarity. Relevant bond distances (Å): Pd1-P1 = 2.287, Pd1-C1 = 2.019, Pd1-I2 = 2.687, Pd1-I1 = 2.751, Pd1-Pd2 = 3.411.

The NMR spectra of **11** in CDCl<sub>3</sub> solution shows that the dimer **11-d** is, as shown in Scheme 7, in slow equilibrium with the monomer **11-m**, where the halo-bridges are split and the biphenyl distal aryl is presumably interacting with the fourth coordination position. The equilibrium constant between the two isomers was determined in CDCl<sub>3</sub> and has a value of K<sub>eq</sub> = 75.4 at 25 °C.



**Scheme 7.** Monomer/dimer equilibrium of complex **11**.

For the oxidations with C<sub>6</sub>H<sub>2</sub>F<sub>3</sub>I and C<sub>6</sub>H<sub>2</sub>BrF<sub>3</sub>, the X-ray structures display also dimeric *anti*-[Pd(C<sub>6</sub>H<sub>2</sub>F<sub>3</sub>)(μ-X)(SPhos)]<sub>2</sub> structures, although in these cases the two Pd coordination planes are practically coplanar (complex **12** and **13** in Figure 5). These structural variations of planarity or non-planarity of the bridging halides are quite common and are within the low energy accessible structural differences that participate in the search of the molecules for its best crystallographic packing, such as aryl rotations, tilting or retention of solvent molecules among others. Interesting, solution behavior is different for these two complexes. While **12** is in a monomer/dimer equilibrium in solution like **11**, complex **13** is only observed as the monomer species in solution.

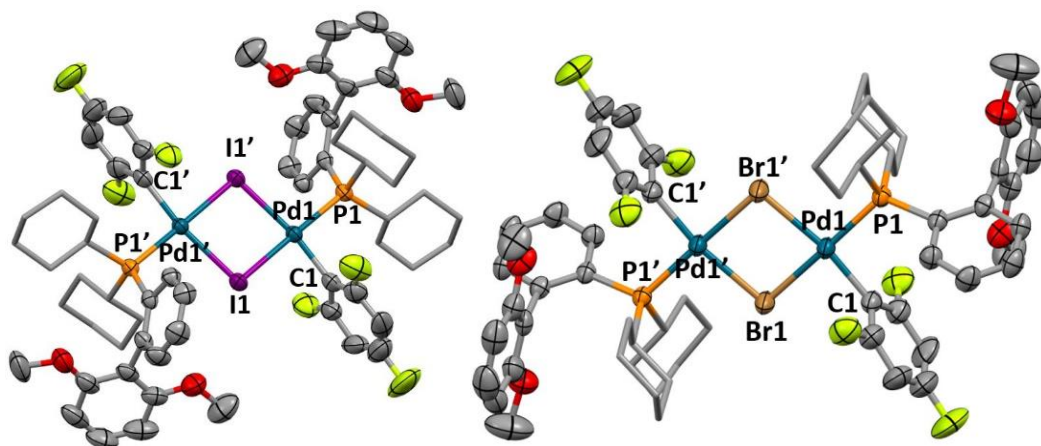


**Figure 5.** X-ray diffraction structure of **12**·2 CH<sub>2</sub>Cl<sub>2</sub> (left) and **13** (right). H atoms and solvent molecules omitted for clarity. Relevant bond distances (Å): **12**: Pd1-P1 = 2.311, Pd1-C1 = 2.030, Pd1-I1' = 2.686, Pd1-I1 = 2.664, Pd1-Pd1' = 3.925. **13**: Pd1-P1 = 2.279, Pd1-C1 = 2.013, Pd1-Br1' = 2.529, Pd1-Br1 = 2.515, Pd1-Pd1' = 3.721.

The variety observed in these structures can be considered as a photographic album of the fluxionality and dynamics of these molecules in solution or during a reaction pathway. Table 5 collects the distances from Pd to the *C*<sub>ipso</sub>, *C*<sub>ortho</sub> and *C*<sub>ortho'</sub> *distal* aryl atoms of the biaryl, potentially involved in interactions with Pd, as well as the Pd-O distance to the closest methoxy group. These distances can be compared to the sum of van der Waals (vdW) radii and the sum of covalent radii of the atoms involved. All the distances are above the sum of covalent radii and only those of complex **10** (highlighted in bold) are below the sum of vdW radii, quite close to the sum of covalent radii. Hence, they are located in a range where weak orbital interactions may be acting along with non-covalent interactions (NCI). A qualitative but clear estimation of the importance of orbital *vs.* NCI interactions can be obtained by comparison of the data for **10** with the data of [AuCl(PR<sub>2</sub>{biaryl})] complexes, in which the Au-*C*<sub>ipso</sub> interactions are exclusively NCI.<sup>13</sup> The Au-*C*<sub>ipso</sub> distances are in the range 3.06-3.20 Å while the Pd-*C*<sub>ipso</sub> in **10** is only 2.413 Å, clearly supporting orbital overlap, probably with π-electron donation from the *distal* aryl to Pd, producing a weak covalent bond.

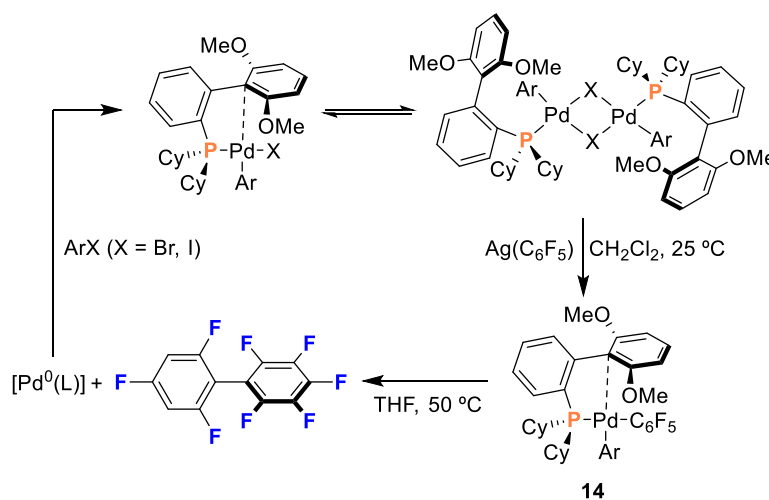
<sup>13</sup> Ponce-de-León, J.; Infante, R.; Pérez-Iglesias, M.; Espinet, P. Fluorinated *vs.* Nonfluorinated PR<sub>2</sub>(biaryl) Ligands and Their [AuCl(L)] Complexes: Synthesis, X-ray Structures, and Computational Study of Weak Interactions. Bond, No Bond, and Beyond. *Inorg. Chem.*, **2020**, *59*, 16599–16610.

**Table 5.** Pd to *distal* aryl distances in [Pd(Ar)<sub>2</sub>(SPhos)] and [Pd(Ar)X(SPhos)] complexes. Sum of covalent radii (Å): Pd+C = 2.12. Sum of vdW radii (Å): Pd+C = 3.92.

Entry/ Compound	Pd···C <sub>ipso</sub> / Å	Pd···C <sub>ortho</sub> / Å	Pd···C <sub>ortho'</sub> / Å	Pd···OMe/ Å
1/ 10	2.413	2.728	2.942	3.272
2/ 11	4.110	3.677	5.261	3.120
3/ 12	5.397	5.786	6.251	5.380
4/ 13	5.422	5.675	6.330	5.228

The monomeric species **10** is formed in preference to a potential alternative structure [Pd(Ar)(μ-Ar)(SPhos)]<sub>2</sub> with two bridging C<sub>ipso</sub> atoms, because bridging aryls are quite electron deficient. In the case of the oxidative addition complexes [Pd(Ar)X(SPhos)], the high bridging strength of halides, which involve two electron pairs in the bridge, leads to very preferential formation of [Pd(Ar)(μ-X)(SPhos)]<sub>2</sub>, with monodentate P coordinate SPhos. The existence of monomer/dimer equilibria in solution suggests that their interconversions are easily accessible. The Pd-C<sub>ipso</sub> distances allow to observe that, once the *distal* aryl is uncoordinated, it can remain relatively close to Pd, as in **11**, or move quite far, as in **12** and **13**. This flexibility requires easy aryl rotation about the P-Ar<sub>proximal</sub> and the Ar<sub>proximal</sub>-Ar<sub>distal</sub> bonds, which could be hindered in more substituted dialkyl biarylphosphines.

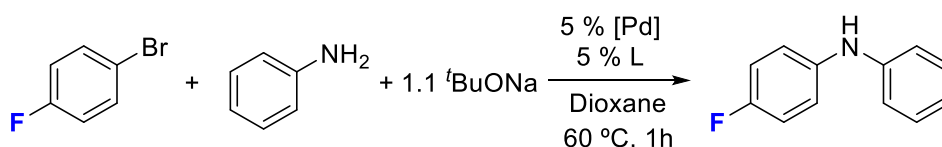
After the *in situ* sequence Pd<sup>II</sup>-precursor/[Pd<sup>0</sup>(L)]/[Pd(Ar)X(L)] that produces the catalyst with the desired Ar and L groups, the catalysis must be followed by transmetalation from the chosen nucleophile and reductive elimination. These two last steps were accessed stoichiometrically for the C<sub>6</sub>H<sub>2</sub>F<sub>3</sub>-C<sub>6</sub>F<sub>5</sub> coupling with SPhos as ligand, out of catalytic conditions, using AgC<sub>6</sub>F<sub>5</sub> as nucleophile, as shown in Scheme 8. The reaction of [Pd(C<sub>6</sub>H<sub>2</sub>F<sub>3</sub>)(X)(SPhos)] (X = Br, I) with AgC<sub>6</sub>F<sub>5</sub> in CH<sub>2</sub>Cl<sub>2</sub> at room temperature led to the transmetalation product [Pd(C<sub>6</sub>H<sub>2</sub>F<sub>3</sub>)(C<sub>6</sub>F<sub>5</sub>)(SPhos)] (**14**), which was isolated and fully characterized. This complex is monomeric and exhibits a P<sub>2</sub>C<sub>Ar</sub>-coordination of SPhos, as previously observed for the homoleptic [Pd(C<sub>6</sub>H<sub>2</sub>F<sub>3</sub>)<sub>2</sub>(SPhos)] (**10**). Then, **14** was heated in THF solution at 50 °C in the presence of (C<sub>6</sub>H<sub>2</sub>F<sub>3</sub>)X, producing reductive elimination of C<sub>6</sub>H<sub>2</sub>F<sub>3</sub>-C<sub>6</sub>F<sub>5</sub> and subsequent reoxidation, generating the starting complex [Pd(C<sub>6</sub>H<sub>2</sub>F<sub>3</sub>)(X)(SPhos)] (X = Br, I).

**Scheme 8.** Stoichiometric reactions with SPhos Pd complexes. Ar = C<sub>6</sub>H<sub>2</sub>F<sub>3</sub>.

*Compared activity of 2b and 4b in catalysis*

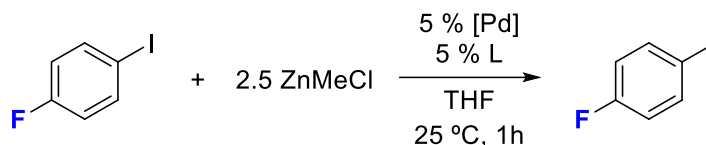
As discussed previously, LS and RE processes from **2b** and **4b** are very dependent on the reaction conditions employed. Some catalytic cross-coupling reactions were carried out to evaluate the possible consequences of this dependence. The catalytic reactions were conducted out of optimized conditions so that the different behavior of **2b** and **4b** is easily observed.

Since biarylphosphines have been widely employed in Buchwald-Hartwig amination,<sup>14</sup> a C–N coupling between *p*-C<sub>6</sub>H<sub>4</sub>BrF and aniline was first tested. The reaction was run in dioxane at 60 °C, with 5 % of the Pd complexes **2b** or **4b** and tBuXPhos as ligand (Scheme 9). After 60 min, the amount of reaction product formed is very different in each case. For **4b**, 91 % yield of amination product is obtained, while for **2b**, only 3 % is observed. This is in good agreement with the results obtained in Table 4, where full ligand substitution was achieved after one 1 hour with **4b**, but not with **2b**, where a large percentage of COD complex **2b** remains unreacted and the actual percentage of the active [Pd(*p*-C<sub>6</sub>H<sub>4</sub>F)Br(tBuXPhos)] catalyst formed is very low (<< 5%). Thus, the use of **4b** is highly preferred to **2b**. Alternatively, the formation of [Pd(*p*-C<sub>6</sub>H<sub>4</sub>F)Br(tBuXPhos)] should be ascertained by <sup>19</sup>F NMR monitoring, allowing the necessary time for catalyst activation previous to aniline addition.



**Scheme 9.** C–N coupling catalysis. [Pd] = **2b** or **4b**. L = tBuXPhos. Yield determined by <sup>19</sup>F NMR.

A second study case is the C–C Negishi coupling of 4-C<sub>6</sub>H<sub>4</sub>FI with ZnMeCl at room temperature (Scheme 10). In this case, the two precatalysts **2b** and **4b** provided almost full conversion (99 % and 98 % yield, respectively) in 60 min at room temperature. These results are totally unexpected because they overcome the rates expected for the relatively slow C<sub>6</sub>H<sub>2</sub>F<sub>3</sub>–C<sub>6</sub>H<sub>2</sub>F<sub>3</sub> coupling at 25 °C (Table 3), particularly when using **2b**.



**Scheme 10.** Negishi catalysis. [Pd] = **2b** or **4b**. L = tBuXPhos. Yield determined by <sup>19</sup>F NMR.

The results in Table 6 show that C<sub>6</sub>H<sub>2</sub>F<sub>3</sub>–C<sub>6</sub>H<sub>2</sub>F<sub>3</sub> formation from precatalyst activation is hardly observed when **2b** is employed, while a big amount of Zn(C<sub>6</sub>H<sub>2</sub>F<sub>3</sub>)Cl is observed instead (entry 1). Zn(C<sub>6</sub>H<sub>2</sub>F<sub>3</sub>)Cl is formed after undesired C<sub>6</sub>H<sub>2</sub>F<sub>3</sub>/Me transmetalations between **2b** and ZnMeCl. This kind of undesired transmetalation when fluorinated aryls

<sup>14</sup> Surry, D. S.; Buchwald, S. L. Biaryl phosphane ligands in palladium-catalyzed amination. *Angew. Chem., Int. Ed.*, **2008**, *47*, 6338–6361.

are involved has been thoroughly studied previously.<sup>15</sup> With **4b**, both C<sub>6</sub>H<sub>2</sub>F<sub>3</sub>-C<sub>6</sub>H<sub>2</sub>F<sub>3</sub> (25%) and Zn(C<sub>6</sub>H<sub>2</sub>F<sub>3</sub>)Cl (75%) are produced (entry 2).

**Table 6.** Catalytic results and catalyst activation products for the Negishi reaction shown in Scheme 10.

Negishi Catalysis Results. % F in C <sub>6</sub> H <sub>4</sub> F				% F in C <sub>6</sub> H <sub>2</sub> F <sub>3</sub> <sup>c</sup>	
Entry/Precat.	ArI	ArMe	ArZnCl	(Ar <sup>F</sup> ) <sub>2</sub>	(Ar <sup>F</sup> )ZnCl
1/ 2b <sup>a</sup>	1	96	3	0	100
2/ 4b <sup>a</sup>	2	95	3	25	75
3/ 2b <sup>b</sup>	1	97	2	6	94
4/ 4b <sup>b</sup>	2	97	1	85	15

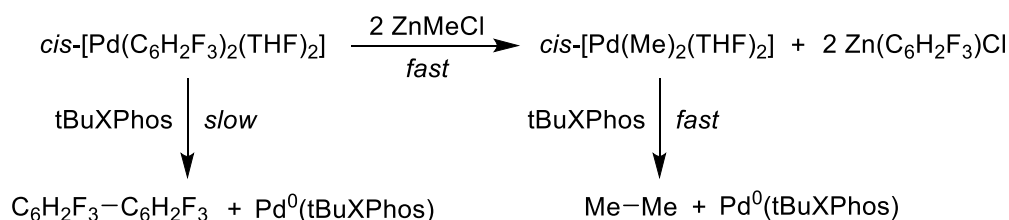
<sup>a</sup> All the reagents at the start of catalysis. <sup>b</sup> [Pd], L and ArI mixed for 1h, before ZnMeCl addition.

<sup>c</sup> MeMe is observed in <sup>1</sup>H RMN.

The catalysis were repeated, mixing the [Pd] and ligand in the presence of the ArI for 1 hour before ZnMeCl addition (entries 3 and 4). The yield of the catalysis did not differ, and catalyst activation products fit well with the previous results from Table 3.

- For **2b**, with a slow LS+RE process, Me–Me coupling product is observed in the <sup>1</sup>H NMR spectra, alone in entry 1 and mostly in entry 3, as shown by the scarce formation of C<sub>6</sub>H<sub>2</sub>F<sub>3</sub>-C<sub>6</sub>H<sub>2</sub>F<sub>3</sub>. This implies that transmetalation is faster than substitution + C<sub>6</sub>H<sub>2</sub>F<sub>3</sub>-C<sub>6</sub>H<sub>2</sub>F<sub>3</sub> coupling and the formation of active catalyst [Pd(*p*-C<sub>6</sub>H<sub>4</sub>F)I(L)] mainly occurs after coupling on a transmetalated [Pd(Me)<sub>2</sub>(L)] intermediate.
- For **4b**, the couplings from [Pd(C<sub>6</sub>H<sub>2</sub>F<sub>3</sub>)<sub>2</sub>(L)] and from transmetalated [Pd(Me)<sub>2</sub>(L)] are competitive. As the ligand substitution on **4b** is very fast, this supports that the undesired transmetalation + Me–Me coupling is faster than the C<sub>6</sub>H<sub>2</sub>F<sub>3</sub>-C<sub>6</sub>H<sub>2</sub>F<sub>3</sub> coupling (Scheme 11).

Overall, this effect can be considered as a positive one when more stable [PdR<sub>2</sub>(L)] precatalysts are employed, as it can be employed to accelerate the rate of formation of [Pd<sup>0</sup>(L)].

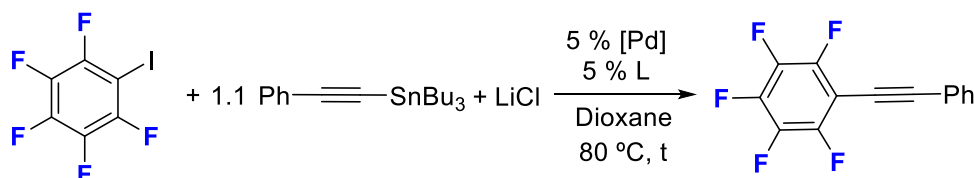


**Scheme 11.** Undesired transmetalation between Pd and Zn and subsequent coupling.

Finally, a Stille coupling involving a fluorinated aryl iodide (C<sub>6</sub>F<sub>5</sub>I) and an alkynylstannane (PhCCSnBu<sub>3</sub>) was tested (Scheme 12), which again displayed an interestingly unexpected behavior. The reaction, run at 80 °C in dioxane (stannanes are mild nucleophiles that benefit from higher temperature), proceeded similarly with both

<sup>15</sup> del Pozo, J.; Salas, G.; Álvarez, R.; Casares, J. A.; Espinet, P. The Negishi Catalysis: Full Study of the Complications in the Transmetalation Step and Consequences for the Coupling Products. *Organometallics*, **2016**, *35*, 3604–3611.

**2b** and **4b**. The high temperatures required for this catalysis have made the formation of the [Pd(C<sub>6</sub>F<sub>5</sub>)I(L)] catalyst similarly efficient from the two precursors, and the catalytic yield is almost the same. For this reason, only the results obtained with **2b** are shown in Table 7 (entries 1-3). Considering a previous work in Stille couplings with bulky reagents,<sup>16</sup> it is probable that the overall efficiency of this coupling is decreased due to the presence of a very bulky substituent both on Pd (tBuXPhos) and the stannane (butyl). Therefore, [AuCl(PPh<sub>3</sub>)<sub>3</sub>] was added as cocatalyst, working as a shuttle of the alkynyl group between Sn and Pd. This produced an increase in the reaction rate (entry 4), as well as a slightly higher yield after 24 hours (entry 6).



**Scheme 12.** Stille catalysis. [Pd] = **2b** or **4b**; L = tBuXPhos. Yields determined by <sup>19</sup>F NMR.

**Table 7.** Stille catalysis, and Pd/Au co-catalysis. AlkSnBu<sub>3</sub>:(C<sub>6</sub>F<sub>5</sub>)I = 1.1:1; [Pd] = **2b**; L = tBuXPhos. Yields determined by <sup>19</sup>F NMR

Entry/ Co-catalyst	t/ h	% Ar-I	% Ar-Alk	% Ar-H	% Ar-Sn
1/ No	1	60	32	5	3
2/ No	5	41	49	6	4
3/ No	24	20	57	18	5
4/ AuCl(PPh <sub>3</sub> ) (5%)	1.5	30	53	12	5
5/ AuCl(PPh <sub>3</sub> ) (5%)	5	25	56	14	5
6/ AuCl(PPh <sub>3</sub> ) (5%)	24	16	64	15	5

The catalysis rate could be further accelerated by increasing the equivalents of stannane employed, from 1.1 to 2 (Table 8). Full conversion is obtained after 24 hours without cocatalyst, and in 3 hours in the cocatalyzed reaction. Reaction yields also increased, up to 85 % in both cases.

**Table 8.** Stille catalysis, and Pd/Au co-catalysis. AlkSnBu<sub>3</sub>:(C<sub>6</sub>F<sub>5</sub>)I = 2:1; [Pd] = **2b**; L = tBuXPhos. Yields determined by <sup>19</sup>F NMR.

Entry/ Co-catalyst	t/ h	% Ar-I	% Ar-Alkyn	% Ar-H	% Ar-Sn
1/ No	1	48	39	8	5
2/ No	5.5	12	72	9	7
3/ No	24	0	85	8	7
4/ AuCl(PPh <sub>3</sub> ) (5%)	1	8	74	9	8
5/ AuCl(PPh <sub>3</sub> ) (5%)	3	0	83	9	9

The complexes *cis*-[Pd(C<sub>6</sub>H<sub>5-n</sub>F<sub>n</sub>)(THF)<sub>2</sub>] (n = 2, 3, 5), with increasing stability with the number of F atoms, are convenient precursors of [Pd(Ar)X(L)] complexes in a wide range

<sup>16</sup> del Pozo, J.; Carrasco, D.; Pérez-Temprano, M. H.; García-Melchor, M.; Álvarez, R.; Casares, J. A.; Espinet, P. Stille Coupling Involving Bulky Groups Feasible with Gold Cocatalyst. *Angew. Chem., Int. Ed.*, **2013**, *52*, 2189–2193.



of conditions, due to the ease of ligand substitution and coupling processes followed by reoxidation. The evolution toward the oxidative addition complex can be easily monitored by <sup>19</sup>F NMR through the formation of (C<sub>6</sub>F<sub>n</sub>H<sub>5-n</sub>)<sub>2</sub>. In contrast, *cis*-[Pd(C<sub>6</sub>F<sub>n</sub>H<sub>5-n</sub>)(COD)] and the previously reported *cis*-[Pd(neophyl)(COD)] exhibit slower ligand substitution, retarding the complex formation. This difficulty is clearly observed when bulky ligands are employed.

The ease of ligand substitution at *cis*-[Pd(Ar<sup>F</sup>)(THF)<sub>2</sub>] complexes allows the isolation of elusive *cis*-[Pd(Ar<sup>F</sup>)(L)] intermediates, both with XantPhos and SPhos ligands. The latter show a P,C-chelation of SPhos, with the biaryl interacting with the fourth coordination site of Pd both in solution and in the solid state. On the other hand, [Pd(Ar)X(SPhos)] complexes, obtained after oxidative addition, exists as a mixture of monomer and dimer in equilibrium in solution, while they crystallize as the dimeric [Pd(Ar)(μ-X)(SPhos)]<sub>2</sub> species in the solid state.

The catalysis tests clearly show the reaction conditions where each *cis*-[Pd(Ar<sup>F</sup>)(L)] (L = 2 THF or COD) is preferred as precatalyst. When mild reaction conditions and nucleophiles are applied (C–N coupling), it is the THF precatalyst the one to be used, as it is easily activated. However, when high temperatures (Stille coupling) or strong nucleophiles (Negishi coupling) that open new activation pathways are employed, both can be used almost indistinctly.



## Chapter IV: Analysis of Metal-Ligand Interactions in [AuCl(L)] Complexes with Fluorinated PR<sub>2</sub>(biaryl) Phosphines

Biaryl phosphines have been frequently used in gold(I) catalysis, often in cyclization or cycloaddition reactions catalyzed by cationic complexes.<sup>1</sup> In the X-ray diffraction structures of [AuX{PR<sub>2</sub>(biaryl)}] complexes, whether cationic or neutral, the distal aryl of the biaryl group is systematically located roughly parallel to the Au–X bond, with one or two aryl carbon atoms at distances from gold in the range 3.02–3.30 Å. These structures have been examined on several occasions (Figure 1).<sup>2</sup> The proximity of the distal aryl to gold suggests mutual interactions, often referred to as weak interactions and sometimes as  $\pi$ -interactions. Recently, two theoretical studies on [AuX{PR<sub>2</sub>(biaryl)}] complexes have been published: one on the R<sup>F</sup> effect in a family of [Au(SR<sup>F</sup>)(JohnPhos)] thiolate complexes, with JohnPhos = P(*t*-Bu)<sub>2</sub>(*o*-C<sub>6</sub>H<sub>4</sub>-C<sub>6</sub>H<sub>5</sub>),<sup>3</sup> and another on Tolman cone angles of phosphine ligands in different metal coordinations, including [AuCl{PR<sub>2</sub>(biaryl)}] examples.<sup>4</sup>

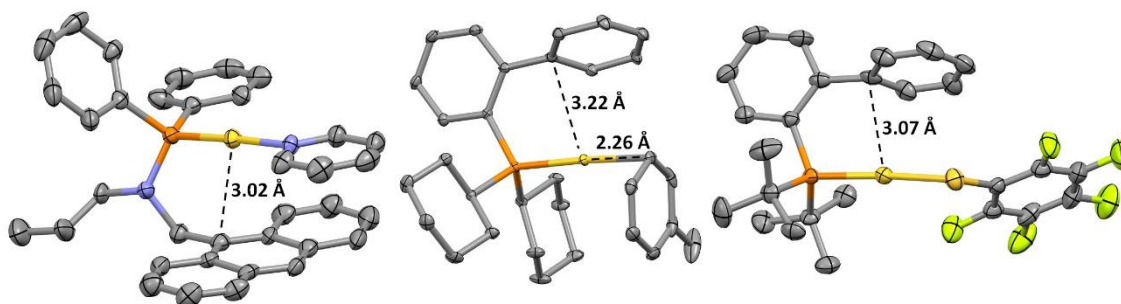


**Figure 1.** X-ray structures of selected Au complexes showing Au-arene interactions.

Considering these previous studies, we decided to evaluate the interaction with the Au–Cl zone of electronically different PR<sub>2</sub>(biaryl) phosphines. To meet this purpose, phosphines with varying fluorine substitution were synthesized (**L1–L6**, Figure 2). Including in the study the reported nonfluorinated PhJohnPhos (PhJ) and CyJohnPhos (CyJ) phosphines, we complete, for R = Ph, Cy, the sequences HH, HF, FH, and FF relative to proximal and distal aryl perfluorination or non-fluorination. Their Au(I) complexes (**1–6**) were obtained by ligand substitution from AuCl(*t*ht) in high yields (85–98 %), and their X-ray structures were determined. As expected, all of the X-ray diffraction structures display almost linear Cl–Au–P coordination, with the distal aryl

<sup>1</sup> (a) Nieto-Oberhuber, C.; López, S.; Echavarren, A. M. Intramolecular [4 + 2] Cycloadditions of 1,3-Enynes or Arylalkynes with Alkenes with Highly Reactive Cationic Phosphine Au(I) Complexes. *J. Am. Chem. Soc.*, **2005**, *127*, 6178–6179; (b) Liu, L.; Zhang, J. Gold-Catalyzed Transformations of  $\alpha$ -Diazocarbonyl Compounds: Selectivity and Diversity. *Chem. Soc. Rev.*, **2016**, *45*, 506–516; (c) Mascareñas, J. L.; Varela, I.; López, F. Allenes and Derivatives in Gold(I)- and Platinum(II)-Catalyzed Formal Cycloadditions. *Acc. Chem. Res.*, **2019**, *52*, 465–479.

<sup>2</sup> (a) Li, Q.-S.; Wang, C.-Q.; Zou, R.-Y.; Xu, F.-B.; Song, H.-B.; Wan, X.-J.; Zhang, Z.-Z. Gold(I)  $\eta^2$ -Arene Complexes. *Inorg. Chem.*, **2006**, *45*, 1888–1890; (b) Herrero-Gómez, E.; Nieto-Oberhuber, C.; López, S.; Benet-Buchholz, J.; Echavarren, A. M. Cationic  $\eta^1/\eta^2$ -Gold(I) Complexes of Simple Arenes. *Angew. Chem. Int. Ed.*, **2006**, *45*, 5455–5459.

<sup>3</sup> Moreno-Alcántar, G.; Hess, K.; Guevara-Vela, J. M.; Rocha-Rinza, M. T.; Pendás, A. M.; Flores-Álamo, M.; Torrens H.  $\pi$ -Backbonding and non-covalent interactions in the JohnPhos and polyfluorothiolate complexes of gold(I). *Dalton Trans.*, **2017**, *46*, 12456–12465.

<sup>4</sup> Jover, J.; Cirera, J. Computational assessment on the Tolman cone angles for P-ligands. *Dalton Trans.*, **2019**, *48*, 15036–15048.

group lying close to parallel to the Au–Cl bond. To be more precise, the distal aryl ring bends away from the Au–Cl bond so that C<sup>1</sup> has a noticeably shorter distance to this line than C<sup>4</sup>. The shortest distance for each complex is Au–C<sup>1</sup>, always shorter than the sum of Bondi vdW radii (3.36 Å).<sup>5</sup> Two structurally different kinds of X-ray structures are observed, as shown by the two examples in Figure 3. Most of them (**1**, **5**, [AuCl(CyJ)], **2**, **6**), are quite symmetrical, with the Au–Cl line almost exactly over the C<sup>1</sup>–C<sup>4</sup> line. In the others (AuCl(PhJ), **3**, and **4**), these two lines deviate. This observation suggest that the X-ray structures are altered by crystal forces.

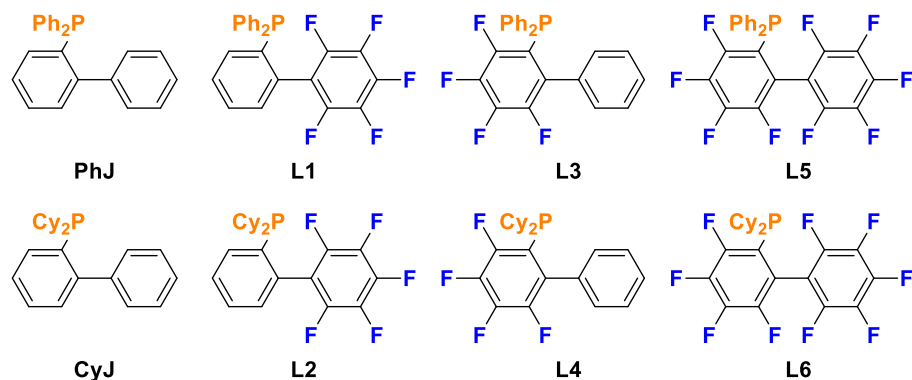


**Figure 2.** New fluorinated Buchwald-type biaryl phosphines and their two reference non-fluorinated phosphines.

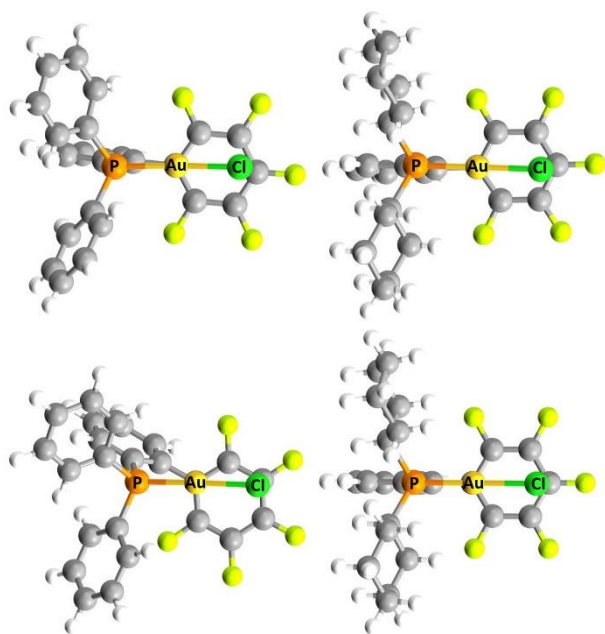


**Figure 3.** Examples of X-ray (the two above) and gas phase DFT optimized (the two below) structures of [AuCl(L1)] (**1**) (left) and [AuCl(L2)] (**2**) (right), viewed along the Au...C<sup>1</sup> imaginary line (in this view, C<sup>1</sup> is eclipsed by the Au above it).

<sup>5</sup> (a) Bondi, A. Van der Waals Volumes and Radii. *J. Phys. Chem.*, **1964**, *68*, 441–451; (b) Bondi, A. van der Waals Volumes and Radii of Metals in Covalent Compounds *J. Phys. Chem.*, **1966**, *70*, 3006–3007.

To avoid the alterations produced in the solid state, DFT calculations were carried out to obtain gas-phase optimized structures.<sup>6</sup> These structures would be only subjected to intramolecular forces. There are calculated structures more symmetrical (all the Cy complexes) and less symmetrical (all the Ph complexes). This does not always coincide with their X-ray cases (Figure 3, structures at the left). It seems that the less regular structural behavior of the DFT optimized Ph series is caused by different rotational arrangements of the aryls.

A consequence of this asymmetry in Ph complexes is that the Au–Cl moiety mainly interacts with one half of the distal aryl. Moreover, the tilting of the distal aryl, which is not evident from the view in Figure 3, brings this half of the distal aryl closer to the Au–Cl. This tilting is observed for all the structures and, in consequence, the Au–C<sup>2</sup> distance is smaller than the Au–C<sup>6</sup> in all cases.

An interesting study of biaryl phosphine gold(I) cationic [Au{PR<sub>2</sub>(biaryl)}-(arene)]<sup>+</sup> complexes provides information on covalent Au<sup>I</sup>–arene bond distances trans to P.<sup>7</sup> The study concluded that significant interactions with arenes should show distances of less than 2.95 Å for Au<sup>I</sup>. Obviously, the term “significant interactions” means covalent interactions involving positive orbital overlapping and net charge transfer between atoms. Above this distance (2.95 Å), calculations indicate conclusively that no electron transfer occurs from the arene to the metal and that the interaction does not have any covalent character.<sup>7</sup> If we take 2.95 Å as the “bond” limit for gold(I) and arenes, moving beyond 2.95 Å from Au, we are getting into the “beyond bond” domain. There, we speak of “weak interactions”, “no-bond” interactions, or noncovalent interactions (NCI). These interactions include attractive and repulsive electrostatic interactions, dipole inductions (polarizations), and attractive interactions between instantaneous multipoles (London dispersion) and, as a whole, are often referred to as van der Waals (vdW) forces. The term “closed shell” is also applied to them in contrast with the “shared-shell” (covalent) interactions.

The vdW radius is well-defined for simple entities not prone to exchange electron density, as in the case of two contacting noble-gas atoms. If we take the most used values proposed by Bondi, the expected Au–C vdW distance is 3.36 Å. In our complexes, the Au–C<sup>1</sup> and Au–C<sup>2</sup> distances are significantly shorter (e.g., 3.066 and 3.237 Å in complex **4**). It makes sense to ask why, in the isolated molecule and in the absence of covalent Au–C interactions, the biphenyl ring still chooses to get so close to gold (structure **A** in Figure 4), forcing the ligand to adopt unnatural bending angles (15–20°) between the Au–P and the inter-ring C<sub>ipso</sub>–C<sup>1</sup> bond lines,<sup>8</sup> as well as “no bond” distances shorter than the sum of vdW radii, instead of taking any other orientation not requiring structural distortion of the ligand (e.g. **B** in Figure 4).

<sup>6</sup> Calculations were made using the dispersion-corrected hybrid functional ωB97X-D, considered to be better for long-range distances compared to B3LYP and B3LYP-D3.

<sup>7</sup> Pérez-Galán, P.; Delpont, N.; Herrero-Gómez, E.; Maseras, F.; Echavarren, A. M. Metal-Arene Interactions in Dialkylbiarylphosphane Complexes of Copper, Silver, Gold. *Chem. - Eur. J.*, **2010**, *16*, 5324–5332.

<sup>8</sup> Partyka, D. V; Robilotto, T. J.; Zeller, M.; Hunter, A. D.; Gray, T. G. Dialkylbiarylphosphine Complexes of Gold(I) Halides. Gold-Aryl π-Interactions in the Solid State. *Organometallics*, **2008**, *27*, 28–32.

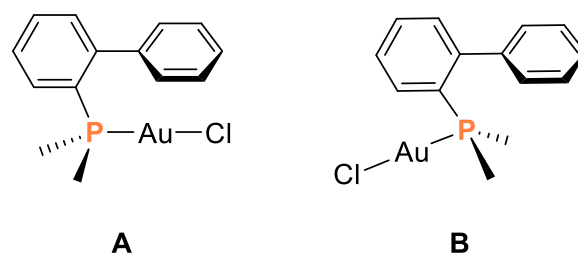


**Figure 4.** Alternative structures with (A) and without (B) a short Au–C<sup>1</sup> distance.

The thermodynamic net stabilization of structure **A** vs **B** was calculated for all the [AuCl{PR<sub>2</sub>(biaryl)}] complexes of this study, affording values in the range 1–10 kcal mol<sup>-1</sup> (Table 1). For structure **A** to be the preferred thermodynamic result, the “weak interactions”, certainly enhanced at shorter distances, should compensate and overcome the cost of structurally forcing the ligand. There is a clear higher stabilization for the fluorinated Cy complexes **2**, **4**, and **6** than for their nonfluorinated reference [AuCl(CyJ)]. The adoption of structure **A** occurs with similar success for any complex, be it fluorinated or not. In order to get additional information about the F effect on the interactions existing in the zone beyond the Au–C covalent bond frontier, QTAIM studies were carried out.<sup>9,10</sup>

**Table 1.** Calculated Higher Stability of Structure **A** vs **B** ( $\Delta\Delta G^\circ$  in kcal mol<sup>-1</sup>) for [AuClL<sup>n</sup>] in the Gas Phase

Complex	$\Delta\Delta G^\circ$ A-B	Complex	$\Delta\Delta G^\circ$ A-B
[AuCl(PhJ)] (PhHH)	-5.2	[AuCl(CyJ)] (CyHH)	-0.9
[AuCl(L1)] (PhHF)	-2.3	[AuCl(L2)] (CyHF)	-3.4
[AuCl(L3)] (PhFH)	-6.6	[AuCl(L4)] (CyFH)	-5.7
[AuCl(L5)] (PhFF)	-3.4	[AuCl(L6)] (CyFF)	-8.9

#### Topological analysis of the distal aryl region

The gradient line maps (GLMs) of the distal aryls for structures **A** were examined, looking for possible effects of H and F substitution in the ligands. Figure 5 compares the distal aryls of complexes [AuCl(CyJ)] (CyHH) and **6** (CyFF), which differ in the fluorination of the biphenyl aryl in **6**. These GLM display 12 (3, -1) critical points (CP), corresponding to the 6 C–C<sub>(ring)</sub> bonds, 1 C<sup>1</sup>–C<sub>ipso</sub> bond, and 5 C–H bonds or 5 C–F bonds (blue); in addition, the (3, +1) ring CP (orange) appears. The positions of the bond CPs reflect clearly their polarization: the 6 CP(C–C)<sub>ring</sub> are centered, the CP(C–H) are closer to H than to the C(sp<sup>2</sup>) atom, and the CP(C–F) are much closer to C(sp<sup>2</sup>) than to F.

<sup>9</sup> Atoms in Molecules: A Quantum Theory. Bader, R.F.W. Oxford University Press: Oxford, U.K., 1990.

<sup>10</sup> The Quantum Theory of Atoms in Molecules. Matta C. F. and Boyd R. J., eds. WILEY-VCH Verlag GmbH & Co. KGaA, Weinheim, 2007.

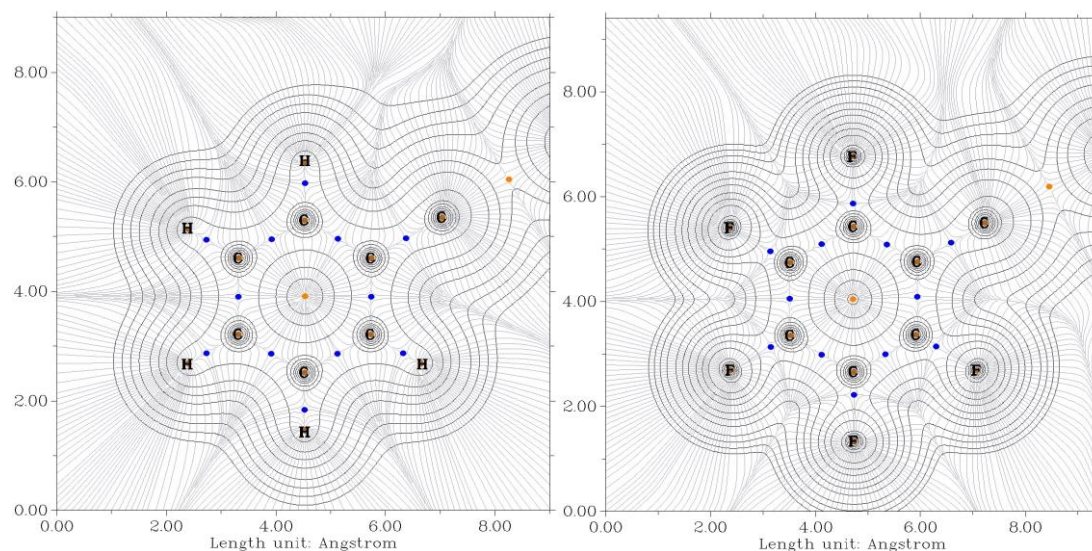


**Figure 5.** GLMs with contour lines for the distal aryls of complexes [AuCl(CyJ)] (left) and [AuCl(L6)] (right). Blue dots are (3, -1) CPs, and orange dots are (3, +1) CPs.

The data of atomic charges provides interesting information. The  $C^2$ – $C^6$  and  $H^2$ – $H^6$  Bader charges in [AuCl(CyJ)] are very close to zero, as expected for C–C and C–H bonds of very low polarity. In contrast, the very polar C–F bonds in [AuCl(L6)] give rise to large positive charges for  $C^2$ – $C^6$  (about 0.59–0.67 au) and large negative charges of similar magnitude for  $F^2$ – $F^6$ . For  $C^1$ , a moderate positive charge of 0.0555 au is found in [AuCl(L6)], in comparison to the small negative charge of -0.0125 au in [AuCl(CyJ)], with a total variation of 0.0680 au upon H by F substitution.

#### *Topological analysis of the gold region*

Since the Au– $C^1$  distance is noticeably shorter in complex **6**, this suggests that, against initial intuition, the effect of distal aryl fluorination on carbon atoms is contracting its electronic cloud, thus reducing the repulsive interelectronic interactions with gold and allowing for a closer approximation of the two nuclei at an attraction–repulsion equilibrium.

The eight complexes show the presence of two (3, -1) critical points, as displayed in the GLM of complex **1** (Figure 6): one between the two aromatic carbon atoms more involved in gold interaction,  $CP(C^1-C^2)$ , and one between the Au atom and  $C^1$ ,  $CP(C^1-Au)$ . It is noteworthy that the latter is placed practically on the Au... $C^1$  line and far from the Au... $C^2$  line in all the complexes, with  $C^1$ –CP–Au angles in the range 172.5–177.1°. This supports that, in the interaction between gold and the  $C^2$ – $C^1$ – $C^6$  triangle,  $C^1$  is dominant as commented above.

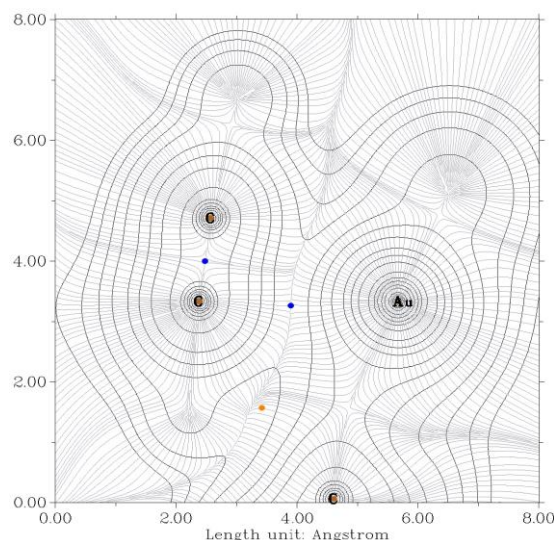


**Figure 6.** GLM with contour lines for complex **1**. The plane chosen is defined by Au (right), C<sup>1</sup> (bottom left), and C<sup>2</sup> (top left). Blue dots are (3, -1) CPs.

The electron density  $\rho(r_{cp})$  values at the CP(C<sup>1</sup>–C<sup>2</sup>) (Table 2, column 2, entries 1–8) are quite high ( $>0.30$  au), consistent with multiple covalent bonds. In contrast  $\rho(r_{cp})$  values at CP(C<sup>1</sup>–Au) (Table 2, column 3) are extremely low (about 0.01 au), consistent with NCI contacts between C<sup>1</sup> and Au. The CP(C<sup>1</sup>–Au) position marks the boundary of atomic domains (basins) of the two interacting atoms in the C<sup>1</sup>–Au direction. Consequently, we can assign the C<sup>1</sup> to CP and Au to CP distances as the corresponding local vdW radii of C<sup>1</sup> and Au under the interaction pressure (Table 2, columns 4 and 5).

**Table 2.** Electron Density at (3, -1) CPs (eu) and vdW Contact Radii (Å) in [AuCl{PR<sub>2</sub>(biphenyl)}] Complexes

Entry/ Complex	$\rho(r_{cp})$ C <sup>1</sup> –C <sup>2</sup>	$\rho(r_{cp})$ C <sup>1</sup> –Au	d CP–C <sup>1</sup> / Å	d CP–Au/ Å	Au–C <sup>1</sup> / Å
<b>1</b> / [AuCl(PhJ)]	0.3095	0.0111	1.541	1.816	3.351
<b>2</b> / [AuCl(L1)] (HF)	0.3138	0.0126	1.520	1.772	3.289
<b>3</b> / [AuCl(L3)] (FH)	0.3105	0.0127	1.499	1.762	3.258
<b>4</b> / [AuCl(L5)] (FF)	0.3152	0.0145	1.480	1.722	3.199
<b>5</b> / [AuCl(CyJ)]	0.3101	0.0120	1.518	1.772	3.287
<b>6</b> / [AuCl(L2)] (HF)	0.3153	0.0136	1.494	1.740	3.233
<b>7</b> / [AuCl(L4)] (FH)	0.3108	0.0129	1.492	1.747	3.237
<b>8</b> / [AuCl(L6)] (FF)	0.3156	0.0145	1.475	1.719	3.193
<b>9</b> / [AuCl(L1)] XRay	0.3265	0.0149	1.466	1.714	3.173

Both *local* radii are shorter or much shorter in all of our complexes than the vdW radii values in the literature,<sup>5</sup> confirming that they are compressed in the direction of interaction, under the effect of intramolecular forces. The C atom radius shrinks to about 88% of its value in literature tables. Very interestingly, the Au<sup>I</sup> radius shrinks more, to about 75% of its value in the literature tables, suggesting that this gold(I) is softer (hence more polarizable) than C(sp<sup>2</sup>) in these complexes. The X-ray structure of complex **1** (Table 2, entry 9), examined as an example of a solid-state circumstance, is consistent with the same analysis. Its parameters afford *local* vdW radii even lower than those for the molecular calculations, under the higher stress of crystal forces.



A similar result can be obtained for the chloro region. In this case, the softer Cl electron density assumes most of the polarization in the interaction and its local vdW radius is clearly expanded in the Cl...C<sup>4</sup> direction.

#### Noncovalent Interaction Analysis (NCI)

Since the meaning of QTAIM analysis has sometimes been disputed when particularly weak noncovalent atomic interactions are involved,<sup>11</sup> as is the case, we have performed a noncovalent interaction analysis (NCI),<sup>12</sup> to visualize the clash zones and get a three-dimensional picture of the interactions between the Au–Cl zone and the distal aryl. The representative cases of complex **1** for the asymmetrical structure and complex **2** for the more symmetrical structure were analyzed.

For the asymmetric complex **1**, the green-brown gradient isosurface (Figure 7) shows a continuum of attractive and repulsive weak interactions, spanning from C<sup>1</sup> to C<sup>4</sup>, between the pentafluorophenyl distal ring and the Au–Cl fragment.

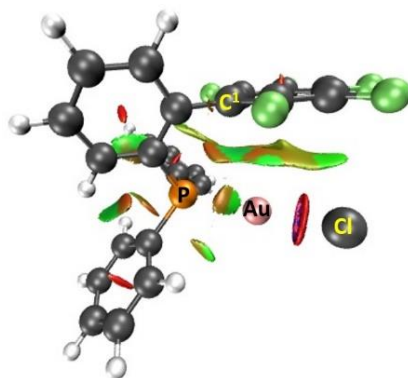


**Figure 7.** Gradient isosurface ( $s = 0.5$  au) for complex **1**, shown on a blue–green–red scale according to values of  $\text{sign}(\lambda_2)\rho$ , ranging from  $-0.04$  to  $0.02$  au: green, weak attractive interactions; red, strong nonbonding overlap.

Reducing the  $s$  value from  $s = 0.5$  au to  $s = 0.35$  au (Figure 8, left) and examining the gradient surface from above the pentafluorophenyl ring (Figure 8, right) provide a more informative view and allows identification of two areas of higher interaction: one that confirms a concentration of weak attractive interaction in the Au/C<sup>1</sup>/C<sup>2</sup> zone and another that recognizes weak attraction forces focused in the Cl/C<sup>3</sup>/C<sup>4</sup> zone. This separation into two zones is in part an artifact provoked on purpose to facilitate the analysis. The truth is that each molecular component has an influence on the others, and the structural equilibrium (distances) and the charges and electronic density at each point are the result of the global effect of many concerted interactions. This explains again why it is not possible to achieve precise correlations in comparing individual local magnitudes observed in the DFT and QTAIM studies (e.g., distances to gold) and local data (e.g., charges on gold).

<sup>11</sup> (a) Shahbazian, S. Why Bond Critical Points Are Not “Bond” Critical Points. *Chem. - Eur. J.*, **2018**, *24*, 5401–5405; (b) Foroutan-Nejad, C.; Shahbazian, S.; Marek, R. Toward a Consistent interpretation of the QTAIM: Tortuous Link between Chemical Bonds, Interactions, and Bond/Line Paths. *Chem. - Eur. J.*, **2014**, *20*, 10140–10152.

<sup>12</sup> Johnson, E. R.; Keinan, S.; Mori-Sánchez, P.; Contreras-García, J.; Cohen, A. J.; Yang, W. Revealing Noncovalent Interactions. *J. Am. Chem. Soc.*, **2010**, *132*, 6498–6506.

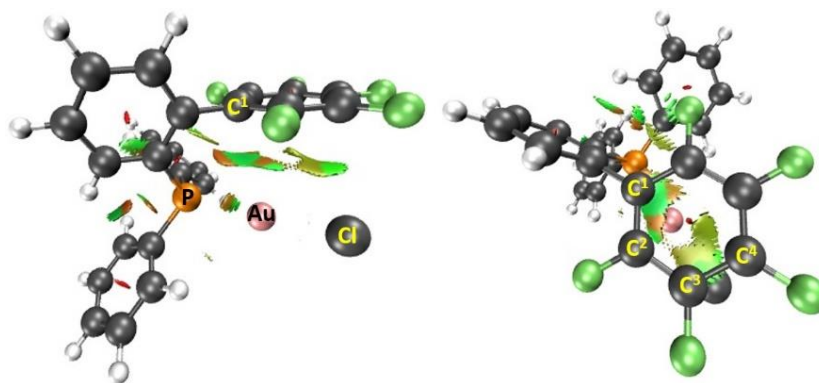


**Figure 8.** Two views of the gradient isosurface ( $s = 0.35$  au) for complex **1**. The same color codes are used as in Figure 7.

Figure 9 allows a direct comparison of asymmetrical *vs.* symmetrical (top *vs.* bottom) and nonfluorinated *vs.* fluorinated (left *vs.* right) in the complexes [AuCl(PhJ)], [AuCl(L1)] (**1**), [AuCl(CyJ)], and [AuCl(L2)] (**2**). It can be noted that, for the symmetrical Cy complexes, the C<sup>4</sup> interactions with Cl (this atom is hidden behind the gradient isosurface) and the C<sup>1</sup> interactions with Au are, according to the color code, apparently well-defined for the nonfluorinated [AuCl(CyJ)] (Figure 9, bottom left), and for **2** (Figure 9, bottom right). For the less symmetrical [AuCl(PhJ)] (Figure 9, top left) and **1** (Figure 9, top right) the asymmetry seems particularly detrimental for the Cl–C<sup>4</sup> interaction, in favor of Cl–C<sup>3</sup>.

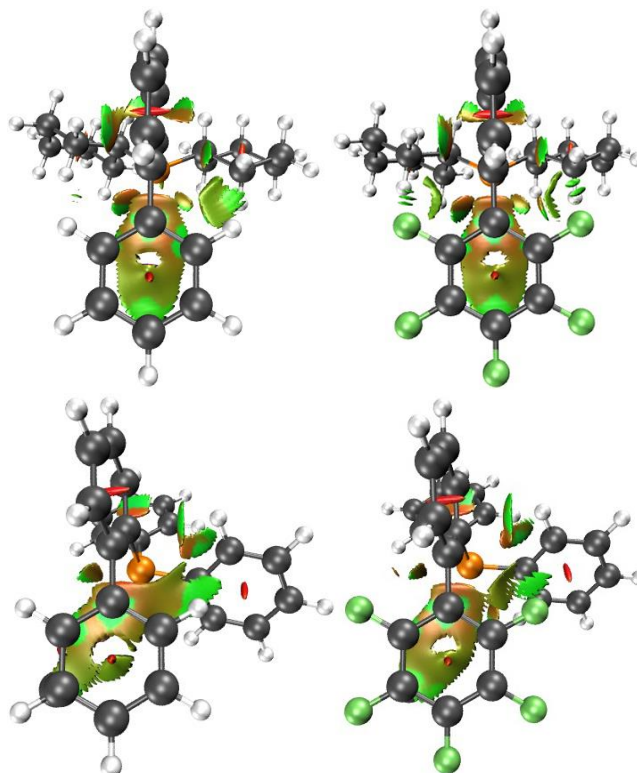


**Figure 9.** Gradient isosurfaces ( $s = 0.50$  au) of [AuCl(CyJ)] (top left), **2** (top right), [AuCl(PhJ)] (bottom left), and **1** (bottom right) viewed along the Au...C<sup>1</sup> imaginary line (Au is eclipsed by the C<sup>1</sup> above it).

## NBO Analysis

In order to have an approximate estimation of the energy of the noncovalent interactions observed, we have carried out an NBO analysis (Table 3 shows the values for **6**). As expected, all of the  $E_{\text{SOPT}}$  contributions are very small, in comparison to the values for covalent bonds. The stronger interactions correspond systematically to several  $\pi$ -bond donations from the ring to an empty (99.4% p) orbital of gold. NBOs representing potential donations from Au to aryl BD\* orbitals are not found, meaning that this kind of interaction is less significant. On the other hand, LP Cl (99.4–99.8% p) donations, not only to BD\* C–C, but also to BD\* F–C bonds are found. These interactions are weak but not insignificant.

**Table 3.** Donor and acceptor NBOs and  $E_{\text{SOPT}}$  values ( $\text{kcal mol}^{-1}$ ) for ring interactions with Au (values above 0.5) and with Cl (values above 0.05) for [AuCl(L**6**)]

Entry	Donor NBO	Acceptor NBO	$E_{\text{SOPT}}/\text{kcal mol}^{-1}$
<b>1</b>	30. BD(1) C <sup>1</sup> -C <sup>6</sup>	111. LP*(8) Au	2.06
<b>2</b>	32. BD(1) C <sup>1</sup> -C <sup>2</sup>	111. LP*(8) Au	1.84
<b>3</b>	39. BD(1) C <sup>6</sup> -C <sup>5</sup>	111. LP*(8) Au	1.50
<b>4</b>	40. BD(1) C <sup>4</sup> -C <sup>3</sup>	111. LP*(8) Au	1.14
<b>5</b>	41. BD(1) C <sup>4</sup> -C <sup>5</sup>	111. LP*(8) Au	1.28
<b>6</b>	49. BD(1) C <sup>3</sup> -C <sup>2</sup>	111. LP*(8) Au	1.23
<b>7</b>	113. LP(2) Cl	574 . BD*(1) F <sup>4</sup> -C <sup>4</sup>	0.06
<b>8</b>	113. LP(2) Cl	598. BD*(2) C <sup>4</sup> -C <sup>5</sup>	0.07
<b>9</b>	114. LP(3) Cl	574. BD*(1) F <sup>4</sup> -C <sup>4</sup>	0.08
<b>10</b>	114. LP(3) Cl	598. BD*(2) C <sup>4</sup> -C <sup>5</sup>	0.23

For the whole series, the sum of computed  $E_{\text{SOPT}}$  is in the range 2–10  $\text{kcal mol}^{-1}$ , which is very consistent with the computed values for the difference in stabilities between structures **A**, where these NCIs exist, and structures **B**, where they have been broken.

In summary, in the distal-aryl/Au–Cl zone of the [AuCl{PR<sub>2</sub>(biaryl)}] complexes, the interactions with gold occur at distances shorter than the sum of vdW radii, whereas the interactions with Cl occur at distances larger than the sum of vdW radii. Consequently, the noncovalent interactions holding the aryl attached to the Au–Cl fragment consist mostly of a significant polarization of the  $\pi$ -aryl electron density (not only that involving C<sup>1</sup>) by gold and a Cl polarization by the aryl carbon atoms, weaker but still operating at a greater distance. The overall balance of interactions is significantly stronger, and the vdW distances shorter, for the phosphines with a fluorinated distal aryl, creating higher charges on the aryl C<sup>2</sup>–C<sup>6</sup> carbon atoms.



## Chapter V: Synthesis of Fluorophosphoranes from Fluorinated Biaryl Phosphines by Intramolecular $S_NAr$

During the synthesis of the  $PR_2$ (biaryl) phosphines, perfluorinated at one or the two aryls, described in Chapter III (Figure 1), we observed that the synthesis of **1** provided the product in much lower yield than the others (47% *vs.* >70%). Since no phosphine oxide formation was detected, we decided to take a closer look to possible decomposition pathways that would eventually lead to the lower yield observed.

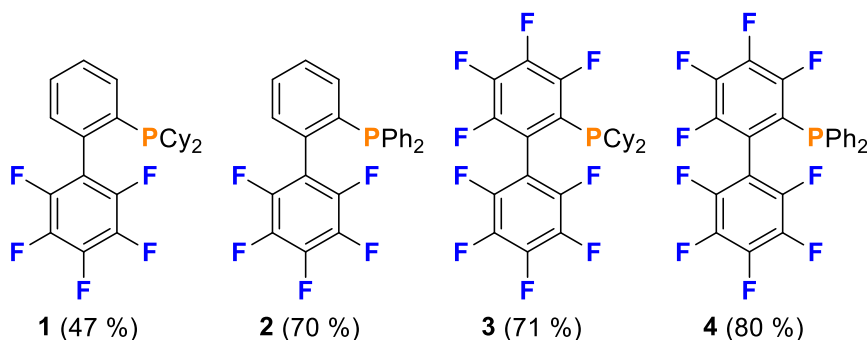


**Figure 1.** Fluorinated  $PR_2$ (biaryl) phosphines (isolated yields in parenthesis) that show thermal decomposition.

When a solution of **1** was left at room temperature for one day, a new species was observed by  $^{19}F$  NMR (Figure 2). This new compound shows a characteristic doublet at -47 ppm, with a  $J = 704$  Hz.

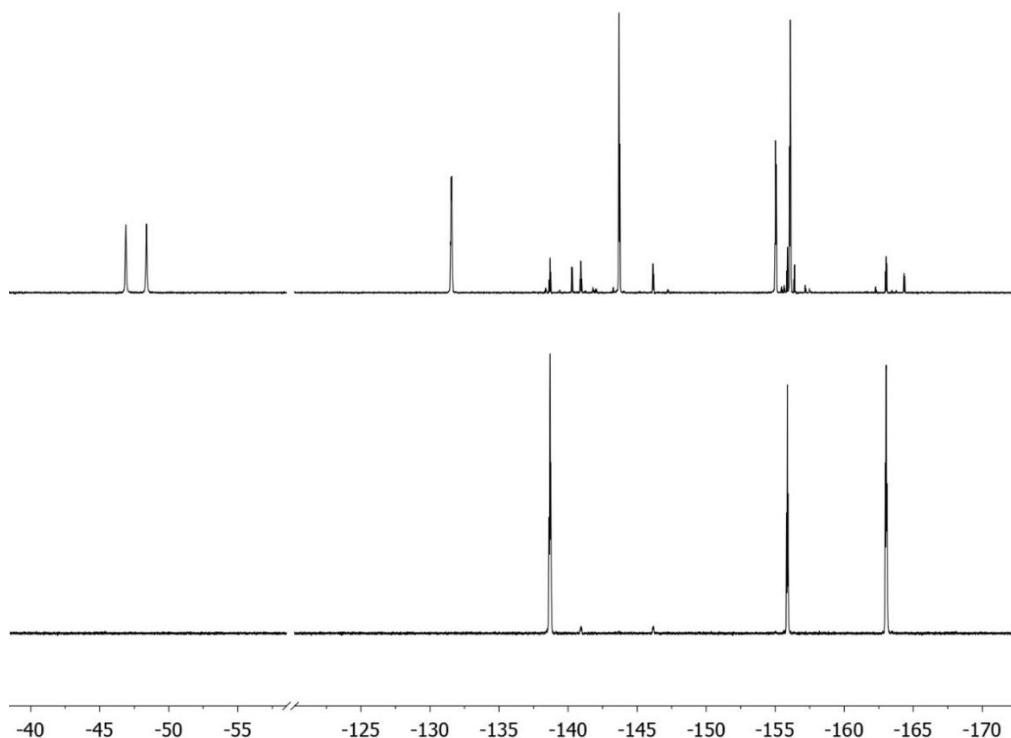


**Figure 2.**  $^{19}F$  NMR spectrum of **1** in  $CDCl_3$  after 5 min (bottom) and 24 h (top) at room temperature.

Such a high coupling constant indicates that the fluorine atom is directly bonded to an NMR active nucleus which, for this molecule, could only be the phosphorous. Indeed, a similar resonance was also observed in the  $^{31}\text{P}$  NMR spectrum, with an upfield chemical shift of -55.9 ppm. This signal is a doublet of doublets, with  $J = 704$  and 19 Hz, thus confirming the P–F bond. Moreover, the second coupling constant indicates that another fluorine atom is part of the P atom spin system. This observation suggests an intramolecular process where the P atom has inserted in the  $C_{ortho}$ -F bond of the distal aryl.

A similar transformation was also observed, although at higher temperatures, for the other phosphines fluorinated at the distal aryl (2–4). After careful examination of the NMR spectra, the products were assigned as the P(V) fluorophosphoranes 5–8 shown in Figure 3.

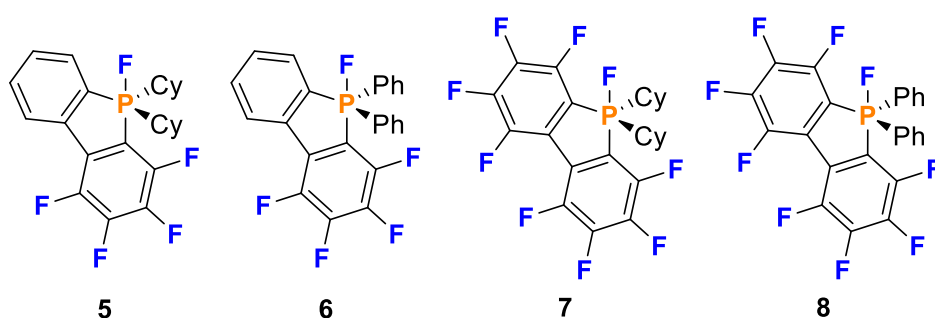
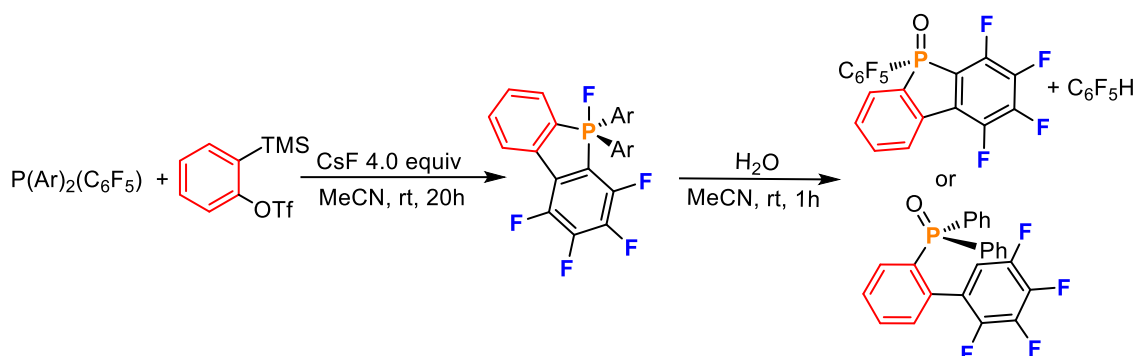


**Figure 3.** Fluorophosphoranes obtained as isomerization products of  $\text{PR}_2(\text{biaryl})$  phosphines.

Fluorophosphoranes are elusive species due to their high reactivity and the first three isolated examples with aryl substituents at the P atom have been recently reported by Tobisu *et al* (Scheme 1).<sup>1</sup> This methodology requires the use of  $\text{P}(\text{C}_6\text{H}_n\text{F}_{5-n})_3$  ligands and the synthesis of a precursor for slow *in situ* generation of an aryne intermediate. Once the fluorophosphorane is obtained, its hydrolysis produces phosphine oxides, which maintain or not the dibenzophosphole moiety depending on the electron density of the aryls in the fluorophosphorane. One of the fluorophosphoranes isolated by Tobisu is compound 6 and this allowed us to confirm the identity of our products by direct comparison of NMR data.

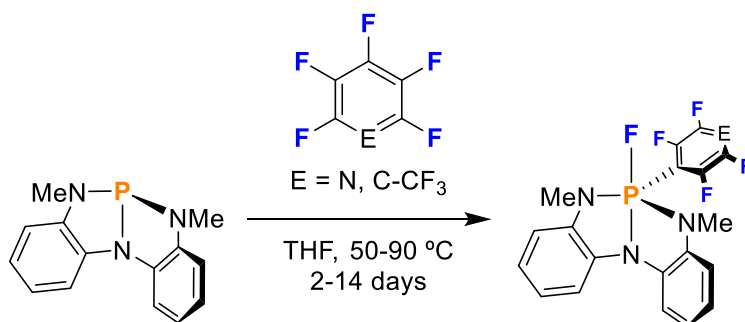
<sup>1</sup> Fujimoto, H.; Kusano, M.; Kodama, T.; Tobisu, M. Aryne-Induced  $S_NAr$ /Dearylation Strategy for the Synthesis of Fluorinated Dibenzophospholes from Triarylphosphines via a P(V) Intermediate. *Org. Lett.*, **2020**, *22*, 2293–2297.



**Scheme 1.** Reported synthesis of fluorophosphoranes and hydrolysis to dibenzophospholes. TMS = trimethylsilyl. OTf = triflate.

The intermolecular oxidative addition to  $Ar^F-F$  bonds of pentafluoroarene derivatives by the  $C_s$ -symmetric electron-rich  $P(N_3)$  ( $N_3 = N[C_6H_4-NMe-o]_2$ ) has also been reported by Radosevich *et al.* (

**Scheme 2**).<sup>2</sup> The X-ray structures of the  $FP(Ar^F)(N_3)$  fluorophosphoranes obtained show  $N_3$  occupying one apical and two equatorial positions. In this case, the use of a geometrically constraining backbone at the phosphine enhances its biphilic (electrophilic and nucleophilic) character, allowing the reaction to take place.<sup>3</sup>



**Scheme 2.** Oxidative addition of perfluoroarenes to a phosphorous triamide.

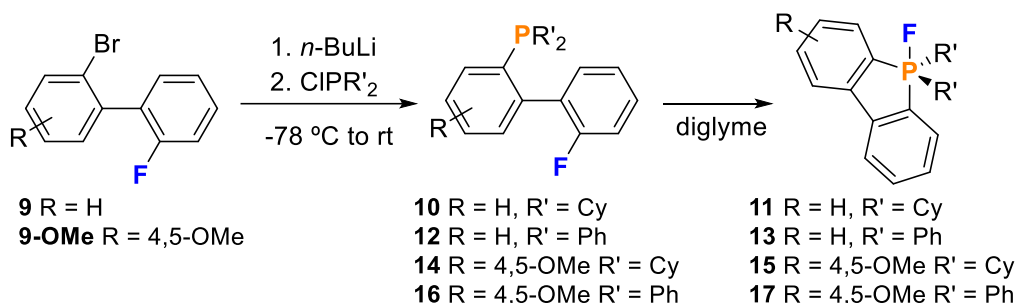
Considering the two reported procedures to obtain fluorophosphoranes, some drawbacks were observed for both of them. In Tobisu's method, the need of an aryne precursor limits the general scope of the reaction to the obtention of this reagent. On the other hand, Radosevich's method is limited to the reaction between highly biphilic phosphines and perfluorinated arenes and requires long reaction times.<sup>4</sup> Hence, based on the decomposition process observed for phosphines **1–4**, we wondered whether a different methodology could be developed. The proposed synthetic procedure shown in Scheme 3 could be a convenient, fairly direct and general alternative for the synthesis of fluorophosphoranes. Requiring the insertion of the P atom to a  $C(sp^2)-F$  bond, it would also be feasible with moderately basic phosphines due to the intramolecular nature of the

<sup>2</sup> Lim, S.; Radosevich, A. T. Round-Trip Oxidative Addition, Ligand Metathesis, and Reductive Elimination in a  $P^{III}/P^V$  Synthetic Cycle. *J. Am. Chem. Soc.*, **2020**, *142*, 16188–16193.

<sup>3</sup> Lee, K.; Blake, A. V.; Tanushi, A.; McCarthy, S. M.; Kim, D.; Loria, S. M.; Donahue, C. M.; Spielvogel, K. D.; Keith, J. M.; Daly, S. R.; Radosevich, A. T. Validating the Biphilic Hypothesis of Nontrigonal Phosphorus(III) Compounds. *Angew. Chem., Int. Ed.*, **2019**, *58*, 6993–6998.

<sup>4</sup> It is important to note that fluorophosphorane synthesis is not the main goal in Radosevich's report.

process. Ideally, this cyclization step would not show any functional group incompatibility, as long as the temperature required to promote the process does not contribute to any other decomposition. Therefore, the scope of the method would only be determined by the existing methods to prepare the fluorinated phosphine to be cyclized and by the cyclization barrier. Fortunately, several methodologies for the synthesis of biaryls and aryl phosphines can be found in the literature.



**Scheme 3.** Two-step synthetic route to access fluorophosphoranes.

The results of some tested conditions are shown in Table 1. The observed cyclization is an isomerization promoted by  $S_NAr$  attack of P to the C2'(F) atom at the distal aryl of the biaryl. Hence, it is possible to establish structure-activity relationships for the process. The relative nucleophilicity of the P atom for the R' Ph/Cy pairs can be estimated based on their  $^{31}\text{P}$  chemical shift. For all cases, cyclohexylic phosphines showed a higher nucleophilicity than the phenylic ones.<sup>5</sup> Therefore, the temperature required to promote the  $S_NAr$  is lower for the cyclohexylic phosphines. On the other hand, phosphines with an electron-rich distal aryl (compared to a perfluorinated aryl) have a less electrophilic C(2)'F carbon and require increasing the temperature. This analysis explains why phosphine **1** evolved detectably fast at room temperature, as it combines the most nucleophilic P atom and a strongly electrophilic C(2)'F carbon (more fluorination in the aryl > less fluorination). Nevertheless, all of them cyclize when heated in toluene or diglyme in the temperature range 90–150 °C. The conversion of the starting phosphine can be brought close to 100 % using longer times or higher temperatures. It is noteworthy that the transformation is highly chemoselective, and significant amounts of phosphine oxide are only exceptionally formed.

<sup>5</sup> Only pairs with identical biphenyl should be compared because different biphenyls produce different anisotropic shielding on P.



**Table 1.** Reaction conditions and yields for the isomerization of 2'-F,2-(PR'<sub>2</sub>)biaryls.

Entry/ Phosphine	$\delta^{31P^a}$	Prod.	T/ °C	t/ h	Yield <sup>b</sup> / %	Phos/Prod/Oxide
1/ 1	-6.9	<b>5</b>	90 <sup>c</sup>	6	95(82)	4/95/1
2/ 2	-10.6	<b>6</b>	100 <sup>c</sup>	23	94 (85)	4.5/94/1.5
3/ 3	+5.8	<b>7</b>	90 <sup>c</sup>	21	97 (78)	2/97/1
4/ 4	-11.3	<b>8</b>	100 <sup>c</sup>	27	83 (75)	6/83/11
5/ 10	-10.5	<b>11</b>	130 <sup>d</sup>	22	98 (86)	0.5/98/1.5
6/ 12	-12.1	<b>13</b>	150 <sup>d</sup>	96	72(63)	26/72/2
7/ 14	-10.6	<b>15</b>	130 <sup>d</sup>	22	95(91)	3/95/2
8/ 16	-12.7	<b>17</b>	150 <sup>d</sup>	96	39(-) <sup>e</sup>	39/39/22

<sup>a</sup> In CDCl<sub>3</sub>. <sup>b</sup> Determined by <sup>19</sup>F and <sup>31</sup>P NMR. Isolated yield in parenthesis. The lower isolated yields are due to the high solubility of these compounds. <sup>c</sup> In toluene. <sup>d</sup> In diglyme. <sup>e</sup> Slow reaction and higher decomposition prevent clean isolation.

Pentacoordinated P(V) compounds usually adopt a trigonal bipyramidal structure. It was possible to obtain the X-ray structures of compounds **6**, **7** and **11** (Figure 4). Along with one structure reported by Tobisu,<sup>1</sup> they all show that the fluorine atom is placed in an apical position and the biaryl takes one equatorial and one apical position, leading to a C1-P-C2 bond angle of approximately 90° that is preferred for 5-member cycles. The two other carbon substituents take the remaining two equatorial positions (approximately 120° bond angle) to minimize electron repulsions.<sup>6</sup>

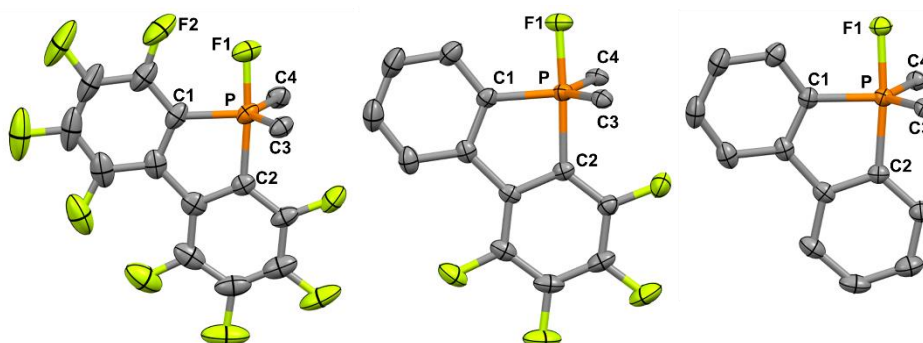


**Figure 4.** X-ray structure of **7** (left), **6** (middle) and **11** (right). H atoms, and Ph and Cy rings (except C3 and C4) omitted for clarity. Relevant bond distances (Å): **7**: P-C1 = 1.848, P-C2 = 1.906. **6**: P-C1 = 1.822, P-C2 = 1.912. **11**: P-C1 = 1.831, P-C2 = 1.902.

The structures observed in solution display NMR signals also coincident with the exclusive existence of the solid state structures. A potential equilibrium between the fluorophosphorane and its corresponding phosphonium fluoride is not observed. For instance, the <sup>19</sup>F NMR spectra of **7** display nine sharp signals, one for the P bounded F atom, and eight corresponding to the non-equivalent F atoms of the biaryl group (Figure 5). This nonequivalence also supports that the biaryl is occupying one equatorial and one apical position. The <sup>1</sup>H and <sup>13</sup>C{<sup>1</sup>H} NMR spectra indicate that the cyclohexyl

<sup>6</sup> VSEPR Theory: (a) Gillespie, R. J.; Nyholm, R. J. *Inorganic stereochemistry. Q. Rev. Chem. Soc.*, **1957**, *11*, 339–380; (b) Bader, R. F. W.; Gillespie, R. J.; MacDougall, P. J. A physical basis for the VSEPR model of molecular geometry. *J. Am. Chem. Soc.*, **1988**, *110*, 7329–7336; (c) Gillespie, R. J. Fifty years of the VSEPR model. *Coord. Chem. Rev.*, **2008**, *252*, 1315–1327.

substituents are equivalent, thus, they are placed in the two equatorial positions left. Finally, the F atom on P is assigned the second apical position.

While the  $^{31}\text{P}$  NMR chemical shifts spans in a 24-ppm range for the obtained fluorophosphoranes, the  $^{19}\text{F}$  NMR chemical shifts of the apical fluorine nucleus vary in a wider range of approximately 74 ppm (Table 2). All the compounds show a large  $^1J_{\text{F-P}}$  coupling for the apical F in the 650–770 Hz range. The perfluorinated compounds **7** and **8** also show a through space coupling between the apical F and one  $\text{C}(\text{sp}^2)\text{-F}$  fluorine atom, with a  $^{\text{ts}}J_{\text{F-F}} = 140\text{--}150$  Hz (Figure 5, zoomed spectra), indicating a short distance between them. This proximity between the apical F atom and the ortho F atom of one aryl is confirmed with the X-ray structure of **7**.  $\text{F}^1$  and  $\text{F}^2$  respectively, in Figure 4, show a 2.364 Å distance, which is below the sum of vdW radii (2.92 Å).<sup>7</sup> This explains the large  $^{\text{ts}}J_{\text{F-F}}$  through space coupling constant observed. For the cases of asymmetric partially fluorinated biaryls this through space coupling is not observed, supporting that **5** and **6** have the structures proposed in Figure 3 in solution, with the apical F and the fluorinated aryl ring at opposite sides of the triangular bipyramid plane, and in agreement with the X-ray structure of **6** (Figure 4).

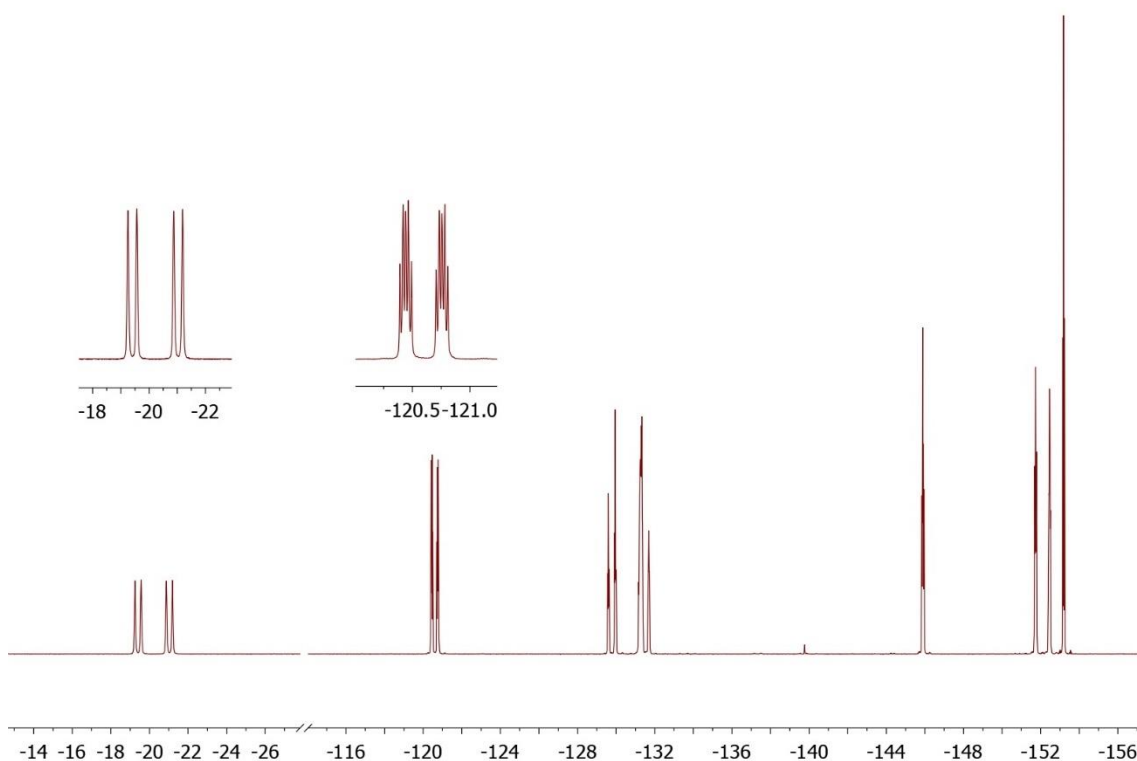


**Figure 5.**  $^{19}\text{F}$  NMR spectrum of **7**. Two resonances overlap at -132 ppm.

<sup>7</sup> Alvarez, S. A cartography of the van der Waals territories. *Dalton Trans.*, **2013**, 42, 8617–8636.

**Table 2.**  $^{19}\text{F}$  and  $^{31}\text{P}$  NMR shifts ( $\delta$  in toluene, acetone- $d_6$  capillary), coupling constants (Hz), and apical distances to P for the fluorophosphoranes.

Entry/ Compound	$^{19}\text{F}$ shift (ppm)	$^{31}\text{P}$ shift (ppm)	$^1\text{J}_{\text{F-P}}$ (Hz)	$^t\text{J}_{\text{F-F}}$ (Hz)	P-F (Å)
1/ 5	-47.3	-57.9	717.7	–	–
2/ 6	0.5	-72.1	675.0	–	1.697
3/ 7	-19.8	-48.2	769.0	148	1.661
4/ 8	27.0	-67.9	737.6	141	–
5/ 11	-32.2	-59.7	675.4	–	1.741
6/ 13	10.2	-70.2	644.7	–	–
7/ 15	-31.9	-59.8	667.6	–	–
8/ 17	11.1	-69.6	623.0	–	–

The fluorophosphoranes obtained are also part of a large family of molecules that contain the dibenzophosphole moiety. These phosphines and their corresponding tetrahedral P(V) dibenzophosphole oxides, OPR(biaryl), are interesting materials due to their luminescent and conductivity properties, centered in their conjugated organic  $\pi$ -systems.<sup>8,9</sup> Amongst them, several luminescent systems with fluorinated aryls have been studied. The presence of F substituents stabilizes the LUMO orbitals and moves the electronic transitions to high wavenumbers despite their short conjugation length.<sup>10</sup> However, the photoluminescence of five-coordinated dibenzophospholes with trigonal bipyramidal geometry has not been studied so far, probably due to the scarcity of stable derivatives. The isolated fluorophosphoranes **5–8**, **11**, **13**, and **15** present fluorescent emission both in THF solution and in the solid state. Representative data in solution are shown in Table 3.

**Table 3.** Excitation and emission data in  $5 \cdot 10^{-5}$  M THF solution.

Entry/ Compound	$\lambda_{\text{abs}}$ / nm	$\log \epsilon$	$\lambda_{\text{em}}$ / nm	$\phi$ / %	$\tau_{\text{av}}$ / ns
1/ 5	304, 315	3.24	339	25.5	3.54
2/ 6	293, 315	3.06	351	30.5	4.40
3/ 7	315	3.63	360	17.6	2.58
4/ 8	315	3.53	366	6.4	3.38
5/ 11	294, 321	3.37	350	6.7	4.97
6/ 13	277, 290	3.69	366	13.5	4.56
7/ 15	255, 306	3.86	382	37.5	7.82

For the fluorinated compounds **5–8**, a common maximum absorption peak is observed at 315 nm, and emission bands covering the range 320–450 nm (Figure 6). The maxima of the emission bands are found in the blue-UV region for all the compounds, in the range 339–382 nm. Their short average lifetimes support fluorescence processes. The values

<sup>8</sup> Hibner-Kulicka, P.; Joule, J. A.; Skalika, J.; Bałczewski, P. Recent studies of the synthesis, functionalization, optoelectronic properties and applications of dibenzophospholes. *RSC Adv.*, **2017**, *7*, 9194–9236.

<sup>9</sup> Nishida, J.; Kawakami, Y.; Yamamoto, S.; Matsui, Y.; Ikeda, H.; Hirao, Y.; Kawase, T. Synthesis and Photophysical Studies of Dibenzophosphole Oxides with D–A–D Triad Structures. *Eur. J. Org. Chem.*, **2019**, 3735–3743.

<sup>10</sup> Geramita, K.; McBee, J.; Tilley, T. D. 2,7-Substituted Hexafluoroheterofluorenes as Potential Building Blocks for Electron Transporting Materials. *J. Org. Chem.*, **2009**, *74*, 820–829.

for compound **8** can be directly compared with those found for the identical phosphine oxide OPPh(C<sub>6</sub>F<sub>4</sub>C<sub>6</sub>F<sub>4</sub>) (solution:  $\lambda_{\text{abs}} = 325$  nm;  $\log \epsilon = 3.6$ ;  $\lambda_{\text{em}} = 365$  nm;  $\phi = 18$  %; solid:  $\lambda_{\text{em}} = 378$  nm).<sup>10</sup> While the  $\lambda_{\text{em}}$  value is almost identical for both compounds, the quantum yield  $\phi$  is only about one third for the bipyramidal fluorophosphorane. For **5-8**, **11** and **13**, a blue shift of the maximum is observed when increasing the donor character of the R substituents at P atom, from Ph to Cy, (**5** vs. **6**, **7** vs. **8**, **11** vs. **13**). This blue-shift effect is also observed when the fluorine substitution degree at the phosphole core is reduced (**5** vs. **7**, **6** vs. **8**). In addition, a marked increase in the quantum yield is observed. The most electron rich fluorophosphorane **15**, with OMe substituents, shows the shortest emission wavelength of all, exhibiting emission in the blue region. Moreover, it is also the compound with the highest quantum yield (37.5 %).

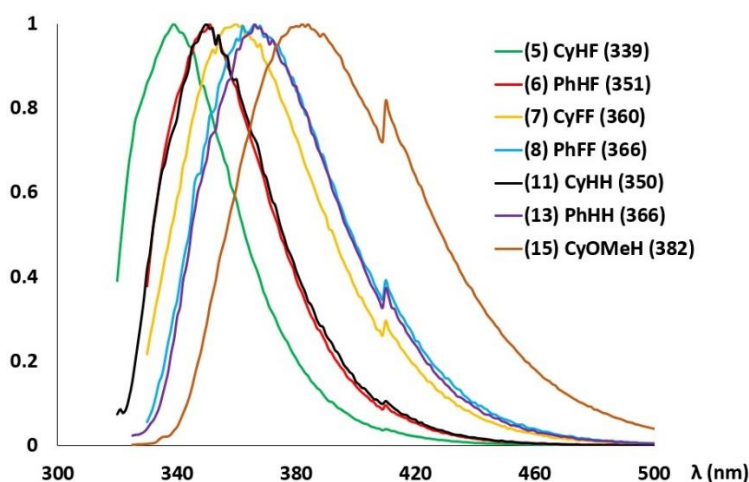


**Figure 6.** Normalized emission spectra for compounds **5-8**, **11**, **13**, and **15** in THF. The peak at *ca.* 400 nm is an instrument artifact.

The described synthesis of fluorophosphoranes, by means of a  $S_NAr$  cyclization, offers an excellent opportunity for a combined experimental and theoretical mechanistic study to gain insight into the process. Experimentally, the cyclization proceeds smoothly for phosphine **1**, with almost full conversion and only trace amounts of byproducts detected. Therefore, it is the best substrate to carry out a <sup>19</sup>F NMR monitoring of the intramolecular cyclization under mild conditions. The product formation of **5** from **1** was followed in a toluene solution of **1** at 60 °C (Figure 7, dots). No intermediate species were detected during the monitoring of the reaction, which indicates an initial high activation energy, with any processes taking place after it lower in terms of activation free energy. Complementary linear regression analysis with COPASI software provided excellent fitting of the experimental data to a first order reaction, as expected for an intramolecular process (Figure 7, lines). The kinetic constant of formation of **5** was determined, with a value of  $k = 1.367 \times 10^{-4} \text{ s}^{-1}$ , corresponding to a  $\Delta G^\ddagger_{333\text{K}} = 25.5 \text{ kcal mol}^{-1}$  (Table 4).

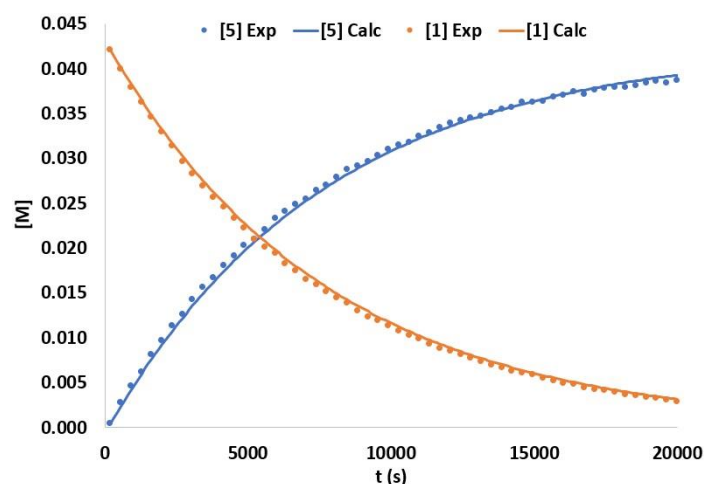


**Figure 7.** Monitoring of the isomerization of **1** to **5** by <sup>19</sup>F NMR, and COPASI fitting.

Some of the described cyclizations were carried out in diglyme, since the required temperature for the process to take place was much higher than the boiling point of toluene. For this reason, we found it appropriate to evaluate possible solvent effects during the process. Therefore, the kinetic analysis for phosphine **1** was also performed in diglyme. A similar reaction profile was obtained, confirming the intramolecular nature of the process regardless of the solvent employed. However, the kinetic rate constant obtained was slightly higher than in toluene. This suggests that the use of polar solvents such as diglyme produces, to some extent, a stabilization of the rate-determining transition state and, consequently, reduces the activation barrier of the process. The same behavior was also observed for compound **3**. Compared to **1**, the activation barriers obtained are approximately 1 kcal/mol higher both in toluene and diglyme, due to the lower nucleophilicity of the P atom in **3** (Table 4).

**Table 4.** Kinetic constants and activation barrier for the cyclization process at 333 K.

Entry/ Comp.	Solvent	$k \times 10^4$ (s <sup>-1</sup> )	$\Delta G^\ddagger_{333\text{K}}$ (kcal mol <sup>-1</sup> )
1/ 1	Toluene	1.367	25.5
2/ 1	Diglyme	3.637	24.8
3/ 3	Toluene	0.297	26.5
4/ 3	Diglyme	1.006	25.7

Altogether, the data obtained from the kinetic analysis are compatible with a S<sub>N</sub>Ar mechanism. To confirm this hypothesis, DFT calculations were performed to determine the complete reaction profile. The ωb97X-D/6-31+G(d,p) (SMD=toluene) level of theory was chosen, as it has been previously validated in other S<sub>N</sub>Ar processes.<sup>11</sup> Starting from phosphine **1**, the rate determining transition state **TS1** features a S<sub>N</sub>Ar attack: as the P atom approaches the C<sub>ortho</sub> of the distal aryl, the C⋯F distance increases (Figure 8). The calculated energy barrier in toluene is 26.5 kcal mol<sup>-1</sup>, in excellent agreement with the experimental value (25.5 kcal mol<sup>-1</sup>). This rds step is computationally so cheap and simple

<sup>11</sup> Rohrbach, S.; Murphy, J. A.; Tuttle, T. Computational Study on the Boundary Between the Concerted and Stepwise Mechanism of Bimolecular S<sub>N</sub>Ar Reactions. *J. Am. Chem. Soc.*, **2020**, *142*, 14871–14876.

to obtain that it is clearly worth evaluating *in silico* the feasibility of any new cyclization step, in advance to undertaking any synthetic work on the precursors.

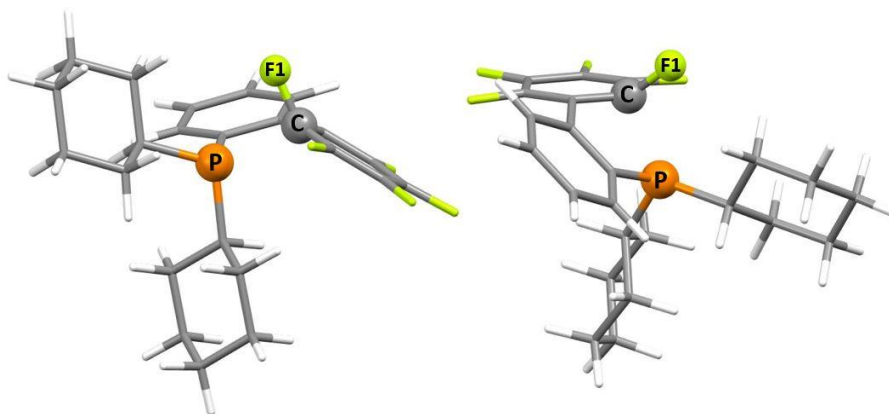


**Figure 8.** Two views of **TS1**. Selected distances (Å) and angles (°): P–C = 2.183, P–F1 = 2.650, C–F1 = 1.423. P–C–F1 = 92.14.

The possible subsequent evolution from **TS1** towards the observed final product **5** finds a fluorophosphorane intermediate **I2** at  $-4.9$  kcal mol $^{-1}$  (in red in Figure 9) which is, however, not experimentally observed. This intermediate has the biaryl moiety coordinated in two equatorial positions. Isomerization of this compound is necessary to reach the much more thermodynamically stable **5** (at  $-22$  kcal mol $^{-1}$ ).

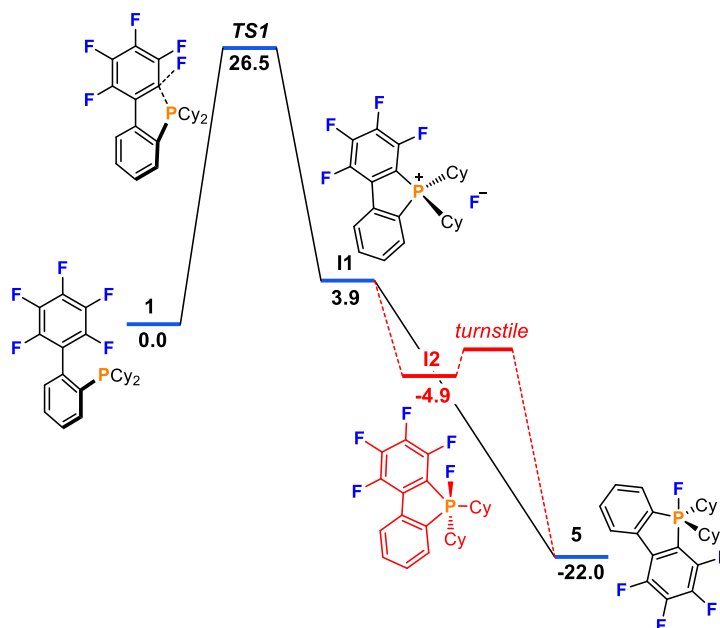


**Figure 9.** DFT calculations for **1** → **5** evolution (energy in kcal mol $^{-1}$ , 333 K, 1 atm, toluene).

The intermediate **I2** is, a priori, a plausible molecule that should isomerize to its isomer **5** by a mechanism with an isomerization barrier lower than 26.5 kcal mol $^{-1}$ , in order to disappear as soon as it is formed and not to be observed during the course of the reaction. This evolution requires switching the less stable equatorial–equatorial biphenylene coordination to the more stable equatorial–apical one, which is a quite reasonable possibility. Pentacoordinate compounds have usually low energy isomerization

mechanisms, such as Berry pseudo-rotation, turnstile, etc., with transition states, usually very difficult to find, below 10 kcal mol<sup>-1</sup>.<sup>12,13</sup> Indeed, with the level of theory employed in the profile calculation, it was not possible to obtain such transition state.

However, careful examination of the evolution from **TS1** to **I2** shows that the coordination of the released anion (F1)<sup>-</sup> to P is more likely an independent step subsequent to the  $S_NAr$  attack, after complete heterolytic breaking of the C'-F1 bond occurs. In fact, at **TS1** the F...P distance is already 2.650 Å (*vs.* 1.64 Å sum of covalent radii) and it further increases to 3.771 Å (*vs.* 3.36 Å for the sum of vdW radii) at the DFT point labelled **I1**, which corresponds to the structure found when F1 reaches the farthest distance to P before falling back towards P. Intermediate **I1**, observed in a local minimum of energy, corresponds structurally to a phosphonium, a class of ionic species with tetrahedral P cations (Figure 10, left) very frequently observed for phosphoranes with other anions (*e.g.* Cl<sup>-</sup> or BF<sub>4</sub><sup>-</sup> instead of F<sup>-</sup>). In **I1**, the (F1)<sup>-</sup> leaving group is essentially independent of the phosphonium cation, far from P, and only weakly interacting with one H atom of a Cy group. As only this ionic pair exists in the computation, F1 is eventually attracted by the P cation following the shortest direction from the place where it was released, giving rise to a possibly deceptive intramolecular step that directly leads to **I2**.<sup>14</sup>

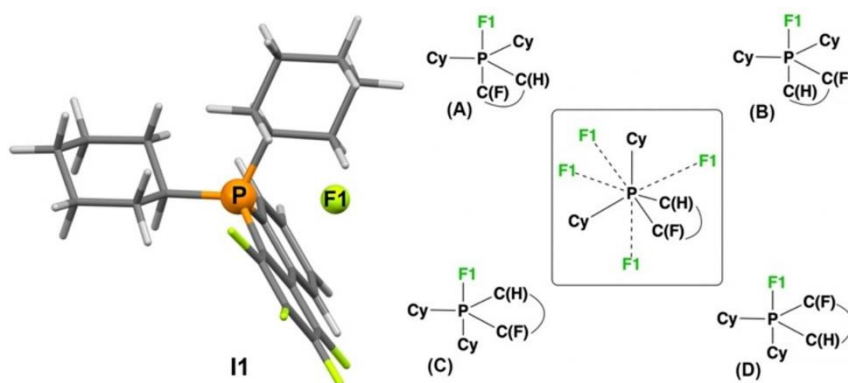


**Figure 10.** Left: Calculated structure of [P(biaryl)(Cy)<sub>2</sub>](F) (**I1**). Right: Four trigonal bipyramidal isomers of [P(biaryl)(Cy)<sub>2</sub>(F)] formed depending on the face of the tetrahedron chosen for F<sup>-</sup> approximation.

The mechanistic perspectives change when moving to *in vitro* conditions. At this point, the presence of many anions, cations, and solvent molecules must be taken into account. Freed from the constraints imposed by the *in silico* calculations, the multiple choice of the nearby F1<sup>-</sup> that coordinates to P can now become an intermolecular step. Statistically, the F1<sup>-</sup> anion that is chosen for approximation to P could be one in any of the four

<sup>12</sup> Asatryan, R.; Ruckenstein, E.; Hachmann, J. Revisiting the polytopal rearrangements in penta-coordinate d<sup>7</sup>-metallocomplexes: modified Berry pseudorotation, octahedral switch, and butterfly isomerization. *Chem. Sci.*, **2017**, *8*, 5512–5525.

<sup>13</sup> The turnstile mechanism is preferred for Pd complexes with chelating ligands conditioning 90° angles at the bpt: Casares, J. A.; Espinet, P. Dynamic Behavior of [Pd(C<sub>6</sub>F<sub>5</sub>)<sub>2</sub>(SPPy<sub>n</sub>Ph<sub>3-n</sub>)] Complexes: Evidence for a Turnstile Mechanism in Intramolecular Exchange. *Inorg. Chem.*, **1997**, *36*, 5428–5431.

<sup>14</sup> Interestingly, one of these phosphonium salts was isolated when attempting to obtain the fluorophosphorane [(C<sub>6</sub>H<sub>4</sub>-C<sub>6</sub>H<sub>4</sub>)P(F)(NEt<sub>2</sub>)<sub>2</sub>] (**18**) Although the compound with the typical J<sub>P-F</sub><sup>19</sup>F doublet was observed by NMR in the crude reaction solution, only a much less soluble tetrahedral [(C<sub>6</sub>H<sub>4</sub>-C<sub>6</sub>H<sub>4</sub>)P(NEt<sub>2</sub>)<sub>2</sub>]Cl (**18-Cl**) could be easily isolated. Probably its low solubility displaces the reaction towards it, easing the dissociation of the P-F bond.

tetrahedral faces of the phosphonium (Figure 10, right). This determines the formation of four possible isomers. Presumably, the major product should be the one following the easiest pathway and, according to the experimental results, the cyclization is fully selective to **A** (**5**). According to our assumption, pathways passing through fewer stable intermediates or transition states with the biaryl group in the equatorial plane (**C** and **D**) are consequently less likely *in vitro* than the direct one to **A** (**5**). Of course, we cannot discard that this might be altered in specific cases with significantly different steric hindrance for the four passages. Nevertheless, formation of this intermediates should not be discarded, as they would also lead to the thermodynamic product, **5**, through low-energy barrier intramolecular isomerization processes (Berry, turnstile).

In conclusion, our synthesis protocol allows the easy synthesis of new fluorophosphoranes through selective thermal-promoted intramolecular  $S_NAr$  cyclization of modularly accessible 2'-F,2-PR<sub>2</sub>(biaryl)phosphines. The only requirement for these cyclizations to take place is the presence of a fluorine atom in the 2'-position of the distal aryl of the biaryl phosphine. The simplicity of the process (an intramolecular isomerization) allows to evaluate the feasibility of the decisive cyclization step by means of an easy and short calculation prior to any synthesis of precursors. Inasmuch as the cyclization step does not add any group tolerance requirement, the scope of the process should cover any variation where the corresponding biaryl and phosphine can be synthesized and the calculated cyclization barrier is accessible.

Finally, two thoughts should be taken into account. Firstly, the observed cyclization processes advise the use of moderate or low temperatures in the synthesis of biarylphosphines with fluorine at the 2'-position, in order to prevent yield losses due to the cyclization of the desired product. Secondly, for their application in catalysis requiring medium or high temperatures, such as some cross-coupling reactions, utilization of preformed catalysts with the biarylphosphine already coordinated to the metal, rather than *in situ* preparation of the catalyst from a mix of pre-catalyst and phosphine, may prevent undesired side reactions or the total inhibition of the catalysis due to ligand isomerization or decomposition.



## Chapter VI: Luminescent Behavior of Chalcone-derived Phosphines (PEWO) and their Metal Complexes

Phosphine-Electron Withdrawing Olefin (PEWO) ligands have been successfully applied to reduce the reductive elimination barrier in Pd and Ni.<sup>1</sup> Moreover, PhPEWO-F enabled the Pd- and Ni-catalyzed synthesis of highly fluorinated biaryls.<sup>2</sup> These processes are possible due to the  $\pi$ -acceptor properties of the olefin moiety once it is coordinated to the metal center.<sup>3</sup> If a closer look to the ligand design is taken, a chalcone skeleton can be clearly observed in PEWO ligands (Figure 1), with the chalcone moiety fluorinated (left) or not (right, previously reported by Lei).<sup>4</sup>

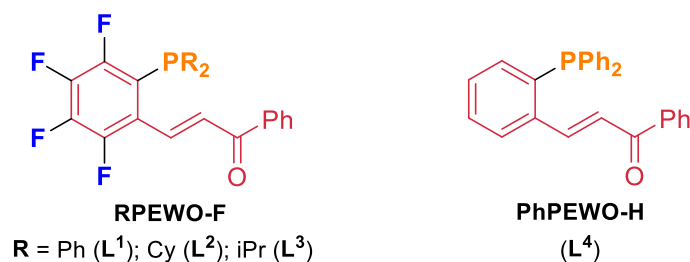


**Figure 1.** Hemilabile PEWO ligands with the chalcone group highlighted in red.

Chalcone derivatives (Ar-CH=CH-C(=O)-Ar') are not only known for their biologic activity and pharmacological applications,<sup>5</sup> but also because some of them display interesting luminescent properties.<sup>6</sup> These compounds typically exhibit aggregation induced emission, determined by their lack of planarity that hinders  $\pi$ -stacking interactions and by *push-pull* conjugation effects at the enone moiety.<sup>7</sup> Very recently, a rare crystal jumping behavior was found for a highly luminescent chalcone derivative, due to a reversible intermolecular [2+2] cycloaddition process in the solid state.<sup>8</sup>

<sup>1</sup> (a) Gioria, E.; del Pozo, J.; Martínez-Ilarduya, J. M.; Espinet, P. Promoting Difficult Carbon-Carbon Couplings: Which Ligand Does Best? *Angew. Chem., Int. Ed.*, **2016**, *55*, 13276–13280; (b) Ponce-de-León, J.; Gioria, E.; Martínez-Ilarduya, J. M.; Espinet, P. Ranking Ligands by Their Ability to Ease (C<sub>6</sub>F<sub>5</sub>)<sub>2</sub>Ni<sup>II</sup>L → Ni<sup>0</sup>L + (C<sub>6</sub>F<sub>5</sub>)<sub>2</sub> Coupling versus Hydrolysis: Outstanding Activity of PEWO Ligands. *Inorg. Chem.*, **2020**, *59*, 18287–18294.

<sup>2</sup> Ponce-de-León, J.; Espinet, P. Selective synthesis of fluorinated biaryls by [MCl<sub>2</sub>(PhPEWO-F)] (M = Ni, Pd) catalysed Negishi cross-coupling. *Chem. Commun.*, **2021**, *57*, 10875–10878.

<sup>3</sup> Gioria, E.; del Pozo, J.; Lledós, A.; Espinet, P. Understanding the Use of Phosphine-(EWO) Ligands in Negishi Cross-Coupling: Experimental and Density Functional Theory Mechanistic Study. *Organometallics*, **2021**, *40*, 2272–2282.

<sup>4</sup> Luo, X.; Zhang, H.; Duan, H.; Liu, Q.; Zhu, L.; Zhang, T.; Lei, A. Superior Effect of a  $\pi$ -Acceptor Ligand (Phosphine-Electron-Deficient Olefin Ligand) in the Negishi Coupling Involving Alkylzinc Reagents. *Org. Lett.*, **2007**, *9*, 4571–4574.

<sup>5</sup> (a) Zhuang, C.; Zhang, W.; Sheng, C.; Zhang, W.; Xing, C.; Miao, Z. Chalcone: A Privileged Structure in Medicinal Chemistry. *Chem. Rev.*, **2017**, *117*, 7762–7810; (b) Elkanzi, N. A. A.; Hrichi, H.; Alolayan, R. A.; Derafa, W.; Zahou, F. M.; Bakr, R. B. Synthesis of Chalcones Derivatives and Their Biological Activities: A Review. *ACS Omega*, **2022**, *7*, 27769–27786; (c) Gaonkar, S. L.; Vignesh, U. N. Synthesis and pharmacological properties of chalcones: a review. *Res. Chem. Intermed.*, **2017**, *43*, 6043–6077.

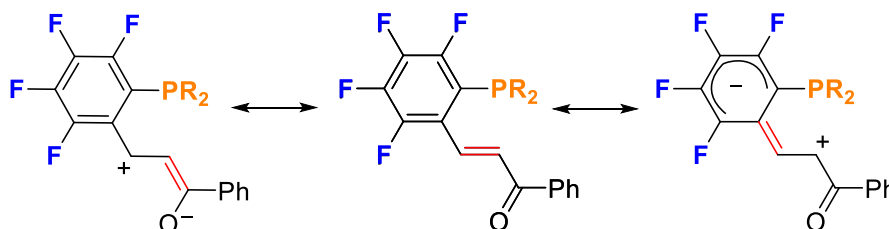
<sup>6</sup> a) Komarova, K. G.; Sakipov, S. N.; Plotnikov, V. G.; Alfimov, M. V. Luminescent properties of chalcone and its aminoderivatives. *J. Lumin.*, **2015**, *164*, 57–63; (b) Mahesha, P.; Shetty, N. S.; Kulkarni, S. D. A Review on Metal Ion Sensors Derived from Chalcone Precursor. *J. Fluoresc.*, **2022**, *32*, 835–862.

<sup>7</sup> Kagatkar, S.; Sunil, D. Aggregation induced emission of chalcones. *Chem. Pap.*, **2021**, *75*, 6147–6156.

<sup>8</sup> Cheng, X.; Yang, F.; Zhao, J.; Ni, J.; He, X.; Zhou, C.; Sun, J. Z.; Tang, B. Z. Microscopic visualization and mechanism investigation of the crystal jumping behavior of a cyclic chalcone derivative. *Mater. Chem. Front.*, **2020**, *4*, 651–660.

Chemosensors with chalcone-based chromophores have been applied for the selective detection of  $\text{Cu}^{2+}$  in aqueous media.<sup>9</sup> Applications of chalcone-derived liquid crystals for  $\text{NH}_3(\text{g})$  sensing are also worth mentioning.<sup>10</sup>

Fluorination of the chalcone moiety has a tremendous effect in the properties of the ligand. It increases its solubility as well as that of their complexes, allowing to obtain crystal structures more easily, and fluorine atoms can be employed as a tag by  $^{19}\text{F}$  NMR, which ease monitoring of reactions. Moreover, it can lead to new reactivity upon coordination, since the C–F bond is more prone to  $\text{S}_{\text{N}}\text{Ar}$  reactions than a C–H bond.<sup>11</sup> The olefin configuration also deserves some comments. While the free ligand exhibits an E-configuration, the Z-isomer is obtained upon reaction of the ligand with one equivalent of  $[\text{PdCl}_2(\text{NCMe})_2]$ . The E/Z isomerization takes place at room temperature, indicating a low activation barrier for the process.<sup>12</sup> This is due to the great delocalization of the double bond into both extremes of the fluorinated chalcone moiety ( $\text{C}_6\text{F}_4$  and  $\text{C}(=\text{O})\text{Ph}$ ) (Scheme 1). Considering the potential applications of phosphine ligands bearing a chalcone moiety with a special *pull-pull* conjugation, a series of metal complexes bearing PEWO ligands have been prepared, and their photophysical evaluated.



**Scheme 1.** Proposed resonance forms that ease double bond Z/E isomerization of PEWO ligands.

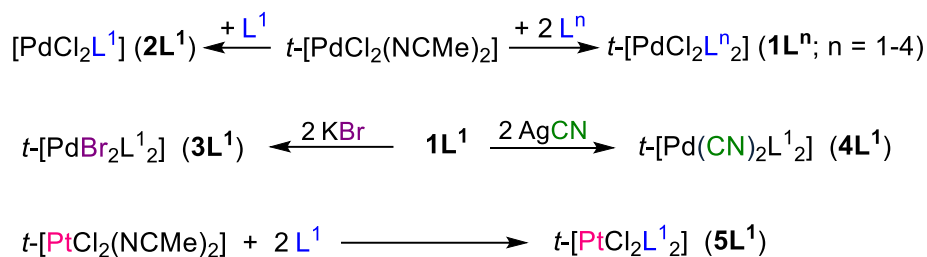
Reaction of *trans*- $[\text{PdCl}_2(\text{NCMe})_2]$  with two equivalents of the appropriate ligand yields the corresponding Pd complexes  $\mathbf{1L}^1\text{--}4$  as yellow solids in yields higher than 80% (Scheme 2). These complexes exhibit a *trans* coordination of the two phosphine ligands, with the olefin uncoordinated to Pd with an E-configuration. On the other hand, addition of one equivalent of  $\mathbf{L}^1$  to *trans*- $[\text{PdCl}_2(\text{NCMe})_2]$  yields  $[\text{PdCl}_2(\text{Z-L}^1)]$  ( $\mathbf{2L}^1$ ), with the phosphine acting as a chelate ligand with the olefin coordinated to Pd. Treatment of complex  $\mathbf{1L}^1$  with KBr or AgCN leads respectively to *trans*- $[\text{PdBr}_2(\text{L}^1)_2]$  ( $\mathbf{3L}^1$ , 86 % yield) and *trans*- $[\text{Pd}(\text{CN})_2(\text{L}^1)_2]$  ( $\mathbf{4L}^1$ , 67 % yield). Finally, the platinum compound *trans*- $[\text{PtCl}_2(\text{L}^1)_2]$  ( $\mathbf{5L}^1$ ), synthesized analogously to  $\mathbf{1L}^1$ , is obtained as a colorless solid.

<sup>9</sup> Gomes, L. J.; Moreira, T.; Rodriguez, L.; Moro, A. J. Chalcone-based fluorescent chemosensors as new tools for detecting  $\text{Cu}^{2+}$  ions. *Dyes Pigm.*, **2022**, *197*, 109845.

<sup>10</sup> Mohammad, A.-T.; Abbas, W. R. Liquid crystal behavior, photoluminescence and gas sensing: A new series of ionic liquid crystal imidazole and benzoimidazole bearing chalcone groups, synthesis and characterization. *RSC Adv.*, **2021**, *11*, 38444–38456.

<sup>11</sup> Peñas-Defrutos, M. N.; Vélez, A.; Espinet, P. Reactivity of Fluorinated-Chalcone Phosphines, RPEWO-F<sub>4</sub>, Induced by C–F Activation upon Coordination to  $\text{PdCl}_2$ . *Organometallics*, **2020**, *39*, 841–847.

<sup>12</sup> Peñas-Defrutos, M. N.; Vélez, A.; Gioria, E.; Espinet, P. E–Z Isomerization of Phosphine-Olefin (PEWO-F<sub>4</sub>) Ligands Revealed upon  $\text{PdCl}_2$  Capture: Facts and Mechanism. *Organometallics*, **2019**, *38*, 4701–4707.



**Scheme 2.** Synthesis of complexes  $\mathbf{1L}^n$ ,  $\mathbf{2L}^1$ ,  $\mathbf{3L}^1$ ,  $\mathbf{4L}^1$  and  $\mathbf{5L}^1$ .

Once the complexes were synthesized, they and the free ligands were subjected to UV irradiation in a benchtop lamp. Unfortunately, none of them showed emissive properties in solution, regardless of the solvent employed (CHCl<sub>3</sub>, THF, acetone). However, in the solid state the result was strikingly different. The free ligands  $\mathbf{L}^1$  and  $\mathbf{L}^2$  show yellow emission upon irradiation, and the Pd complexes  $\mathbf{1L}^{1-3}$  and  $\mathbf{3L}^1$  show very bright orange emission.<sup>13</sup> As an example, the emission spectra of CyPEWO-F ( $\mathbf{L}^2$ ) and its Pd complex ( $\mathbf{1L}^2$ ) are shown in Figure 2. The photographs taken upon UV irradiation clearly show how different the emissions of both compounds are: yellow for the ligand and deep orange for the complex. Since the emission bands are very broad, the  $\lambda_{\text{em}}$  is not enough to guess the observed colour.

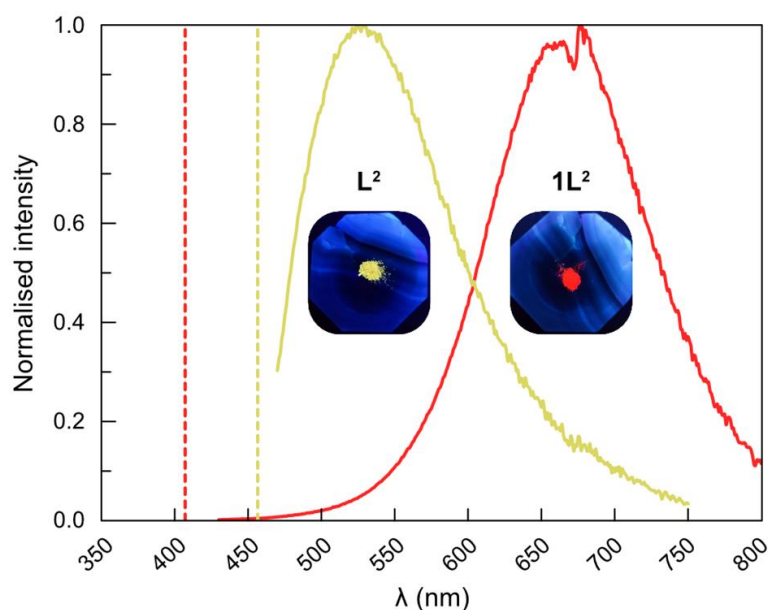


**Figure 2.** Emission spectra, with normalised intensity, of  $\mathbf{L}^2$  (yellow line) and  $\mathbf{1L}^2$  (red line); dashed lines represent the maximum of excitation.

Table 1 collects the experimental data (excitation and emission maxima, quantum yield percentages and average lifetimes) measured for the luminescent microcrystalline solids. Except the chelated *Z* complex  $\mathbf{2L}^1$ , non-luminescent and with a drastic structural difference, as the olefin is coordinated to Pd, in all the other compounds (free ligands and complexes) the uncoordinated olefins have *E*-configuration. The chalcone moieties are

<sup>13</sup> For an example of luminescent chalcones in the solid state but not in solution see: Zhang, L.; Liu, J.; Gao, J.; Lu R.; Liu, F. Adjustment of the solid fluorescence of a chalcone derivative through controlling steric hindrance. *RSC Adv.*, **2017**, *7*, 46354–46357.

submitted in the free ligands to orbital influences by the R substituents at the P atom, and, additionally, by the MX<sub>2</sub> metal fragment at which the phosphine is coordinated to in the complexes.

**Table 1.** Excitation and emission data of the ligands and complexes in the solid state.

Entry/ Comp.	$\lambda_{\text{exc}}$ (nm)	$\lambda_{\text{em}}$ (nm) <sup>a</sup>	$\Phi$ (%)	$\tau_{\text{av}}$ (ns) <sup>b</sup>
<b>1/ L<sup>1</sup></b>	413	606	10.1	2.4
<b>2/ L<sup>2</sup></b>	460	530	4.1	3.5
<b>3/ L<sup>4</sup></b>	472	552	< 3	3.0
<b>4/ 1L<sup>1</sup></b>	405	649	28.0	$1.3 \times 10^3$
<b>5/ 1L<sup>2</sup></b>	412	676	21.8	$1.6 \times 10^3$
<b>6/ 1L<sup>3</sup></b>	405	643	15.6	$1.4 \times 10^3$
<b>7/ 1L<sup>4</sup></b>	469	680	< 3	$6.4 \times 10^2$
<b>8/ 2L<sup>1</sup></b>	<i>Undetected emission</i>			
<b>9/ 3L<sup>1</sup></b>	415	666	15.7	$5.4 \times 10^3$
<b>10/ 4L<sup>1</sup></b>	<i>Undetected emission</i>			
<b>11/ 5L<sup>1</sup></b>	<i>Undetected emission</i>			

Firstly, emissive properties of the free ligands were analyzed, for which the electronic and steric properties must be considered. **L<sup>1</sup>** (fluorinated, R = Ph) shows the highest emission maxima wavelength, at 606 nm. In comparison, the fluorinated **L<sup>2</sup>** (R = Cy) has a blue-shifted maxima wavelength closer to the value of **L<sup>4</sup>**, 530 and 552 nm respectively. This suggest that the donor inductive effect of the Cy substituents to the P atom is strong enough to compensate the electron withdrawing effect of fluorination in the chalcone ring. Moreover, increasing the electron density in the chalcone moiety, be it by lack of fluorination or by donor inductive effect, looks detrimental to the quantum yield, which is clearly reduced to the point of almost non-existence in **L<sup>4</sup>**.

Luminescence is clearly modified upon coordination to MX<sub>2</sub>. Apart from the previously discussed electronic effects, coordination to a metal center introduces new electronic factors to be considered: the P atom acts as  $\sigma$ -donor to M, and  $\pi$ -backdonation from M to P, and globally to the whole chalcone moiety, takes place. The direct consequence of these new electronic effects is a shift on the emission maxima. Complex **1L<sup>1-4</sup>** and **3L<sup>1</sup>** show red-shifted emissions, in the range 643-680 nm. This is in good agreement with the trend observed for the free ligands, the lesser electron density in the chalcone, the more red-shifted the emission maximum. For the complexes, the  $\sigma$ -donation from P to M is greater than the  $\pi$ -backdonation, lowering the overall electron density in the chalcone and, therefore, making the emissions for the complexes more red-shifted than for the free ligands.

Coordination to PdX<sub>2</sub> (X = Br, Cl) also led to an increased quantum yield, to the range of 15-28 %, while the free ligands had less than 10%. It is noteworthy that, even after coordination to Pd, the non-fluorinated **1L<sup>4</sup>** is scarcely luminescent, highlighting the importance of fluorination in the chalcone for the emissive properties. Figure 2 showed the particular example of the CyPEWO-F ligand **L<sup>2</sup>** and its corresponding PdCl<sub>2</sub> complex **1L<sup>2</sup>**. Interestingly, the colour change is associated to a substantially higher Stokes shift for **1L<sup>2</sup>** than for **L<sup>2</sup>** (*i.e.*  $9.5 \times 10^3 \text{ cm}^{-1}$  and  $2.9 \times 10^3 \text{ cm}^{-1}$ ) along with longer lifetimes, in

the order of ms for the Pd complexes and ns for the ligands (Table 1, Column 5). These variations are strongly indicative of a change in the nature of the luminescent process from fluorescent to phosphorescent emission upon coordination to PdX<sub>2</sub> (X = Br, Cl).<sup>14</sup>

On the other hand, neither *trans*-[Pd(CN)<sub>2</sub>(L<sup>1</sup>)<sub>2</sub>] (**4L**<sup>1</sup>) nor *trans*-[PtCl<sub>2</sub>(L<sup>1</sup>)<sub>2</sub>] (**5L**<sup>1</sup>) are luminescent in the solid state, despite having an almost identical structure to **1L**<sup>1</sup> (Figure 3). Therefore, this extreme difference must be related to orbital differences. The two halide ligands in **1L**<sup>1-3</sup> and **3L**<sup>1</sup> are medium-strength  $\sigma$ -donor and slightly  $\pi$ -donor, while the cyanide ligands in **4L**<sup>1</sup> are more  $\sigma$ -donor but very strongly  $\pi$ -acceptor. The change from Pd to Pt in **5L**<sup>1</sup> produces large orbital energy differences between the two isoelectronic metal centers due to the lanthanide contraction along with the relativistic effects in Pt. Overall, the cases of **4L**<sup>1</sup> and **5L**<sup>1</sup> end up being quite similar. They both have a less electron-rich metal center which is less susceptible to be polarized.

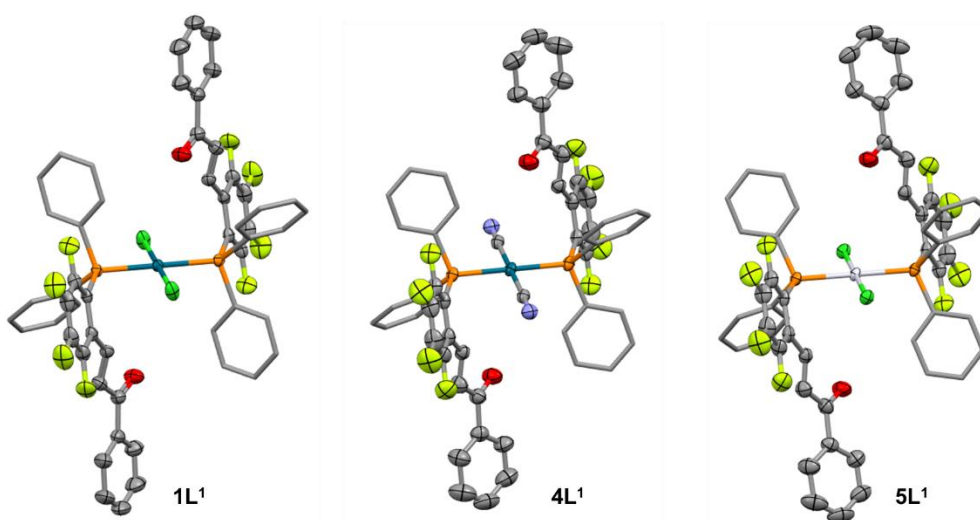


**Figure 3.** X-ray structures of **1L**<sup>1</sup>, **4L**<sup>1</sup> and **5L**<sup>1</sup>. H atoms omitted for clarity. Relevant distances (Å): **1L**<sup>1</sup>: Pd-Cl = 2.2903, Pd-P = 2.3231, C=C(olefin) = 1.314. **4L**<sup>1</sup>: Pd-C = 1.990, Pd-P = 2.3388, C=C(olefin) = 1.320. **5L**<sup>1</sup>: Pt-Cl = 2.3029, Pt-P = 2.3241, C=C(olefin) = 1.303.

To validate this hypothesis, based on experimental observations, and identify the orbitals involved in the process, DFT calculations were carried out. Since the emission only takes place in the solid state, gas phase geometry optimizations were carried out using the X-ray structures as initial guesses, leading to minimal modifications of the solid structures. Specifically, we studied the ligand PhPEWO-F (**L**<sup>1</sup>, luminescent) and its derived complexes **1L**<sup>1</sup> (luminescent) and **4L**<sup>1</sup>/**5L**<sup>1</sup> (non-luminescent). Absorption spectra were simulated employing time-dependent DFT methods (TD-DFT), which allowed the identification of the electronic transitions responsible for the excitation maxima observed in **L**<sup>1</sup> and **1L**<sup>1</sup>.

For **L**<sup>1</sup>, the calculated HOMO-LUMO gap is in good agreement with the experimental excitation wavelength observed ( $\lambda_{\text{calc}} = 402$  nm;  $\lambda_{\text{exp}} = 413$  nm). The HOMO orbital is mainly located in the Ph<sub>2</sub>P moiety (87%), while the LUMO is purely a chalcone orbital.

<sup>14</sup> Forward, J. M.; Bohmann, D.; Fackler Jr J. P.; Staples, R. J. Luminescence Studies of Gold(I) Thiolate Complexes. *Inorg. Chem.*, **1995**, *34*, 6330–6336.

For **1L**<sup>1</sup>, the experimental  $\lambda_{\text{exc}}$  maximum, at 405 nm, fits well with the calculated transition from the HOMO-2 to the LUMO orbital ( $\lambda_{\text{calc}} = 395$  nm). In this case, orbital contribution is slightly more complex, due to the involvement of Pd orbitals: 58% Ph<sub>2</sub>P, 22% PdCl<sub>2</sub>, 20% EWO for HOMO-2, and 42% PdCl<sub>2</sub>, 38% EWO, 20% Ph<sub>2</sub>P for LUMO; these orbitals involve both **L**<sup>1</sup> ligands in a symmetric fashion, instead of being localized in just one of them. Interestingly, for the Pt analogue **5L**<sup>1</sup> a similar transition (HOMO-2 to LUMO) is computed to be markedly more energetic ( $\lambda_{\text{calc}} = 349$  nm), while the HOMO-LUMO transition for Pd(CN)<sub>2</sub> complex **4L**<sup>1</sup> should originate a band at a similar wavelength ( $\lambda_{\text{calc}} = 350$  nm). These results support the qualitative interpretation of similar behavior of these last two complexes.

TD-DFT was also employed to calculate the emission wavelengths and the states taking part in them. The emission experimentally observed for **1L**<sup>1</sup> ( $\lambda_{\text{exp}} = 649$  nm) was assigned to the monodeexcitation from the first triplet state (*T*<sub>1</sub>), computed to be very similar ( $\lambda_{\text{calc}} = 667$  nm). The emission band mainly involves the LUMO→HOMO phosphorescent transition. This result explains the high Stokes shift and long lifetime values experimentally obtained. Reoptimization of both *S*<sub>1</sub> and *T*<sub>1</sub> states led to profound structural change. However, since the emissive properties are only observed in the solid state, geometry relaxation was discarded as structural deformation is quite limited in the solid state. Furthermore, computed results for other emissions, fluorescent and phosphorescent, were far from the experimentally observed data and, consequently, were discarded.

For **4L**<sup>1</sup> and **5L**<sup>1</sup>, the computed phosphorescent emissions (decay from triplet states) are experimentally unobservable, as direct consequence of the changes in the frontier molecular orbitals (FMOs). Figure 4 depicts the (FMOs) for **1L**<sup>1</sup>, **4L**<sup>1</sup> and **5L**<sup>1</sup> for graphical comparison. For **5L**<sup>1</sup>, the PtCl<sub>2</sub> HOMO resembles its PdCl<sub>2</sub> analogue, but the contribution of the PtCl<sub>2</sub> fragment in the LUMO drops to the 7% (*vs* 42% for **1L**<sup>1</sup>) and the deexcitation from the first triplet state is computed to be much more energetic (*i.e.* 555 nm). The effect of the Cl by CN substitution is also clear, with reduced participation of the Pd(CN)<sub>2</sub> fragment in the LUMO of **4L**<sup>1</sup> (casually similar to the PtCl<sub>2</sub> compound) and negligible in the HOMO.

Once the key orbitals involved in the luminescent behavior have been identified, mainly located in the PdCl<sub>2</sub> fragment for **1L**<sup>1</sup>, the experimental data can be better explained: *i*) the PdBr<sub>2</sub> substitution in **3L**<sup>1</sup> (Br is electronically very similar to Cl) or the PR<sub>2</sub> modification in **1L**<sup>2</sup> and **1L**<sup>3</sup> move in the range of variations of polarization, and therefore only slight variations are observed; *ii*) totally different emissions (in fact experimentally undetectable) must be expected from the Pd(CN)<sub>2</sub> (**4L**<sup>1</sup>) or PtCl<sub>2</sub> (**5L**<sup>1</sup>) congeners, with LUMOs hardly participated by their MX<sub>2</sub> moieties.

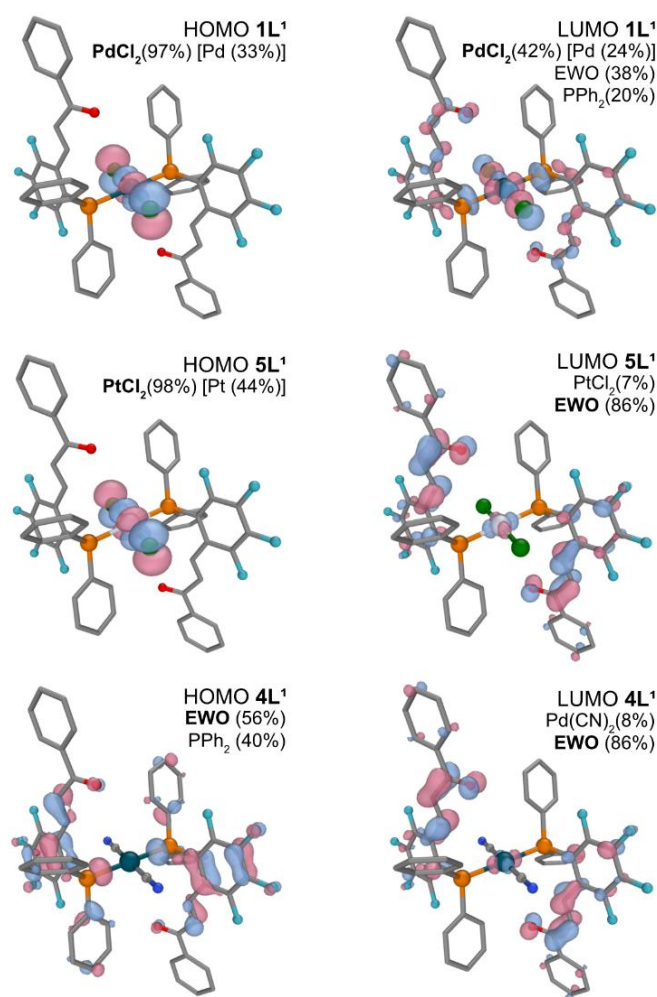


**Figure 4.** FMOs of complexes  $1L^1$  (above),  $5L^1$  (middle) and  $4L^1$  (below). Contribution percentages of the different fragments are included (main participation in bold). Relevant contributions of the metal atom (higher than 10%) are also showed.

Finally, the computed deexcitations from the triplet states are not able to explain the experimentally observed emission of the PhPEWO-F free ligand ( $L^1$ ,  $\lambda_{\text{exp}} = 606$  nm) discarding the phosphorescent behavior in this case. Nevertheless, it is possible to find a  $S_1 \rightarrow S_0$  transition from a singlet state where a slight bending of the chalcone group is observed. It afforded a satisfactory value of fluorescent emission at  $\lambda_{\text{calc}} = 580$  nm, strongly supported by the short experimental lifetime of *ca.* 2 ns. In this case, the contribution of the R<sub>2</sub>P fragment in the orbitals involved is significant, and consequently the effect of the Cy substitution is appreciable, as observed experimentally.

In summary, the luminescent properties of a family of chalcone-derived PEWO ligands and their metal complexes have been studied, with strikingly different results. While the fluorinated ligands show fluorescent yellow emission in the solid state upon UV irradiation, the PdX<sub>2</sub> (X = Br, Cl) complexes show red-shifted phosphorescent emissions with increased quantum yields. In contrast, Pd(CN)<sub>2</sub> and PtCl<sub>2</sub> complexes did not show luminescent behavior. TD-DFT calculations allowed us to identify the reasons of such a different outcome. Pd(CN)<sub>2</sub> and PtCl<sub>2</sub> complexes would require a much more energetic excitation than PdX<sub>2</sub>. Moreover, while the LUMO orbital involved in the PdX<sub>2</sub> complexes emission is delocalized between the metal center and the ligand, it is mainly localized in

the chalcone moiety for Pd(CN)<sub>2</sub> and PtCl<sub>2</sub> complexes. The need of a more energetic excitation in combination with a different frontier orbital contribution explains why the Pd(CN)<sub>2</sub> and PtCl<sub>2</sub> complexes are not luminescent whereas the PdX<sub>2</sub> (X = Br, Cl) are.



## Chapter VII: Synthesis of Group 10 Metallophosphoranes (M = Ni, Pd) and Selective Substitution Reactions

Previously, we have described the application of different types of phosphine ligands with  $\pi$ -acceptor moieties, such as electron deficient olefins and biaryls. In this chapter, the consequences of employing a phosphine ligand having a geometrically constrained P atom, exemplified by **L1**, upon coordination to some group 10 metal precursors will be evaluated (Figure 1).

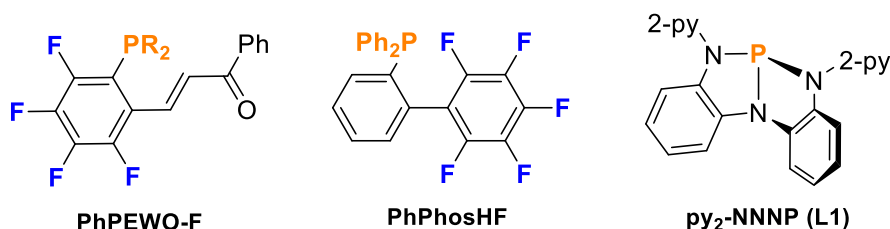


**Figure 1.** Phosphine ligands with  $\pi$ -acceptor ability. 2-py = 2-pyridine.

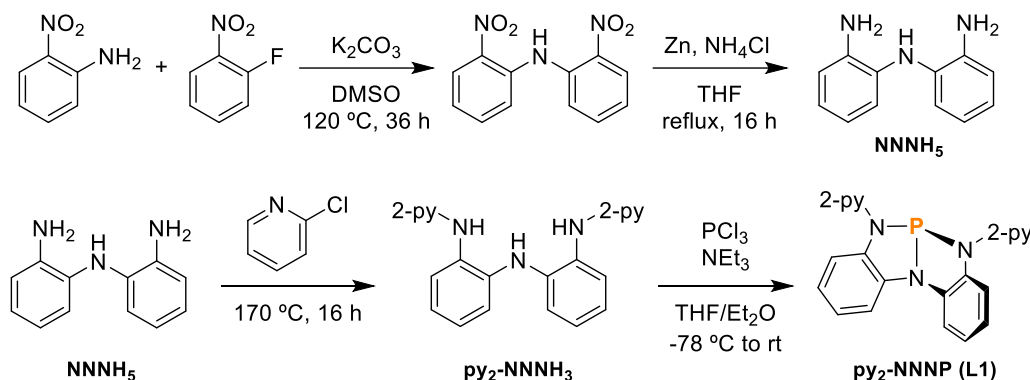
Tricoordinate phosphorous compounds usually have a trigonal pyramidal geometry, with  $C_{3v}$  symmetry around the P atom, where their lone pair often exhibit reactivity toward electrophiles. However, reactivity of these compounds toward nucleophiles is very rare. This is due to the high energy of the antibonding empty orbitals of P. In contrast, the design of tricoordinate phosphorous compounds with a geometrically distorted environment at the P atom ( $C_s$  symmetry) has led to the development of new processes thanks to their enhanced biphilic reactivity.<sup>1</sup> A combined experimental and theoretical (DFT) study evaluated how geometrical distortions affect the frontier orbital energies and consequently, the biphilic character of these compounds.<sup>2</sup> Interestingly, it was shown that the energy of the P atom lone pair orbital is not significantly affected by geometric distortion from  $C_{3v}$  to  $C_s$  to  $C_{2v}$ . However, degeneracy between the two unfilled antibonding orbitals decreases and, consequently, the energy gap between the lone pair and one antibonding orbital is lowered. The direct consequence is that, while the nucleophilicity of the P atom remains, its electrophilicity is greatly enhanced, opening the way to biphilic reactivity.

This reactivity can be further modulated through coordination of the phosphine to a metal center. To this end, py<sub>2</sub>-NNNP (**L1**) ligand was designed as a  $C_s$ -symmetric chelating dipyridyl phosphine ligand related to the previously reported Me<sub>2</sub>-NNNP phosphine.<sup>1c</sup> **L1**

<sup>1</sup> (a) Abbenseth, J.; Goicoechea, J. M. Recent developments in the chemistry of non-trigonal pnictogen pincer compounds: from bonding to catalysis. *Chem. Sci.*, 2020, 11, 9728–9740; (b) Lipshultz, J. M.; Li, G.; Radosevich, A. T. Main Group Redox Catalysis of Organopnictogens: Vertical Periodic Trends and Emerging Opportunities in Group 15. *J. Am. Chem. Soc.*, 2021, 143, 1699–1721; (c) Zhao, W.; McCarthy, S. M.; Lai, T. Y.; Yennawar, H. P.; Radosevich, A. T. Reversible Intermolecular E–H Oxidative Addition to a Geometrically Deformed and Structurally Dynamic Phosphorous Triamide. *J. Am. Chem. Soc.*, 2014, 136, 17634–17644; (d) Lin, Y. C.; Hatzakis, E.; McCarthy, S. M.; Reichl, K. D.; Lai, T. Y.; Yennawar, H. P.; Radosevich, A. T. P–N Cooperative Borane Activation and Catalytic Hydroboration by a Distorted Phosphorous Triamide Platform. *J. Am. Chem. Soc.*, 2017, 139, 6008–6016

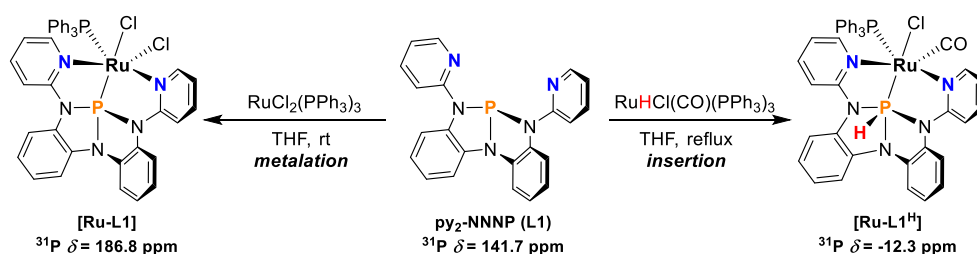
<sup>2</sup> Lee, K.; Blake, A. V.; Tanushi, A.; McCarthy, S. M.; Kim, D.; Loria, S. M.; Donahue, C. M.; Spielvogel, K. D.; Keith, J. M.; Daly, S. R.; Radosevich, A. T. Validating the Biphilic Hypothesis of Nontrigonal Phosphorus(III) Compounds. *Angew. Chem., Int. Ed.*, 2019, 58, 6993–6998.

is obtained after a 4-step synthesis (Scheme 1).<sup>3</sup> Starting from commercially available 2-nitroaniline and 2-fluoronitrobenzene, an intermolecular  $S_NAr$  reaction, followed by reduction of the dinitro product with Zn leads to the triamine compound  $NNNH_5$ . Then, refluxing  $NNNH_5$  in 2-chloropyridine overnight furnishes the ligand backbone, featuring two 2-pyridine moieties ( $py_2$ - $NNNH_3$ ). Finally, reaction of  $py_2$ - $NNNH_3$  with  $PCl_3$  in the presence of  $NEt_3$  leads to **L1**, which is obtained as an off-white solid.



**Scheme 1.** Synthetic pathway to **L1**.

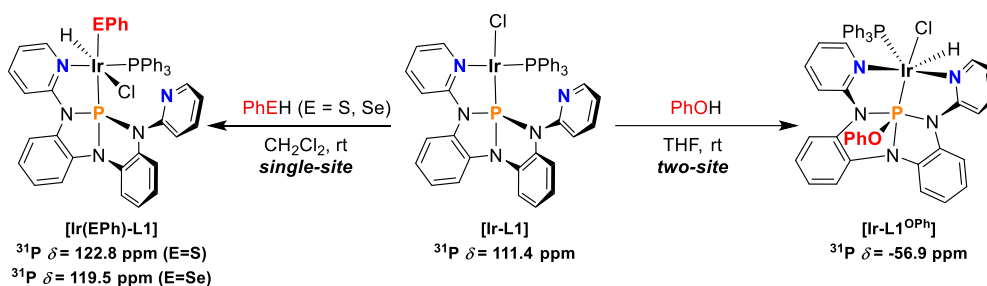
**L1** displays a singlet at 141.7 ppm in the  $^{31}P\{^1H\}$  NMR spectra. Moreover, its X-ray diffraction structure confirmed the  $C_s$  symmetry around the P atom. Reactivity of **L1** with some metal precursors has already been evaluated. Depending on the ligands on the Ru precursor employed,  $\kappa^3$ -N,P,N chelating coordination of **L1** to the metal center to form **[Ru-L1]**, or insertion of the P in a Ru-H bond giving **[Ru-L1<sup>H</sup>]** were observed (Scheme 2).<sup>3</sup>  $^{31}P$  NMR chemical shift is a great tool to know the coordination number around the P atom of **L1** after complexation. **[Ru-L1]** features a doublet, due to coupling with the  $PPh_3$  ligand, at a downfield shift compared to the free ligand (186.8 vs 141.7 ppm). This is the typical behavior observed for phosphine ligands chemical shifts upon coordination to a metal center. In contrast, **[Ru-L1<sup>H</sup>]** exhibits a doublet highly upfield compared to the free ligand, at -12.3 ppm, in the  $^{31}P\{^1H\}$  NMR spectra. This resonance is observed as a doublet of doublets in the non-decoupled experiment. This split of the NMR resonance confirms the hydride migration to the P atom, which is only possible due to the highly Lewis acidic character of the P atom resulting from the  $C_s$  symmetry. Hence, while simple coordination to a metal center shifts the P resonance downfield, an increase of the coordination number around the P atom leads to an upfield shift.



**Scheme 2.** Divergent reactivity of **L1** upon addition to selected Ru complexes.

<sup>3</sup> Tanushi, A.; Radosevich, A. T. Insertion of a Nontrigonal Phosphorus Ligand into a Transition Metal-Hydride: Direct Access to a Metallohydrophosphorane. *J. Am. Chem. Soc.*, **2018**, *140*, 8114–8118.

When **L1** is added to a mixture of  $[\text{IrCl}(\text{COD})]_2$  and  $\text{PPh}_3$ , the corresponding  $[\text{IrCl}(\text{PPh}_3)(\text{L1})]$  complex [**Ir-L1**] is obtained, with **L1** acting as a  $\kappa^2$ -P,N chelating ligand. Interestingly, [**Ir-L1**] shows divergent reactivity upon addition of PhEH (E = O, S, Se). While typical metal-centered oxidative addition at Ir was observed for PhSH and PhSeH, a cooperative two-site oxidative addition took place when PhOH was employed (Scheme 3). The higher oxophilic character of the P atom along with the better interaction of the heavier chalcogen elements with Ir, based on the hard-soft acid-base theory, explains the different reactivity observed in this case.<sup>4</sup> Again, a higher upfield shift of the  $^{31}\text{P}$  resonance of **L1** compared to the starting [**Ir-L1**] was observed when the coordination around the P atom was increased.



**Scheme 3.** Reactivity of [**Ir-L1**] upon addition of chalcogenophenols.

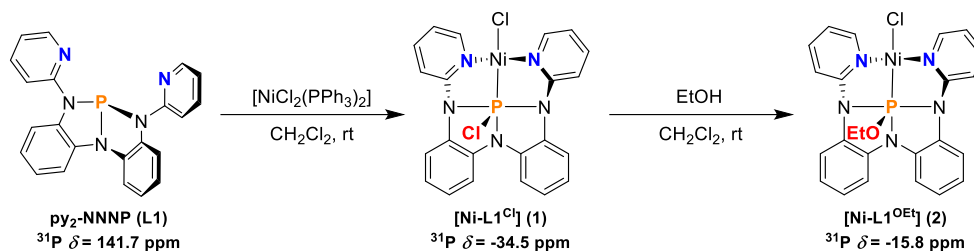
So far, **L1** has been reacted with metals capable of expanding its coordination number, such as Ru and Ir. Therefore, evaluation of the ligand behavior upon addition to metals with defined coordination number may lead to different reactivity. To this end, reactions between **L1** and some group 10 metal precursors were conducted.

Coordination experiments started with the addition of **L1** to simple  $\text{NiCl}_2$  complexes (Scheme 4). When **L1** was added to a solution of *trans*- $[\text{NiCl}_2(\text{PPh}_3)_2]$  in  $\text{CH}_2\text{Cl}_2$ , an upfield shift of the P resonance of **L1** to  $-34.5$  ppm was observed. Considering the previous results with Ru and Ir, this shift suggests a change in the coordination number of the P atom, which in this case can be explained by the migration of one chlorido ligand from Ni to P, giving the metallophosphorane complex  $[\text{NiCl-L1}^{\text{Cl}}]$  (**1**). This is the first observed case where halogen migration takes place at a  $[\text{M-L1}]$  complex.<sup>5</sup> No coupling of **L1** to  $\text{PPh}_3$  is observed and only free  $\text{PPh}_3$  is detected. Hence, a  $\kappa^3$ -N,P,N chelating coordination of **L1** to Ni is proposed. This proposal was confirmed by X-ray diffraction analysis (Figure 2, left). **L1** is coordinated by the P and the two pyridine moieties to the Ni atom, which shows a square planar geometry. The pyridines are slightly bent over and below the plane defined by Ni, in order to accommodate the ligand to the small Ni radius. Interestingly, the P atom features a pseudo square pyramidal geometry, with the Cl ligand in the apical position. On the other hand, when **L1** was reacted with *cis*- $[\text{NiCl}_2(\text{dme})]$ , instead of the expected singlet at  $-34.5$  ppm, a singlet at  $-15.8$  ppm was obtained. X-ray diffraction analysis allowed us to identify the product as  $[\text{NiCl-L1}^{\text{OEt}}]$  (**2**) (Figure 2, right). We wonder if formation of **2** may be due to reaction of the expected **1** with adventitious EtOH from the commercial  $[\text{NiCl}_2(\text{dme})]$ . To test this hypothesis, a solution of **1** in  $\text{CH}_2\text{Cl}_2$  was treated with EtOH. Indeed, upon EtOH addition,  $^{31}\text{P}$  NMR chemical shift

<sup>4</sup> Drance, M. J.; Tanushi, A.; Radosevich, A. T. Two-Site O–H Addition to an Iridium Complex Featuring a Nonspectator Tricordinate Phosphorus Ligand. *J. Am. Chem. Soc.*, **2022**, *144*, 20243–20248.

<sup>5</sup> Halogen migration was not observed in the previously reported Ru and Ir complexes.

moved from -34.5 (**1**) to -15.8 ppm (**2**) confirming the origin of **2**. It is noteworthy that the Cl/OEt exchange takes place only at the P atom, even if excess of EtOH was employed, with the Ni–Cl bond remaining intact.



**Scheme 4.** Coordination of **L1** to Ni precursors.

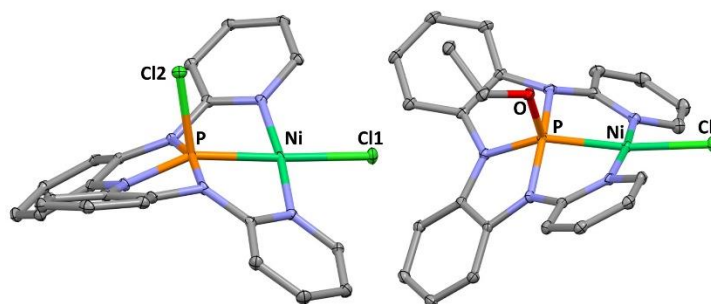
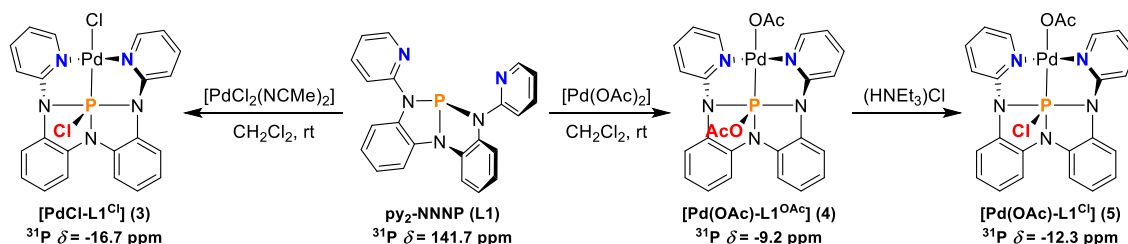


**Figure 2.** X-ray structures of Ni insertion complexes **1** (left) and **2** (right). H atoms omitted for clarity. Relevant bond distances (Å): **1**: Ni–P = 2.163, Ni–Cl1 = 2.241, P–Cl2 = 2.104. **2**: Ni–P = 2.164, Ni–Cl = 2.258, P–O = 1.610.

In order to check if these migrations were common to other group 10 complexes, reactions between **L1** and Pd precursors were carried out (Scheme 5). Addition of **L1** to *trans*-[PdCl<sub>2</sub>(NCMe)<sub>2</sub>] in CH<sub>2</sub>Cl<sub>2</sub> led to the analogous Pd complex of **1**, [PdCl–L1<sup>Cl</sup>] (**3**), where Cl ligand migration from Pd to P has happened. A solution of **3** in CDCl<sub>3</sub> shows a singlet at -16.7 ppm in the <sup>31</sup>P NMR, consistent with an increased coordination number of the P atom due to the proposed migration. This process was also observed when **L1** was added to [Pd(OAc)<sub>2</sub>]. Coordination of **L1** to Pd and migration of an OAc moiety to P formed [Pd(OAc)–L1<sup>OAc</sup>] (**4**), which displays a singlet at -9.2 ppm in the <sup>31</sup>P NMR. Interestingly, if this reaction was carried out with impure fractions of **L1** contaminated with (HNEt<sub>3</sub>)Cl from the ligand synthesis, a new resonance in the <sup>31</sup>P NMR at -12.3 ppm was observed. Instead of the expected complex **4**, protonolysis of the P-bounded OAc ligand followed by coordination of Cl took place and [Pd(OAc)–L1<sup>Cl</sup>] (**5**) was obtained.



**Scheme 5.** Synthesis of [Pd–L1] complexes.

Similarly to Ni, when Pd complexes **3** and **4** were treated with alcohols, exchange at the P atom was observed. When PhOH was employed, complexes [PdCl–L1<sup>O<sub>Ph</sub></sup>] (**6**) and

[Pd(OAc)-L1<sup>O<sub>Ph</sub></sup>] (**7**) were obtained respectively. Their X-ray structures were determined and are shown in Figure 3.

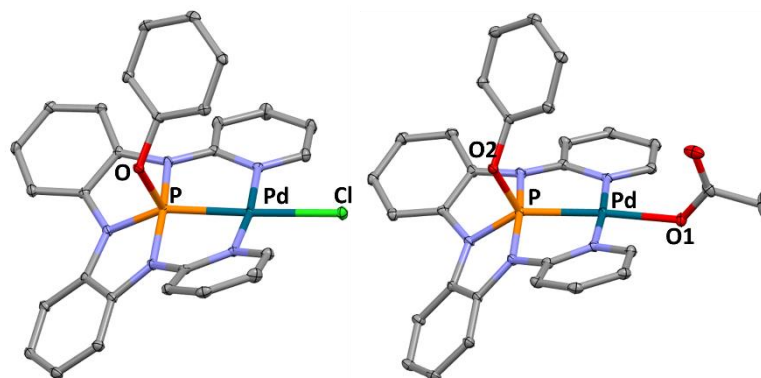


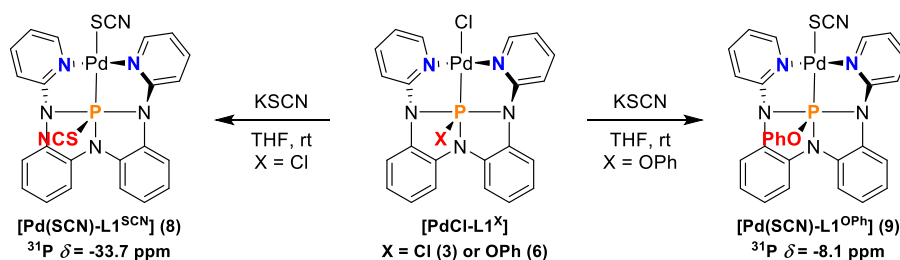
**Figure 3.** X-ray structures of Pd complexes **6** (left) and **7** (right). H atoms and solvent molecules omitted for clarity. Relevant bond distances (Å): **6**: Pd-P = 2.235, Pd-Cl = 2.420, P-O = 1.649. **7**: Pd-P = 2.223, Pd-O1 = 2.111, P-O2 = 1.644.

These observations indicate that selective substitution might be achieved under certain conditions, depending on the substituents at P and Pd, and the nucleophiles employed. Therefore, substitution selectivity was evaluated with two anionic ligands that exhibit soft character, SCN<sup>-</sup> and I<sup>-</sup>. [PdCl-L1<sup>Cl</sup>] (**3**) and [PdCl-L1<sup>O<sub>Ph</sub></sup>] (**6**) were chosen as palladium complexes.

When a solution of **3** in THF was treated with excess KSCN, substitution of both Cl ligands by SCN was observed, obtaining [Pd(SCN)-L1<sup>SCN</sup>] (**8**) as the only product. In contrast, when **6** was employed as starting Pd complex, only the chlorido ligand was substituted, forming the complex [Pd(SCN)-L1<sup>O<sub>Ph</sub></sup>] (**9**) (Scheme 6).<sup>6</sup> A similar reactivity was observed when NaI was added, producing [PdI-L1<sup>I</sup>] (**10**) and [PdI-L1<sup>O<sub>Ph</sub></sup>] (**11**), respectively. It is noteworthy that, in the <sup>1</sup>H NMR spectra of these complexes, it is possible to identify some resonance shifts that are characteristic of the ligands bounded to the Pd and P atoms (Figure 4). The dichloro complex **3** shows a doublet at 9.50 ppm, which correspond to the H atom in ortho position to N of the pyridine. This signal is slightly affected by the P atom substituent, as it has a chemical shift of 9.43 ppm in the phenoxy complex **6**. On the other hand, chloride substitution by iodide at the Pd atom has a strong deshielding effect on the signal, which appears at 9.88 ppm in **11**. This deshielding effect is mainly due to the anisotropic effect of the iodide ligand.<sup>7</sup> In contrast, substitution by SCN is associated with an upfield shift of the signal (8.79 and 8.77 ppm in complexes **8** and **9** respectively). Finally, presence of P-bounded OPh moiety is easily identify by an upfield resonance in the range 6.55–6.65 ppm.

<sup>6</sup> S-coordination of SCN moiety to both P and Pd atoms is proposed.

<sup>7</sup> (a) Anbalagan, V. *J. Coord. Chem.*, **2003**, *56*, 161–172. (b) Pazderski, L.; Tousek, J.; Sitkowski, J.; Kozerski, L.; Szlyk, E. *Magn. Reson. Chem.*, **2007**, *45*, 1045–1058.



**Scheme 6.** Substitution reactions with KSCN.

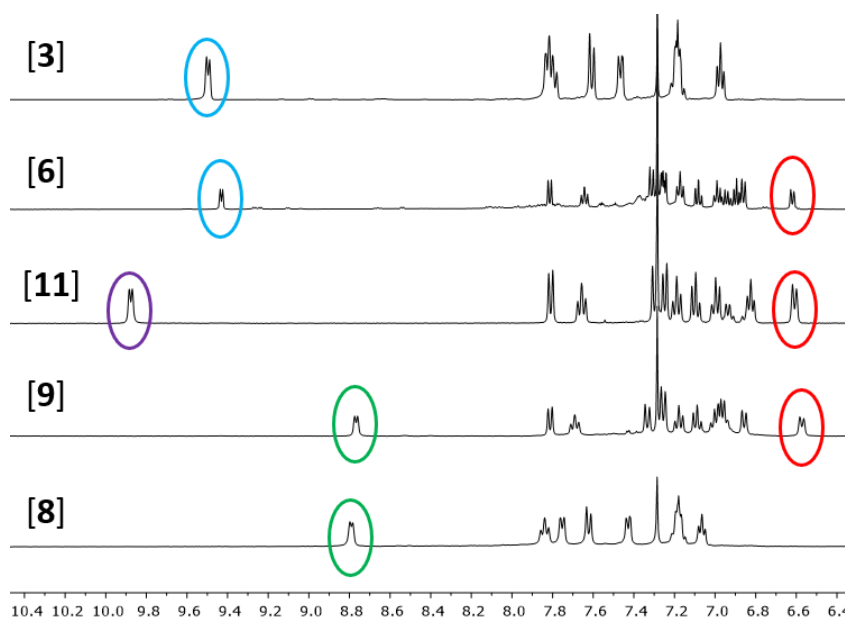
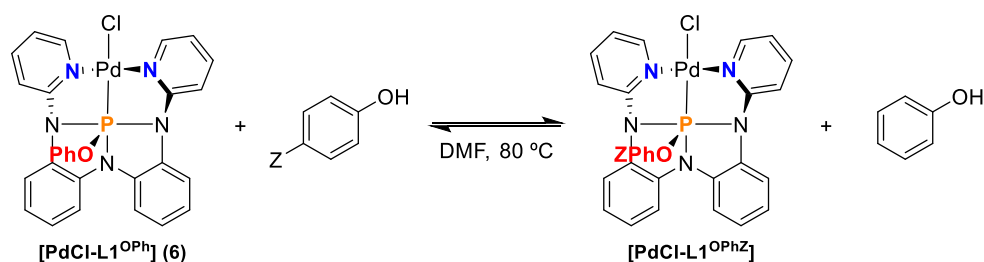


**Figure 4.**  $^1\text{H}$  NMR spectra of the substitution complexes. Color code: Blue: Cl; Purple: I, Green: SCN; Red: OPh.

These reactions showed that substitution can be selectively achieved either at P or Pd, depending on the starting complex and the nucleophile employed. With one eye on the potential application of this metal-ligand combination in catalysis, reversibility of substrate binding was evaluated. To this end, exchange at  $[\text{PdCl-L1}^{\text{OPh}}]$  (**6**) with different para-substituted phenols was tested. Solutions of **6** in DMF in the presence of 1 equivalent of the corresponding phenol were heated at 80 °C. P-bounded OPh exchange was observed. However, in contrast to the previous substitution reactions where the system was displaced toward a single product, the reaction is in this case an equilibrium (Scheme 7).



**Scheme 7.** Equilibrium reaction with different para-substituted phenols.

Depending on the substituent in para position of the phenol, the equilibrium is shifted toward reactants or products (Table 1). When electron rich phenols were employed, a higher degree of substitution was observed compared to electron poor phenols. A Hammett plot of the equilibrium constant logarithm versus  $\sigma_p$  parameter is depicted in Figure 5. It shows a negative slope, with a  $\rho$  value = -2.07, which indicates the buildup of positive charge in the rate determining step of the reaction. This observation could be consistent with a dissociative mechanism for the phenol substitution. However, an associative mechanism where nucleophilic attack of PhOH to P takes place, generating a  $[P-OPh-H]^+$  intermediate, seems more plausible.<sup>8</sup>

**Table 1.** Hammett plot values for the PhOH exchange equilibrium in Scheme 7.

Entry/ <i>p</i> -ZPhOH	$K_{eq}$	$\sigma_p$	$\text{Log}(K_{eq})$
1/ -OMe	3.77	-0.26	0.58
2/ -Me	2.89	-0.17	0.46
3/ -H	1	0	0.00
4/ -Br	0.242	0.25	-0.62
5/ -CN	0.01	1	-2.00

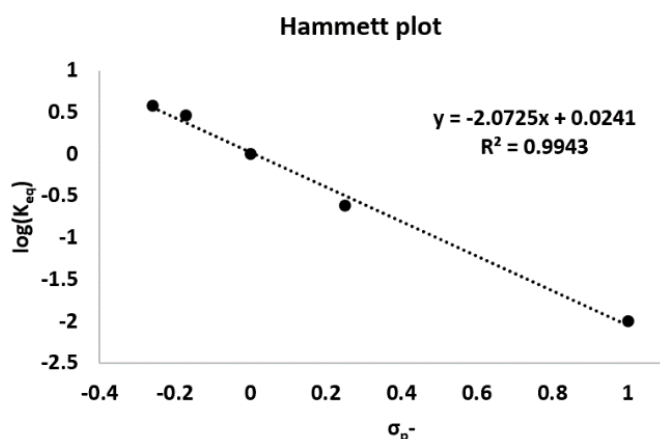


**Figure 5.** Hammett plot for the equilibria between **6** and para substituted phenols.

In summary, reactions between a geometrically constrained phosphine ligand, **L**<sup>1</sup>, and group 10 metal complexes led to the formation of metallophosphoranes, where one of the anionic ligands migrated from the metal center to the ligand P atom. This migration is easily identified by the high upfield chemical shift in <sup>31</sup>P NMR of the complexes compared to the free ligand and was further confirmed by X-ray diffraction studies. Metathesis reactions were tested for some Pd complexes, obtaining selective substitution at P, Pd or both atoms depending on the substituents in the starting complex and the nucleophile employed. Finally, the binding reversibility of substituents at P atom was confirmed upon addition of different para-substituted phenols. The results obtained in this system open the way to new catalytic methodologies for selective bond activation, based on metal-ligand cooperation, employing group 10 metals and geometrically constrained phosphines.

<sup>8</sup> Arantes, G. M.; Chaimovich, H. Thiolysis and Alcoholysis of Phosphate Tri- and Monoesters with Alkyl and Aryl Leaving Groups. An ab Initio Study in the Gas Phase. *J. Phys. Chem. A*, **2005**, *109*, 5625–5635.





## Conclusions

### **Chapter I: Reductive Elimination from Ni<sup>II</sup>-Meter**

The evaluation of ligand effects on the Ni<sup>II</sup> → Ni<sup>0</sup> reductive elimination rate, using *cis*-[Ni(C<sub>6</sub>F<sub>5</sub>)<sub>2</sub>(THF)<sub>2</sub>] as Ni-meter, allows to understand the different behavior of some ligands in Ni and compare it to Pd.

The high flexibility of PEWO ligands allows their use both with Ni and Pd, in contrast to the more rigid PR<sub>2</sub>(biaryl) ligands, which fail in Ni-mediated processes.

### **Chapter II: Selective Synthesis of Fluorinated Biaryls**

The use of PEWO ligands that accelerate the reductive elimination rate, or of a bimetallic Pd/Cu system that diminishes the competitive unwanted transmetalations, enhance the selectivity in the catalytic preparation of fluorinated biaryls.

### **Chapter III: *cis*-[Pd(Ar<sup>F</sup>)<sub>2</sub>(L)] Complexes as Precursors**

Fast ligand substitution and Ar<sup>F</sup>-Ar<sup>F</sup> coupling of *cis*-[Pd(Ar<sup>F</sup>)<sub>2</sub>(L)] precursors are key properties for clean and efficient *in situ* generation of *ad hoc* [Pd(Ar)X(L')] catalysts. Extreme bulkiness of 2-biarylphosphines can be a problem.

### **Chapter IV: Au⋯biaryl Non-Covalent Interactions**

The combination of complementary computational techniques (QTAIM, NCI, NBO) allows to explain the experimentally observed gold molecular structures, where the biaryl gets close to Au without establishing covalent interactions.

### **Chapter V: Intramolecular S<sub>N</sub>Ar Access to Fluorophosphoranes**

The presence of F in the appropriate position of 2-biarylphosphines easily produces luminescent fluorophosphoranes via a non-concerted oxidative addition of P(III) to P(V) by S<sub>N</sub>Ar followed by F<sup>-</sup> coordination to P.

### **Chapter VI: Luminescence of PEWOs and their Pd Complexes**

In metal complexes of fluorinated PEWO ligands, apparently small variations at the metal center provoke luminescence/non-luminescence changes due to good or bad M-chalcone communication via phosphorous atom.

**Chapter VII: Biphilic Phosphines as Ligands**

Modification of the P atom geometry expands the phosphine variability beyond the classical electronic and steric properties.

The selective substitution observed in metallophosphorane species bearing biphilic phosphines and its reversibility opens the way to new synthetic methodologies based on metal-ligand cooperative reactivity.

## Methods

The methodology that has been employed in this Thesis is widely applied in high-quality chemical research. Hence, only the general methods will be described here. The Supplementary Information of the published scientific articles collect more specific details, such as the synthesis and characterization of new compounds, structural data or DFT calculations data.

All the manipulations were performed under N<sub>2</sub> or Ar atmosphere by means of standard Schlenk techniques. Solvents were dried using a solvent purification system SPS PS-MD-5 or distilled from appropriate drying agents, and were sparged with nitrogen gas. CDCl<sub>3</sub> was vacuum-transferred from CaH<sub>2</sub> and degassed using freeze-pump-thaw technique. Solvents for experiments in an inert atmosphere were stored into flame-dried Schlenk flasks over freshly activated 3 or 4 Å molecular sieves.

<sup>1</sup>H, <sup>13</sup>C{<sup>1</sup>H}, <sup>19</sup>F and <sup>31</sup>P{<sup>1</sup>H} NMR spectra were recorded with Bruker Avance 400 Ultrashield and Varian 500/54 Premium Shielded instruments equipped with variable-temperature probes. The temperature for the NMR probe was measured with an ethylene glycol standard (high temperature) or methanol (low temperature) as chemical shift thermometer using standard methods. In the <sup>19</sup>F and <sup>31</sup>P NMR spectra registered in non-deuterated solvents, a coaxial tube containing acetone-*d*<sub>6</sub> was used to maintain the <sup>2</sup>H lock signal.

IR spectra were obtained on a Perkin-Elmer Frontier FT-IR spectrometer equipped with an ATR accessory (*Attenuated Total Reflection*) for direct acquisition from solid samples. HRMS (EI) were performed with a MALDI Bruker Autoflex at the LTI facilities of Valladolid University (Spain). Elemental analysis were carried out with a Carlo Erba 1108 Elemental Analyser at the services of Vigo University (Spain) or an Elemental Analyser EA Flash 2000 (Thermo Fisher Scientific at the PCT facilities of the University of Burgos (Spain).

For the X-ray diffraction studies, a crystal was attached to a glass fiber and transferred to an Agilent Supernova diffractometer with an Atlas CCD area detector (Valladolid University facilities). The crystal was kept at constant temperature during data collection. Data collection was performed with Mo-K $\alpha$  radiation ( $\lambda = 0.71073$  Å). Data integration, scaling and empirical absorption correction were carried out using the CrysAlisPro program package. Using Olex2, the structure was solved with the ShelxT structure solution program and refined with ShelxL program. The non-hydrogen atoms were refined anisotropically and hydrogen atoms were placed at idealized positions and refined using the riding model.

Luminescence studies were carried out at the PCT facilities of the University of Burgos (Spain). Steady-state fluorescence measurements were carried out by using a FLS980 fluorescence spectrometer with a 450W Xe lamp as a light source and double excitation and emission monochromators. Monochromator at 400 nm was used at the excitation and emission arms. A photomultiplier tube detector cooled by a Peltier system was used for detection. To measure the emission lifetimes and photoluminescence quantum yield (QY) the FLS980 fluorescence spectrometer is equipped with an integrating sphere. All data were measured at 25 °C. Time-resolved fluorescence measurements were carried out

using the single-photon counting technique with ns time resolution. A high repetition pulsed light source is used to excite the sample and the photons emitted are processed using the TCC1 card in the computer. Fluorescence decays were obtained with the Time Correlated Single Photon Counting (TCSPC) and MCP-PMT counter module (TCC2) of the FLS980 spectrometer (Edinburgh Instruments). Fluorescence decays were analysed with the method of non-linear least squares iterative deconvolution and the quality of the fits was judged by the values of the reduced Chi-square ( $\chi^2$ ) and the autocorrelation function of the residuals using the FAST (Advanced Fluorescence Lifetime Analysis Software) programme provided by the equipment.

## List of Publications

At the time of the completion of the memory, the results summarized in this Thesis have led to five published scientific articles, two manuscripts that are currently under revision (Chapters III and VI) and one manuscript in preparation (Chapter VII).

### Chapter I

I. Ponce-de-León, J.; Gioria, E.; Martínez-Ilarduya, J. M.; Espinet, P. Ranking Ligands by Their Ability to Ease  $(C_6F_5)_2Ni^{II}L \rightarrow Ni^0L + (C_6F_5)_2$  Coupling versus Hydrolysis: Outstanding Activity of PEWO Ligands. *Inorg. Chem.*, **2020**, *59*, 18287–18294. DOI: 10.1021/acs.inorgchem.0c02831.

### Chapter II

II. Ponce-de-León, J.; Espinet, P. Selective synthesis of fluorinated biaryls by  $[MCl_2(PhPEWO-F)]$  ( $M = Ni, Pd$ ) catalysed Negishi cross-coupling. *Chem. Commun.*, **2021**, *57*, 10875–10878. DOI: 10.1039/D1CC04915A.

III. Ponce-de-León, J.; Marcos-Ayuso, G.; Casares, J. A.; Espinet, P. Pd/Cu bimetallic catalysis to access highly fluorinated biaryls from aryl halides and fluorinated arenes. *Chem. Commun.*, **2022**, *58*, 3146–3149. DOI: 10.1039/D2CC00141A.

### Chapter III

IV. Ponce-de-León, J.; Villalba-Antolín, S.; Martínez-Ilarduya, J. M.; Espinet, P. Mechanistic and Catalytic Studies of Coupling Reactions Using 2-Biaryl-dialkyl Phosphines or Xantphos. Experimental Approaches to Catalyst Precursors, Intermediates and Rates. *Manuscript under revision*.

### Chapter IV

V. Ponce-de-León, J.; Infante, R.; Pérez-Iglesias, M.; Espinet, P. Fluorinated vs Nonfluorinated  $PR_2$ (biaryl) Ligands and Their  $[AuCl(L)]$  Complexes: Synthesis, X-ray Structures, and Computational Study of Weak Interactions. Bond, No Bond, and Beyond. *Inorg. Chem.*, **2020**, *59*, 16599–16610. DOI: 10.1021/acs.inorgchem.0c02513.

### Chapter V

VI. Ponce-de-León, J.; Infante, R.; Espinet, P. Easy Wide Scope Access to Luminescent Fluorophosphoranes. *Chem. Commun.*, **2021**, *57*, 5458–5461. DOI: 10.1039/D1CC00976A.

**Chapter VI**

**VII.** Ponce-de-León, J.; Peñas-Defrutos, M.; Vélez, A.; Aullón, G.; Espinet, P. Luminescence in the Solid State of Phosphine-EWO Ligands with Fluorinated Chalcone Skeletons and their PdX<sub>2</sub> complexes. Metal-promoted Phosphorescence Enhancement. *Manuscript under revision.*

**Chapter VII**

**VIII.** Ponce-de-León, J.; Drance, M.; Radosevich, A. T. Title to be determined. *Manuscript in preparation.*

## Ranking Ligands by Their Ability to Ease $(\text{C}_6\text{F}_5)_2\text{Ni}^{\text{II}}\text{L} \rightarrow \text{Ni}^0\text{L} + (\text{C}_6\text{F}_5)_2$ Coupling versus Hydrolysis: Outstanding Activity of PEWO Ligands

Ponce-de-León, J.; Gioria, E.; Martínez-Illarduya, J. M.; Espinet, P. *Inorg. Chem.*, **2020**, *59*, 18287–18294. DOI: [10.1021/acs.inorgchem.0c02831](https://doi.org/10.1021/acs.inorgchem.0c02831)

**Abstract:** The  $\text{Ni}^{\text{II}}$  literature complex *cis*- $[\text{Ni}(\text{C}_6\text{F}_5)_2(\text{THF})_2]$  is a synthon of *cis*- $\text{Ni}(\text{C}_6\text{F}_5)_2$  that allows us to establish a protocol to measure and compare the ligand effect on the  $\text{Ni}^{\text{II}} \rightarrow \text{Ni}^0$  reductive elimination step (coupling), often critical in catalytic processes. Several ligands of different types were submitted to this Ni-meter comparison: bipyridines, chelating diphosphines, monodentate phosphines,  $\text{PR}_2(\text{biaryl})$  phosphines, and PEWO ligands (phosphines with one potentially chelate electron-withdrawing olefin). Extremely different  $\text{C}_6\text{F}_5\text{--C}_6\text{F}_5$  coupling rates, ranging from totally inactive (producing stable complexes at room temperature) to those inducing almost instantaneous coupling at 25 °C, were found for the different ligands tested. The  $\text{PR}_2(\text{biaryl})$  ligands, very efficient for coupling in Pd, are slow and inefficient in Ni, and the reason for this difference is examined. In contrast, PEWO type ligands are amazingly efficient and provide the lowest coupling barriers ever observed for  $\text{Ni}^{\text{II}}$  complexes; they yield up to 96%  $\text{C}_6\text{F}_5\text{--C}_6\text{F}_5$  coupling in 5 min at 25 °C (the rest is  $\text{C}_6\text{F}_5\text{H}$ ) and 100% coupling with no hydrolysis in 8 h at  $-22$  to  $-53$  °C.





**Selective synthesis of fluorinated biaryls by  $[\text{MCl}_2(\text{PhPEWO-F})]$  (M = Ni, Pd) catalysed Negishi cross-coupling**

Ponce-de-León, J.; Espinet, P. *Chem. Commun.*, **2021**, 57, 10875–10878.  
DOI: [10.1039/D1CC04915A](https://doi.org/10.1039/D1CC04915A).

**Abstract:** Highly selective cross-couplings to polyfluorinated asymmetric biaryls, including the symmetric biaryl  $\text{C}_6\text{F}_5\text{--C}_6\text{F}_5$ , are achieved at relatively low temperature (80 °C) and in short times using  $[\text{MCl}_2(\text{PhPEWO-F})]$  catalysts (M = Ni, Pd; PhPEWO-F = 1-(PPh<sub>2</sub>), 2-(CH=CH-C(O)Ph)-C<sub>6</sub>F<sub>4</sub>), ArFI, and  $\text{Zn}(\text{C}_6\text{F}_5)_2$  as example of highly fluorinated nucleophile.



**Pd/Cu bimetallic catalysis to access highly fluorinated biaryls from aryl halides and fluorinated arenes**

Ponce-de-León, J.; Marcos-Ayuso, G.; Casares, J. A.; Espinet, P. *Chem. Commun.*, **2022**, 58, 3146–3149. DOI: [10.1039/D2CC00141A](https://doi.org/10.1039/D2CC00141A).

**Abstract:** An efficient Pd/Cu bimetallic cross-coupling catalysis of fluoroaryl halides and fluoroarenes is reported. In situ generation of the Cu nucleophile by rate determining C–H activation of highly fluorinated aryls ( $\geq 4$  F atoms) leads to high cross-coupling selectivity with little formation of homocoupling products.



## Mechanistic and Catalytic Studies of Coupling Reactions Using 2-Biaryl-dialkyl Phosphines and Xantphos. Experimental Approaches to Catalyst Precursors, Intermediates and Rates

Ponce-de-León, J.; Villalba-Antolín, S.; Martínez-Illarduya, J. M.; Espinet, P. *Manuscript under revision*.

**Abstract:** The steps and conditions for *in situ* formation and use of *ad hoc* cross-coupling catalysts  $[\text{Pd}(\text{Ar})\text{X}(\text{L})]$  ( $\text{X} = \text{Br}, \text{I}$ ;  $\text{L} = 2\text{-biaryl-dialkyl phosphines or Xantphos}$ ) are studied and tested using *cis*- $[\text{Pd}(\text{C}_6\text{F}_n\text{H}_{5-n})_2(\text{THF})_2]$  ( $n = 2, 3, 5$ ) or  $[\text{Pd}(\text{C}_6\text{F}_n\text{H}_{5-n})_2(\text{COD})]$  as *in situ* precursors of  $[\text{Pd}^0(\text{L})]$  that undergo oxidative addition by the chosen  $\text{ArX}$  electrophile. The results are compared with the reported  $[\text{Pd}^{\text{II}}(\text{neophyl})(\text{COD})]$  precursor. The study detects different rates for COD or THF substitution by the entering L ligand. In general, these preliminary steps are much more efficient on *cis*- $[\text{Pd}(\text{C}_6\text{F}_n\text{H}_{5-n})_2(\text{THF})_2]$ , which can produce the *in situ* sequence to  $[\text{Pd}^0(\text{L})]$  in one hour at 25 °C, while the others require working at 60 °C for lower conversions. The ligand substitution can be slow for bulkier phosphines and the use of tBuBrettPhos is very problematic for coordination and steric reasons that are discussed. The oxidative addition rate to the  $[\text{Pd}(\text{Ar})\text{X}(\text{L})]$  catalysts depends on the L ligand, and their X-ray diffraction structures show that they are commonly 4-coordinate dimers with P-monodentate L and bridging halides, that are split in solution to give probably  $[\text{Pd}(\text{Ar})\text{X}(\text{L})]$  monomers with P,C-chelating L. X-ray diffraction also confirms that the coupling species  $[\text{Pd}(\text{Ar}^{\text{F}})(\text{Ar}')(\text{L})]$  are also 4-coordinate square-planar with P,C-chelating L. In this respect the 2-biphenylphosphines and the chalcone derivatives PEWO are very similar. The application of the *in situ* precursors of  $[\text{Pd}(\text{Ar})\text{X}(\text{L})]$  to three specific catalysis (Buchwald-Hartwig amination, Negishi Ar–Me coupling and Stille  $\text{C}_6\text{F}_5$ –alkynyl coupling) with the same phosphine, tBuXPhos, uncovers peculiarities of the reactions as a consequence of the different reagents and intermediates involved in each case, and allow to select appropriate conditions for optimal *in situ* formation of the *ad hoc* catalysts.



## Fluorinated vs Nonfluorinated $\text{PR}_2(\text{biaryl})$ Ligands and Their $[\text{AuCl}(\text{L})]$ Complexes: Synthesis, X-ray Structures, and Computational Study of Weak Interactions. Bond, No Bond, and Beyond

Ponce-de-León, J.; Infante, R.; Pérez-Iglesias, M.; Espinet, P. *Inorg. Chem.*, **2020**, *59*, 16599–16610. DOI: [10.1021/acs.inorgchem.0c02513](https://doi.org/10.1021/acs.inorgchem.0c02513).

**Abstract:** Six fluorinated  $\text{PR}_2(\text{biaryl})$  phosphines,  $\text{L}^n$ , with  $\text{R} = \text{Ph}$ ,  $\text{Cy}$  and  $\text{biaryl} = \text{C}_6\text{H}_4\text{-C}_6\text{F}_5$ ,  $\text{C}_6\text{F}_4\text{-C}_6\text{H}_5$ ,  $\text{C}_6\text{F}_4\text{-C}_6\text{F}_5$ , have been prepared. Their  $[\text{AuCl}(\text{L}^n)]$  complexes and H congeners with PhJohnPhos or CyJohnPhos have been studied in order to examine the interactions that bring the distal aryl close to the Au–Cl bond region. X-ray, DFT structure optimization, QTAIM, and NCI methods allow for some understanding of the forces involved. The “no bond” noncovalent distal-aryl/Au–Cl weak interactions are produced at forced short distances achieved under intramolecular structural ligand pressure. Enhanced vdW distal-aryl/Au interactions at “no bond” distances shorter than the sum of Au and C vdW radii and weaker distal-aryl/Cl interactions at “no bond” distances beyond the sum of Cl and C vdW radii counterbalance the unfavorable structural distortion of the free ligand, providing some extra stability of the molecule on the order of 2–10 kcal mol<sup>-1</sup>. The F substituents in the distal aryl induce shorter aryl distances to the Au–Cl zone, pointing overall to stronger  $\pi$ -aryl polarization as being mainly responsible for the NCIs with gold. The interactions in the  $\text{C}\cdots\text{Cl}$  zone, where the distances are larger than the sum of vdW radii, contribute only about 5%, according to energy estimations using NBOs.





## Easy Wide Scope Access to Luminescent Fluorophosphoranes

Ponce-de-León, J.; Infante, R.; Espinet, P. *Chem. Commun.*, **2021**, 57, 5458–5461.  
DOI: [10.1039/D1CC00976A](https://doi.org/10.1039/D1CC00976A).

**Abstract:** The almost quantitative synthesis of homologous luminescent fluorophosphoranes, by  $S_{\text{N}}\text{Ar}$  cyclization of (2'-F,2-(PR<sub>2</sub>)biaryl) phosphines made from easily accessible reagents, is reported and the DFT cyclization mechanism and alternative pathways to complete this isomerization are studied and discussed.



## **Luminescence in the Solid State of Phosphine-EWO Ligands with Fluorinated Chalcone Skeletons and their PdX<sub>2</sub> complexes. Metal-promoted Phosphorescence Enhancement**

Ponce-de-León, J.; Peñas-Defrutos, M.; Vélez, A.; Aullón, G.; Espinet, P. *Manuscript under revision*.

**Abstract:** *trans*-[PdX<sub>2</sub>L<sub>2</sub>] complexes (X = Cl, Br; L = R-PEWO-F<sub>4</sub>) display remarkable phosphorescent emission in the solid state, which is not observed when using CN<sup>-</sup> instead of halide, or Pt instead of Pd. DFT calculations explain these observations, illustrating the drastic effect of the metal moieties on the frontier orbitals of these structurally identical derivatives: hybridization of the moderately stable orbitals of the PdX<sub>2</sub> core with those of the chalcone fragment of the ligands is found only for the LUMO of the emissive compounds. Attending to their substantially lower lifetimes, the free ligands feature fluorescent behaviour.

